University of Évora

ARCHMAT

(ERASMUS MUNDUS MASTER in ARCHaeological MATerials Science)

Master's degree in Archaeology and Environment (Erasmus Mundus – ARCHMAT)

New insight on south western Iberian rock art by non-invasive analytical approaches – the cases of Ardales and Escoural Cave

Samantha Hruban m40805

António Candeias
(Supervisor – University of Évora)

Ana Teresa Caldeira
(Supervisor – University of Évora)

Évora, October 2019

Universidade de Évora

ARCHMAT

(ERASMUS MUNDUS MASTER in ARCHaeological MATerials Science)

Mestrado em Arqueologia e Ambiente (Erasmus Mundus – ARCHMAT)

Um novo olhar sobre a arte rupestre ibérica do sudoeste por adordagens analíticas não invasivas – os casos das grutas de Ardales e Escoural

Samantha Hruban m40805

António Candeias
(Orientador – Universidade de Évora)

Ana Teresa Caldeira
(Orientador – Universidade de Évora)

Évora, Outubro 2019

Disclaimer: Due to time constraints and authorizations the campaign of Ardales Cave was not conducted.

Panel of Jury

President: Doctor Nicola Schiavon, Universidade de Évora;

Examiner: Doctor Catarina Miguel, Laboratorio HERCULES, Évora;

Supervisor: Professor António Candeias, Universidade de Évora;

Partner Member: Professor Gabriele Favero, Universitá di Roma La Sapienza.

Table of Contents

Abstract

New insight on south western Iberian rock art by non-invasive analytical approaches – the cases of Ardales and Escoural Cave

This thesis focuses on Escoural Cave, in southwestern Iberia, known as the only cave within Portugal to contain Palaeolithic rock art. Estimated to be roughly 20,000 years old, the paintings and engravings found inside the hypogeal environment face possible degradation due to natural and anthropogenic factors. Although previously well documented, the importance of continuous monitoring and documentation of at-risk cultural heritage, specifically rock art, is important for its survival and for the implementation of future conservation efforts. One aim of this thesis was to use non-invasive techniques and methods to document and analyze the rock art at Escoural Cave. Various imaging techniques were used to further reveal parts of the hidden rock art found within Escoural Cave while also documenting the current state of preservation of the eight most well-known paintings. The work completed for this thesis also investigated the effectiveness and reliability of Vis-NIR FORS and hyperspectral imaging in their usefulness and applicability for non-invasive rock art research. The Vis-NIR FORS and hyperspectral camera were determined to be periodically useful for the work completed at Escoural Cave; many factors from, lighting, location of the rock art, and extensive amounts of calcite coverage over the paintings created non-ideal conditions within the cave for the complete effectiveness of these approaches. These methods were useful for non-invasive pigment identification and proved less reliable for the interpretation of possible organic binders. Lastly, the eight locations sampled throughout Escoural Cave for microbial growth showed - through the use of culture-dependent and the culture-independent method of NGS - that the majority of microorganisms in Escoural Cave are naturally found within karstic systems. However, the presence of some strains of *Enterobacter* sp. raises concerns as it can be pathogenic to visitors with compromised immune systems; additionally, the presence of lampenflora is of concern for the protection of the rock art and is a contender for future preventive conservation efforts through its removal.

Resumo

Um novo olhar sobre a arte rupestre ibérica do sudoeste por adordagens analíticas não invasivas – os casos das grutas de Ardales e Escoural

Esta tese centra-se na gruta do Escoural, no sudoeste da península Ibérica, conhecida como a única com arte rupestre Paleolítica, em Portugal. Estima-se que tenham cerca de 20.000 anos de idade, as pinturas e gravuras encontradas na gruta e enfrentam uma possível degradação devido a fatores naturais e antropogénicos. Embora previamente bem documentada, a importância do acompanhamento contínuo e da documentação do património cultural em risco, especificamente a arte rupestre, é importante para a sua sobrevivência e para a implementação de futuros esforços de conservação. Um dos objetivos desta tese foi usar técnicas e métodos não invasivos para documentar e analisar a arte rupestre da gruta do Escoural. Usaram-se várias técnicas de imagem para revelar ainda mais partes da arte escondida na rocha, no interior da gruta, permitindo também documentar o estado atual de preservação das oito pinturas mais conhecidas. Este trabalho também permitiu avaliar a eficácia e a aplicabilidade de FORS Vis-NIR e imagem híper-espectral como metodologias não invasiva em arte rupestre, revelando-se metodologias úteis para o trabalho desenvolvido nesta gruta; muitos fatores, iluminação, localização da arte rochosa, e extensas quantidades de cobertura de calcite sobre as pinturas criaram condições não-ideais dentro da gruta para a completa eficácia destas abordagens. Estes métodos foram úteis para a identificação não invasiva de pigmentos e revelaram-se menos eficazes para a interpretação de possíveis aglutinantes orgânicos. Finalmente, os oito locais amostrados para o crescimento microbiano mostraram-através do uso de cultura-dependente e do método cultura - independente de NGS-que a maioria do microrgnismos na gruta Escoural são naturalmente encontrados em ambientes hipogénicos. No entanto, a presença de algumas estirpes, por exemplo de *Enterobacter* sp. podem apresentar patogenicidade para os visitantes com sistemas imunológicos comprometidos; além disso, a presença de lampenflora é uma preocupação para a proteção da arte rupestre e é um candidato para futuros esforços de conservação preventiva através de sua remoção.

Acknowledgments

"The uniqueness of rock art, as a manifestation of human expression, is its deep antiquity and its geographical universality. It's the essence of human expression in various forms and ways over the entire span of human existence and in every part of the world."

Neville Agnew, Getty Conservation Institute senior principal project specialist

GCI's Southern Africa Rock Art Project

List of Figures

List of Tables

List of Appendices

Appendix 1: The stylistic evolution of Palaeolithic rock art.

Appendix 2: Cleaned calcite crust from painting #5 in Escoural Cave.

Appendix 3: Results from various imaging techniques used to document the rock art.

Appendix 4: Palaeolithic pigment and binder standards used for calibration of Vis-NIR FORS.

Appendix 5: Point analysis locations for Vis-NIR FORS and EDXRF techniques on paintings from Escoural Cave.

Appendix 6: Isolation charts for bacteria isolates from Escoural Cave.

Appendix 7: NGS results of biofilm sampling locations from Escoural Cave.

List of Appendices

Table of Abbreviations

AOI   Area of Interest

ARCHMAT   Archaeological materials science

BCE   Before Common Era

CRB   Cook Rose Bengal

DNA   Deoxyribonucleic Acid

InGaAs   Indium Gallium Arsenide

IR   Infrared

ITS   Internal Transcribed Spacer

MEA   Malt Extract Agar

NA   Nutrient Agar

NGS   Next Generation Sequencing

PC   Principal Component

PCA   Principal Component Analysis

PCR   Polymerase Chain Reaction

TSA   Trypticase Soy Agar

UVF   Ultraviolet Fluorescence

Vis-NIR FORS   Visible-Near Infrared Fiber Optics Reflectance Spectroscopy

XRF   X-Ray Fluorescence

I. INTRODUCTION

1.1 ROCK ART

Rock art is one of the oldest expressions of humankind and one of the oldest forms of cultural heritage, a true living testimony of the past human experience. Cave art, rock art, petroglyphs, pictographs, rock carvings, rock paintings, parietal art, and rock imagery are just some of the terms that have been used to describe one of the most visible parts of the archaeological record.

Rock art, simply put, consists of symbolic markings found on rock surfaces; these rock surfaces can range from caves to rock shelters to open-air sites (Smith, 2014). The graphic markings or pictures are made with many diverse techniques from fingers, paintbrushes, and pencils, to paint sprayed from the mouth, etching, pecking, and engravings made with burins and flint points (Rogerio-Candelera, 2016; Smith, 2014).

As Dr. David S. Whitley, a specialist in North American prehistoric archaeology shares, "rock art is common in all regions worldwide with landscapes containing natural rock surfaces"(Whitley, 2001, p.7). It is found in Europe, with some of the more well-known sites being Lascaux and Chauvet in France and Altamira in Spain. European rock art sites are more commonly found in France and the Iberian regions where some of the oldest rock art exists dating to 40,000 years old (Agnew et al., 2015). In places like Australia's Kakadu National Park, rock art is still being traditionally made and protected by the Aboriginal communities living there, where their artistic tradition has been passed down for generations within the local culture (Agnew et al., 2015). Rock art can be found in Africa, a continent of 54 countries in which more than half contain rock art sites and eight are listed as UNESCO world heritage sites (TARA, n.d.). South eastern Asia contains a remarkable collection of motifs and sites that display their rich cultural heritage spanning from Siberia to India (Agnew et al., 2015). Lastly, rock art has a great expanse across the Americas, from Alaska to Argentina there are many sites that reflect humankind's rich culture.

Traditional rock art was created with an assortment of different materials and techniques. The pigments used to create the majority of rock art were usually from raw materials which were locally sourced from nearby areas of the actual images. The main pigments of rock art were black, red, and yellow (Chalmin, Menu, & Vignaud, 2003). Black is usually found to be

charcoal, bone black, or manganese oxide (Chalmin et al., 2003). Red colors can be from materials rich in ferric oxides like hematite (red ochre), while goethite (yellow ochre) provides a good source for yellow (Smith, 2014). In order to enhance these pigments, the paints were prepared using extenders, binders, and/or various heating methods (Chalmin et al., 2003). After grinding the raw materials; various binders of water, animal fat, plant-derived material, blood, saliva, or urine could have been used; while extenders of feldspar, biotite, talc, or clay could have been added to the mixture to ensure the wet pigment stuck to the substrate of the rock surface (Gunn, 2004; Smith, 2014; Whitley, 2001). Other methods of rock art included drawings with charcoal sticks or ochre crayons (Smith, 2014). Stencils were also a common method found in rock art; for example, the creation of negative hands was produced by spitting paint over the hand which in turn left an outline (Smith, 2014). Engravings were created through abrasion or chipping away at the substrate's surface with tools of flint, or if the substrate was soft enough, such as clay, fingers could have been used to design the motifs (Rogerio-Candelera, 2015).

The humans that created the rock art had many different themes ranging from figurative and abstract imagery to hand imagery (Smith, 2014). Figurative imagery is a theme which depicts animals and humans. In Europe, horses, bison, mammoth, ibex, and deer are the most common figures found depicted in rock art (Smith, 2014). Abstract imagery includes geomorphic signs from dots to lines and shapes like tectiforms or scalariforms (Smith, 2014). Hand imagery is also an important theme seen regularly throughout rock art; negative hand stencils, positive handprints, and stylized hands drawn (Smith, 2014).

Although the tangible aspects of this common cultural phenomenon are easy enough to describe from their geological location, the raw materials used to create them, and the techniques of production, it is harder to describe the intangible aspects. Rock art is not only the physical but the symbolic dynamics of past societies, it includes the emotional impacts felt by those who view it and those who created it (Gallinaro, 2018). The purposes for creating rock art – although most likely not to convey artistic ability like the term 'art' is used today – is believed to have been for a myriad of different possibilities. Many original hypotheses believed rock art to have be created for shamanistic purposes (Smith, 2014). Rock art, especially those images depicting animals were usually connotated with displays of 'hunting

magic', 'fertility magic', shamanism, or trophyism (Smith, 2014). New theories are continually introduced whenever new archaeological and anthropological movements are developed.

However, the profound importance and wealth of information that can be gathered from rock art is greatly diminished if one only considers the aesthetic feelings the imagery provides; rock art can also be an important documentation of history, giving insight into the past as a first form of storytelling and dare I say, language. The images depicted on the rock's surface shares information about the people who once lived there, providing a deeper understanding about past cultures, environments, and climates. In *figure 1*, image (A) and (B), an engraving from Libya depicts the sacrificing of a bull, where an upside-down bull is surrounded by masked humans (Gallinaro, 2018). Particularly fascinating, this ritual is still practiced today in local communities residing nearby (Gallinaro, 2018). Image (C) is believed to be a *Megaloceros*, an extinct type of giant moose, painted in black pigment found in Chauvet Cave, France (Brandshaw Foundation, n.d.). The cattle etched in image (D) is found in the Ennedi Highlands of Chad, a region now engulfed by the Sahara Desert; however, the highlands were once home to pastoralists and grazing cattle when rainfall was more frequent (Heyd & Lenssen-erz, 2012). Now in the Ennedi Highlands, only camels can survive in the harsh environment (Heyd & Lenssen-erz, 2012).
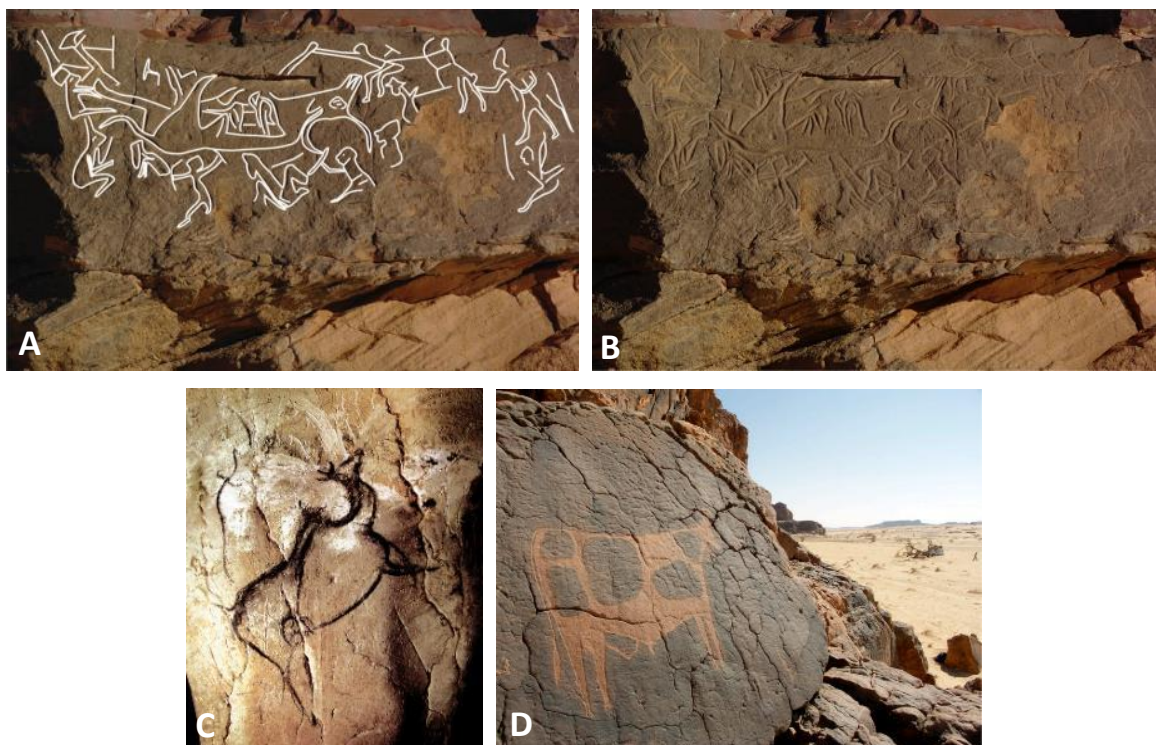
Figure 1: Rock art from around the world depicting various insights into past cultural events, environments, and climate.

As uniquely diverse as rock art is, from what it depicts and what methods were used to create it, it is also uniquely universal when considered as part of the collective human past; in that, rock art can be found all across the world, in all corners of human habitation and has been continuously created for thousands of years. Rock art's importance as a piece of humankind's identity and cultural heritage cannot be understated; and therefore, the efforts to document, analyze, preserve, and create awareness about them should not be either.

1.2 SITE CONTEXT

This thesis focuses on rock art found in the Iberian Peninsula, specifically the Palaeolithic site of Escoural Cave in Portugal. Iberia contains a rich history of rock art dating as far back as the Upper Palaeolithic period. For roughly 30,000 years during the Upper Palaeolithic period, the Iberian Peninsula became a thriving location for rock art, with about 200 Palaeolithic sites found in Portugal and Spain alone (Bicho, Carvalho, Gonz, & Sanchidri, 2007). During the Pleistocene, Palaeolithic hunter gatherers were beginning to create the first tools while at the same time creating relatively remarkable and complex graphics on the side of rock shelters and caves.

The oldest rock art in Europe which occurs in the Upper Palaeolithic can be divided into four time periods based on stylistic techniques employed during each period; the oldest is Aurignacian art from 40,000-25,000 BCE; Gravettian art from 25,000-20,000 BCE; followed by Solutrean art from 20,000-15,000 BCE; and lastly Magdalenian art from 15,000-10,000 BCE (see *appendix 1*) (Whitley, 2001). Typical Upper Palaeolithic rock art consisted of animals and geometric signs, while humans were rarely depicted (Whitley, 2001). Although the Upper Palaeolithic rock art tradition would end during the last ice age, the rock art that was created then can still be found today, some having survived nearly 30,000 years since their creation (Whitley, 2001).

1.2.1 ESCOURAL CAVE

Escoural Cave is located in the municipality of Montemor-o-Novo in the town of Santiago do Escoural, Portugal (Silva, 2011; Silva & Araújo, 1995). Lying between the Tagus and Sado rivers, Escoural Cave finds its home in a natural basin within the Alentejo peneplain (*figure 2*) (Silva, 2011). Due to the natural 'roads' of the rivers, it is surmised that past prehistoric communities would have travelled inland on these roads and found the grotto of Escoural; the only cave within a 50-kilometer radius (Silva, 2011). Escoural's limestone cavern is also

unique within the Alentejo region, which is naturally formed of mostly granite outcrops (Silva, 2011).
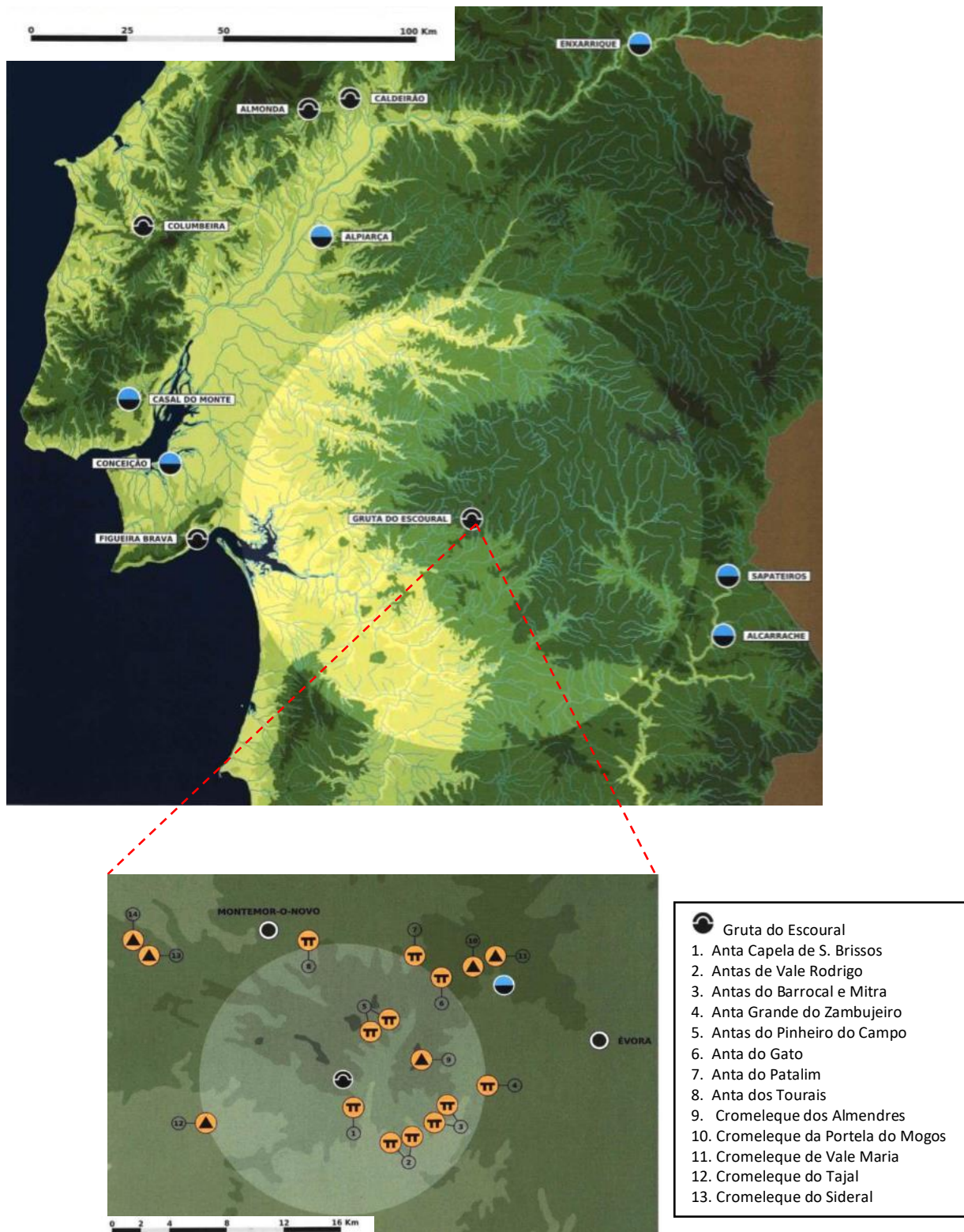
Figure 2: Map of Portugal with location of Escoural Cave and other Palaeolithic sites in south western Iberia; shown below is Escoural Cave in relation to nearby megalithic monuments. Adapted from Silva A.C., Escoural; uma gruta a pré-histórica no Alentejo, 2011.

The Alentejo region in central Portugal is notable for its many megalithic sites and long occupational history. Found nearby to the Cave of Escoural are fourteen other distinct megalithic sites constructed during the Neolithic period (Silva, 2011). These sites include the notably famous, Great Dolmen of Zambujeiro and the Almendres Cromlech (*figure 2*). Escoural Cave itself is known to have been occupied since the Middle Palaeolithic (50,000 BCE) when Neaderthals used the cave as a shelter; during the Upper Palaeolithic (35,000-8,000 BCE) when modern humans used the cave as a sort of 'shrine' where they painted and engraved the walls; to the Neolithic (5,000-3,000 BCE) when it was used as a necropolis to bury the dead (Silva, 2011). Afterwards, outside the cave a Chalcolithic settlement (2,000 BCE) appeared and the nearby megalithic monuments were built (Silva, 2011). However, sometime during the Neolithic settlement, for reasons unknown, the entrance to the cave was sealed preserving the rock art and artifacts inside and would not be reopened until the 17 of April, 1963 when a mining accident in the nearby quarry, Herdade dos Santos, blew open a new entrance to the grotto of Escoural (Marques, 2001).

Escoural Cave itself is a rather small and superficial cave. The natural layout consists of three rooms and narrow passages connecting the rooms and numerous galleries found inside. The main room is approximately twelve by fifteen meters and contains an abundance of the rock art found inside the cave.

Esocural cave is particularly significant due to the fact that it is the only cave in Portugal with Palaeolithic rock art, and one of the few found within the whole of the Iberian Peninsula (Silva & Araújo, 1995). There are nearly 100 figures recorded at Escoural Cave, mostly engravings, but also 30 distinct figures painted in red and black (Mauran, Mirao, Candeias, & Caldeira, 2017). The figures, both engraved and painted, generally consist of animals such as horses, bovines, and bovids; geometric shapes ranging from dots to lines; and a number of unidentified shapes that have either been greatly altered through deterioration, left unfinished, or are simply unrecognizable. Most of the paintings found within Escoural Cave are dated to the Solutrean period (22,000-17,000 BCE), while the majority of the engravings are believed to have been created during the Soluntrean and Magdaleneian periods (18,000-10,000 BCE) (Araújo & Gomes, n.d.).

Originally, the paintings and engravings were dated through a relative dating method of analyzing the rock art stylistically. As *appendix 1* portrays, the Upper Palaeolithic rock art found in Europe displays common themes in regards to the period of when it was created. Older rock art displays a simplistic sense of depiction while the younger images have shifted towards a more anatomically accurate depiction and contain more intricate detailing. Rock art can also be dated directly; however, acquiring funding, permission, and finding enough material to sample are some of the key limitations when it comes to direct dating of rock art. The first attempts to use absolute dating on the paintings of Escoural Cave were undertaken in 2011 using U-Th dating of the calcium carbonate crusts near the paintings; the results obtained confirmed the previously thought age range of approximetly 22,000-17,000 BCE (Mauran et al., 2017).

Other previous analyses at Escoural Cave have included the original analysis in 1997, when projects aimed at the study of the rock art began; the work focused on the recording and deciphering of each painting and engraving found (Peyroteo-stjerna, 2018). Some climatic studies were implemented in the years of 2002-2004 (Barquín, 2015). Between 2010-2012, climatic studies were also conducted at Escoural Cave to monitor the microclimate and implement visitor regulations for preventive conservation of the rock art; calcium carbonate crusts were also removed in attempts to improve visualization of the rock art panels (see *appendix 2*) (Barquín, 2015). Lastly, a campaign in 2016 was conducted to study the pigments and painting techniques used in Escoural Cave; imaging analysis such as infra-red reflectography was used along with microsampling of the pigments (Mauran et al., 2017). In the same campaign of 2016, biofilm sampling was also conducted to analyze the various microorganisms inhabiting the cave (Mauran et al., 2017).

Unfortunately, the rock art at Escoural Cave has struggled to withstand the test of time, having endured for nearly 20,000 years it is astonishing that some of the artwork still remains; nevertheless, the cave and the graphic images themselves face continuous degradation and damaging effects from natural processes to human interventions every single day. Everyday, the cave must balance the unique fragile ecosystem that it supports and still remain open for visitors to explore the rock art. From the visitor regulations implemented in 2012 through a partnership between the Directorate of Regional Culture of Alentejo and the Cabinet of Archaeology and Heritage Management Culture, Escoural Cave has permitted entrance to a

maximum of 40 persons per day; with a maximum of 10,000 visitors per year (Barquín, 2015; Contador, 2019). However, current visitation rates average lower at approximately 3,700 visitors for the previous year of 2018 (Contador, 2019). The work from this thesis will continue to explore the factors threatening the rock art at Escoural Cave and the effects they are causing.

1.3 DETERIORATION AND DEGRADATION

Other than those briefly mentioned earlier, there are a myriad of complex natural and human impacts that can threaten rock art sites; this section will delve deeper into the causes and effects that damage the world's rock art, an irreplaceable form of cultural heritage. Not only can rock art be found all across the globe, they can be discovered on many different surfaces. Rock art is not only limited to the inside of caves and rock shelters, but they can be found on ceilings and floors. Carved images of prehistoric fauna and other abstract imagery can be seen in open-air landscapes as well, like those in the Foz Côa Valley in north eastern Portugal (Silva, 2011). Although these motifs are interesting in their design, they are better known for their survival. As David Lambert, a rock art conservator from Australia's Department of Environment and Climate Change, simply states, "rock art is paradoxically both fragile and enduring" (Lambert, 2007). The unique and marvelous engravings found at the UNESCO World Heritage site of Foz Côa may have miraculously survived these past 25,000 years, but they - along with all rock art encompassing the globe - will continue to face daily threats to their survival; whether it be from natural processes or from anthropogenic factors. In order to save these cultural heritage sites, it is necessary to start with understanding the processes that they undergo.

1.3.1 NATURAL IMPACTS

Natural systems that are present in sites with rock art, whether they be open-air sites or karstic cave systems, contain two basic groups; biotic elements and abiotic elements (Rogerio-candelera, 2015). Both biotic and abiotic elements continue to degrade the rock art surfaces and contribute to the deterioration of the paintings and engravings found there. Biotic elements include natural factors such as microorganisms, insects, and plants. Abiotic elements consist of radiation, air, water, temperature, and rock art itself (Rogerio-candelera, 2015). All sites face specific problems, open-air sites are particularly vulnerable to wind and

rain, while show caves have fragile ecosystems and climates that can be easily disrupted by visitors viewing the rock art (V Jurado et al., 2010; Smith, 2014).

The main natural impacts affecting rock art sites around the world include: weathering and erosion of rock surface and substrate, dust and mineral accretions, vegetation growth, animal and insect impacts, changing climatic conditions, major environmental events, and microorganism growth (Whitley, 2001).

Weathering of rocks is defined as the disintegration and decomposition of rock (Earle, 2019). There are two forms of weathering, mechanical and chemical. Mechanical weathering occurs when a rock is disintegrated into smaller pieces by physical forces usually due to temperature and pressure changes (Earle, 2019). Chemical weathering is when minerals inside a rock are altered through the addition or removal of varying elements; such as water and oxygen (Earle, 2019). Common examples of mechanical weathering that can easily harm rock art painted on the surface include: frost wedging when water freezes and expands causing cracks and fissures, and mechanical exfoliation when water, salts, and changes in temperature and humidity causes the rock to be stripped (see *figure 3*) (Earle, 2019). Chemical weathering includes dissolution; when acidic waters, whether natural or not, dissolve rocks especially limestone (Earle, 2019). Oxidation is also a common form of chemical weathering; when oxygen reacts with ferrous iron to cause rust; oxidation can react with common rock art minerals such as hematite and goethite (Earle, 2019). Hydrolysis, another form of chemical weathering, is when a substance is broken down when combined with water (Earle, 2019). Many factors can influence the process of chemical weathering on rock surfaces; these include changes in climate, the presence of organisms and microorganisms, growth of vegetation, and time.

Erosion can be defined as the weathering of rocks through the transportation of products by mobile agents such as water, wind, or ice (Earle, 2019). Open-air sites like those found at Foz Côa Valley are particularly prone to erosion.

Dust and mineral accretions, such as salt deposits continuously piling on rock art can slowly begin to obscure the paintings and engravings found (see *figure 3*). Another harmful natural impact that can be especially damaging for open-air sites and rock shelter sites includes vegetation growth. Various shrubs and trees near sites can also cause damage such as organic

weathering; when weeds and shrubs rub against the rock surface and when tree roots split rocks ("Documentation and Conservation of Rock Art," n.d.). The presence of plants near rock art can also be potential fire hazards, in which the exposed rock art can be darkened from fire and smoke, effectively destroying any paintings (see *figure 3*). Plants are not the only forms of organic weathering that can harm rock art; animals and insects can also contribute to the problem. Many birds and insects, such as mud wasps, are often a problem at rock shelter sites where they build their nests on the rock surface (see *figure 3*) (Agnew et al., 2015).

Other natural factors include geological and geomorphological risks pertaining to the structural stability of the rock art support which can be affected by landslides, collapses from earthquakes, and other events like flash floods (Ontañón, 2014).
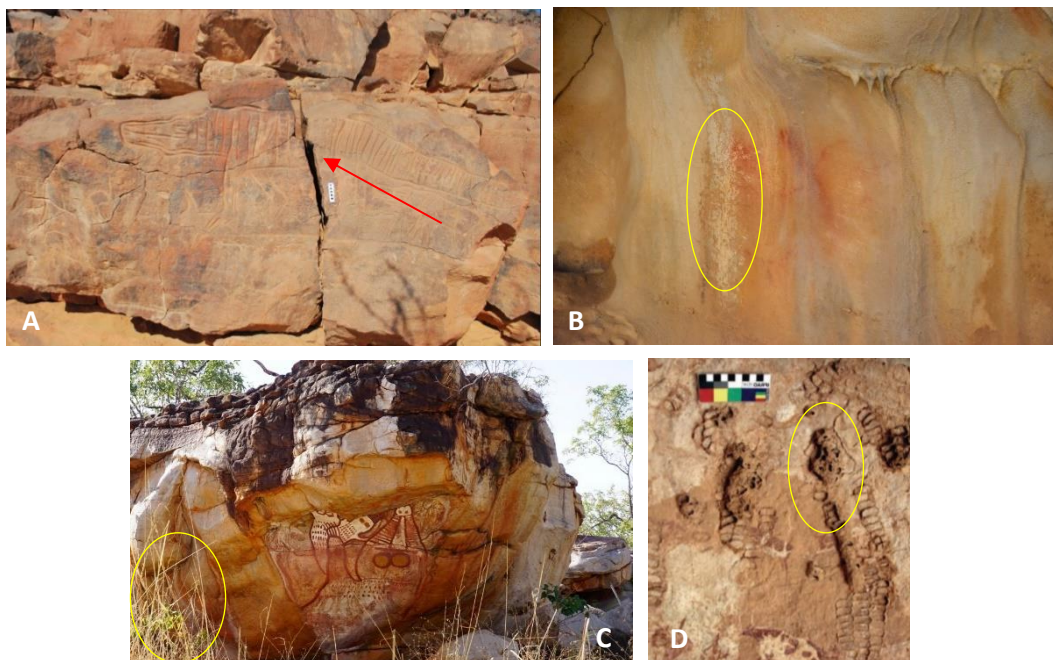
Figure 3: A) Cracks and fissures breaking rock art in half, due to mechanical weathering processes (59); B) water run-off from precipitation of cave causing pigment to run and the buildup of calcite crusts; C) nearby vegetation growth is a fire safety risk, especially for adjacent rock art that would be tarnished by the flames and smoke (97); D) Mud wasps nest covering rock art featuring cattle (59).

Lastly, as mentioned above, microorganisms can be a cause of chemical weathering on rock surfaces. Biodegradation and biodeterioration, usually a secondary process to the weakening of rock substrate by weathering, is caused by both heterotrophic and phototrophic microorganisms that can be found at many rock art sites, especially in closed environments like caves (Rosado et al., 2017). These microorganisms are the result of various interactions

between the other cave organisms, the rock substrate, and the environmental conditions of the site (Gallinaro, 2018; Rosado et al., 2017).

These microorganisms can include various bacteria, fungi, algae, and lampenflora. Microorganisms thrive in rock surfaces where they are able to obtain nutrients essential for their metabolism, such as calcium, aluminum, silicon, iron, and potassium (Rosado et al., 2017) in turn, the metabolic activities of the microorganisms induce more chemical weathering (Earle, 2019).

Microorganisms are naturally found in all rock art sites. However, some microorganisms are introduced to rock art sites by other means and can prove extremely harmful for the rock art residing there. Some methods of microorganism introduction found inside show caves include formation due to artificial illumination (Stomeo, Gonzalez, & Saiz-Jimenez, 2007)(1); underground air renewal from opening vaulted cave doors for visits can also disperse fungi spores throughout a cave (Fernandez-Cortes et al., 2011; Stomeo et al., 2007); human shoes can track in new organic material to feed microorganisms, while human hairs and clothing fibers can also act as nutrient sources for biota growth (Fernandez-Cortes et al., 2011; Novakova, Hubka, Saiz-Jiménez, & Kolarik, 2012; Whitley, 2001); bats and insects also create and distribute organic matter and fungal spores throughout caves (Fernandez-Cortes et al., 2011; Whitley, 2001); lastly, the instability of certain climatic conditions like relative humidity, CO_2, and also the occurrence of organic and inorganic material can promote the growth of fungi, bacteria, and biofilms (V Jurado et al., 2010; Rosado et al., 2017).

There are a few indications that signify if microbial growth is damaging the rock art nearby. Microorganisms, like fungi, can cause both chemical and mechanical processes to occur due to rhizine penetration of the substrate (Rosado et al., 2017). The root-like rhizine attach into the substrate and can cause exfoliation of the substrate walls and detachment of painted layers; while chemically, fungi can also cause discoloration of paintings due to metabolic processes (Gallinaro, 2018; Gonzalez, Laiz, Hermosin, Caballero, & Incerti, 1999; Olivares et al., 2013; Rosado et al., 2017). Biodeterioration is a continual cycle of transformation due to the microorganisms that use the substrate walls as a nutrient source, their metabolic processes that then damage the substrate by the acceleration of the dissolution of carbonate rocks, the releasing of acids furthers the biodeterioration, and this leads to further nutrients

for microorganisms to grow (Olivares et al., 2013; Rogerio-candelera, 2015; Rogerio-Candelera et al., 2018).

In order to preserve and further protect rock art, it is important to be wary of all the natural damages that can occur on rock art and the supporting substrate. Unfortunately, many natural impacts cannot be altered and will continue to happen (e.g. mechanical weathering). On the other hand, the observation, analysis, and prevention of harmful natural impacts - like invasive microorganisms - can be conducted in order to help preserve these cultural heritage sites. The monitoring and analysis of show caves is especially useful due to their fragile climates and environments. In order to analyze the type of microbes thriving in a rock art site, it is necessary to sample various areas of the site to learn what species are naturally found and those that are endangering the site. By identifying the microorganisms that reside near the rock art it is then possible to create a preservation and removal strategy that target specific groups of extremely harmful microorganisms and biofilms (Stomeo et al., 2007).

1.3.2 HUMAN IMPACTS

Rock art could neither exist, nor be given meaning without humans, yet we remain one of the main forces behind its deterioration. It is generally well known the impact tourists can have on rock art sites, especially caves containing rock art (Saiz-Jimenez, 2014). Currently, two of the most famous Upper Palaeolithic rock art caves in the world, Lascaux in France and Altamira in Spain, are permanently closed to tourism (Saiz-Jimenez, 2014). In their place replicas of the caves were created and are used for the masses of tourists that still visit these sites daily (Saiz-Jimenez, 2014). The forced closures of these caves were due to the extreme advanced deterioration observed since their original rediscovery; caused mainly by the staggering number of tourists visiting each year and the required modifications of the caves needed for their convenience and safety (Saiz-Jimenez, 2014). At the time, in 1935, only 56 years following the 'discovery' Altamira, two members of the Conservation and Defense Board for the Cave of Altamira, Henri Breuil and Hugo Obermuier concluded that "the paintings had suffered more in the last fifty years than they had since they were painted [nearly 20,000 years ago]" due to the irreversible stabilization efforts on the cave's galleries and the quickening of biodeterioration rates due to increase in CO_2 levels, temperature, and relative humidity occurring with the surges of tourist visits (Saiz-Jimenez, 2014).

Human impacts consist of two forms, internal factors and external factors. Internal anthropogenic factors include events that occur directly at rock art sites ranging from uncontrolled visits and deliberate destruction like graffiti and theft; to installation of support walls, stairs, lighting systems; also, archaeological excavations and poor attempts at rock art conservation ("Documentation and Conservation of Rock Art," n.d.; Gallinaro, 2018; Ontañón, 2014; Whitley, 2001). These internal human factors can not only lead to the direct destruction of rock art from actions like theft, but also through the introduction of microbial growth through actions like the installation of artificial lighting that can create a food source for phototrophic microorganisms (Mulec & Kosi, 2009). External anthropogenic factors are harder to control, but still threaten the survival of rock art. External factors can include nearby mining and construction works, encroaching urbanization and the pollution that comes with it, agricultural practices located nearby, and fires (Gallinaro, 2018; Ontañón, 2014; Whitley, 2001). Nearby factories or other forms of air pollutants can cause the growth of gypsum crusts that cover the vulnerable rock art; while construction works can encroach into impluvium areas of show caves and potentially endanger the entire karstic systems (Rogerio-Candelera et al., 2018; Saiz-Jimenez, 2014).

Unlike artworks found in museums, artworks that have monetary value and therefore insured protection against all potential threats, rock art is uninsured yet priceless. As Jeffrey Levin, The Getty Conservation Institute, states, "[rock art] is a public art in the very original sense that it can't be acquired. It must remain where it is, or otherwise you destroy it" (*Conservation Perspectives: Rock Art Conservation*, 2019, p.22). As artworks in museums are guarded by security measures and advanced state-of-the-art environmental monitoring systems, rock art is protected by indigenous peoples, local communities, rock art researchers, and conservation professionals; but unfortunately it is common to find that they lack communication and information between them; they lack recognition, funding, and support; and they can lack consistent and set practice standards that follow agreed-upon protocols (Agnew et al., 2015).

The proper management of rock art sites are crucial for their protection. However, many sites are caught between protecting the rock art and allowing the public to enjoy the sites. The consequences of cultural tourism can create rifts between competing interests of the people protecting the sites and those promoting and creating revenue from it (Smith, 2014).

Another factor acting as a double-edged sword is the documentation and analysis of rock art. Many things can be learned from the analysis of rock art, however the methods used for these analyses need to be taken under careful consideration. Analysis methods can range from non-invasive to invasive sampling and complete destruction of a sample. Non-invasive methods can include various imaging techniques like photogrammetry, while destructive techniques involving sampling can be used to date the rock art.

In order to ensure a future for the survival of rock art these local and broader communities need to work together, not only so they can benefit from these invaluable pieces of cultural heritage, but to also manage and conserve them better (Agnew et al., 2015). The long-term survival of rock art is dependent on many factors, some which are controllable and some which are not. This multi-analytical thesis aims to be carried out in a non-invasive manner in order to help prevent further unnecessary damage to the priceless cultural heritage site of Escoural Cave.

1.4 THESIS TOPIC

This project intends to cast new light on the south west Iberian rock art site of Escoural Cave, in the Alentejo region of Portugal through the use of in-situ, non-invasive complementary analytical techniques to document and analyse the rock art and the surrounding environment.

The non-invasive documentation and material study of the rock art and their state of preservation will combine surface imaging techniques with point analysis techniques. Imaging techniques will include visible and raking light photography to document the rock art's visible features and surface irregularities; IR photography with different band-pass filters to observe under calcite coverage of at-risk paintings and to see the superposition of any paintings; UV fluorescence photography to detect materials with varying response to UV, distinguishing them with the naked eye; hyperspectral imaging in the visible range to identify differences in the material's response to different wavelengths including hidden details and images and the ability to identify pigment components; digital enhancement software such as DStretch and Photoshop that enable photographs to be altered in order to enhance the presence of eroded and degraded rock art; and lastly, photogrammetry to create a 3D digital model of the wall surfaces and a continuous picture of the rock art panels for complete documentation of the

current level of preservation. Vis-NIR FORS supported with EDXRF will be used to identify pigment compositions and possible organic binders used in the paintings.

Furthermore, non-destructive microbial sampling will be taken for culture-dependent and culture-independent analysis for the identification of biofilms in Escoural Cave. Molecular analysis of biofilm DNA will be carried out for the identification of microbial genera and species found residing near the at-risk rock art.

1.4.1 AIMS

This master's thesis aims to further the current knowledge of the rock art found inside Escoural Cave. Using non-invasive multi-analytical techniques, this thesis aims to provide new information regarding the rock art including recording their current state of preservation, identifying factors that could potentially be causing damage to the sites such as biofilms and microorganism growth, and using various imaging techniques to possibly reveal previously unknown art. This thesis also aims to determine if two non-invasive techniques new to rock art analysis, hyperspectral imaging and the Vis-NIR FORS, are useful in rock art analysis and documentation.

The purpose of the thesis is to document and analyse rock art in hypogeal environments without the use of destructive techniques on these rare and invaluable pieces of prehistoric art. The methods mentioned above will allow for a qualitative and semi-quantitative analysis of the rock art. As rock art is inherently fragile and is known to face continuous damage, degradation, and deterioration it is therefore a necessity to use non-destructive and non-invasive methods that are portable for fieldwork and are able to provide results that are fast and reliable in the fight to conserve and document the world's remaining rock art narratives.

This project was chosen through an interest in preventive conservation of cultural heritage through minimally invasive campaigns. The use of non-invasive techniques and analyses not only can allow for a deep understanding of the physical and chemical aspects of an archaeological object, but also ensures the preservation of these cultural heritage objects for future generations to enjoy and take meaning from.

1.5 LITERATURE REVIEW

The importance of using non-invasive methods to analyze cultural heritage has been well known for decades (Inés Domingo, Villaverde, López-montalvo, Luis, & Cabrelles, 2013;

15

General Method Policies for All Site Recordation, 2018; Olivares et al., 2013; Whitley, 2001). Although the benefits of invasive and sometimes destructive analysis through sampling are numerous when it comes to cultural heritage objects, it is foremost imperative to perform as many analyses as possible using methods and techniques that will not harm or alter the objects in any way especially if they are at-risk objects. In the case of rock art, many invasive, destructive techniques can be quite useful from absolute dating using Uranium-Thorium dating and Carbon-14 dating to learn the age of the rock art, or sampling of pigment to learn more about the various compositions of the paint and painting techniques used in the prehistoric rock art. However, it is also well known that rock art is an extremely fragile area of cultural heritage due to their physical locations, extreme age, and sometimes unique ecosystems; they suffer from natural deterioration of mechanical weathering and human caused interference like microorganism attacks similar to those see in Lascaux Cave which rapidly began to degrade the pigments of the infamous polychrome wall after the cave was opened to public visits (Saiz-Jimenez, 2014).

Well known non-invasive methods used throughout rock art analysis and documentation include various imaging techniques like IR photography, photogrammetry, and DStretch ("Documentation and Conservation of Rock Art," n.d.; Domingo Sanz, 2014; Whitley, 2001). More and more studies are being published that involve intensive monitoring of caves that contain rock art - analyzing everything from their climate, relative humidity, to their levels of CO_2, and also the microorganisms residing in the caves ("Documentation and Conservation of Rock Art," n.d.; V Jurado et al., 2010; Ontañón, 2014). Research on these microorganisms are mostly centered around the impact they can cause on the rock art or the supporting substrate, but new publications are finding interest if any of these show caves contain pathogenic microorganisms that could cause potential risks for visitors (Valme Jurado et al., 2010).

As the factors affecting rock art survival and rock art deterioration are well outlined in section 1.3, this project was created with the intent to focus on using only non-invasive methods to analyze and document the rock art at Escoural Cave. Therefore, this thesis will be using the traditional methods that are now commonplace in work involving rock art research including imaging techniques and microbiological analysis.

However, this thesis will also be venturing out to determine if two techniques, which have yet to be published in works related to rock art analysis, hyperspectral imaging and Vis-NIR FORS, would in fact be useful for non-invasive analysis of rock art. Relatively few published works can be found where multispectral imaging has been used on rock art, but none in so far regarding a portable hyperspectral camera (Liang, 2011; Robinson & Ware, 2002). That being said, there has also been only three published articles in which a FORS in the NIR range has been used to analyze historical works of art, including illuminated manuscripts and renaissance paintings, but not to my knowledge has the instrument been used on rock art (Cavaleri, Giovagnoli, & Nervo, 2013; Cheilakou, Troullinos, & Koui, 2014; Pronti, Ferrarai, Uccheddu, Pelagottii, & Piva, 2015).

Although other authors have noted the limitations of these instruments (Yivlialin, Galli, Raimondo, Martini, & Sassella, 2019), especially regarding the Vis-NIR FORS - from extremely difficult to read NIR regions, the necessity to create as accurate as possible reproductions for a database, the ability of the NIR to penetrate directly through to the support, or the bands to become altered from chemical alterations due to interaction with each material- it is still of interest to see how these instruments fare when used on rock art. Possible difficulties that could arise with the use of the Vis-NIR FORS and the hyperspectral camera during rock art analysis include difficulties due to the uneven limestone substrate, the extreme calcite coverage found throughout the cave and on top of the paintings, and limited visibility of the paintings. Nevertheless, it is necessary to test these non-invasive in-situ methods in order to prove their effectiveness in working with rock art or to evaluate and expand upon their limitations regarding certain parameters that affect rock art.

II. MATERIALS AND METHODS

2.1 IMAGING ANALYSIS

The Iberian rock art site analyzed for this thesis was Escoural Cave in the Alentejo region of Portugal. Permission to carry out non-invasive analyses at Escoural Cave was given by the Alentejo Regional Directorate of Culture. The majority of the analyses for this thesis were done in-situ during organized field campaigns at the rock art site. Microbial analysis was carried out at the Laboratorio Biotecnologia at the Universidade de Évora and the Laboratorio HERCULES in Évora, Portugal.

Escoural Cave contains nearly 100 documented engravings and paintings, however, due to the limited time available for this research, only the most visible and easily accessible engravings and paintings were analyzed. In total, 8 painted panels (#1-8), with singular or multiple figures, and 4 engraved panels (#1E-4E) were analyzed using imaging techniques and multi-analytical approaches. *Figures 4-6* show a map of Escoural Cave with the location of each panel and a scaled photograph of each rock art panel that was analyzed for this thesis (all scales are in 5 cm increments unless otherwise specified). The in-situ analyses were carried out during multiple return trips to Escoural Cave taking place on 22 May, 31 May, 21 June, and 8 July 2019. Below, *table 1* shows which methods and techniques were used on each panel at Escoural Cave.
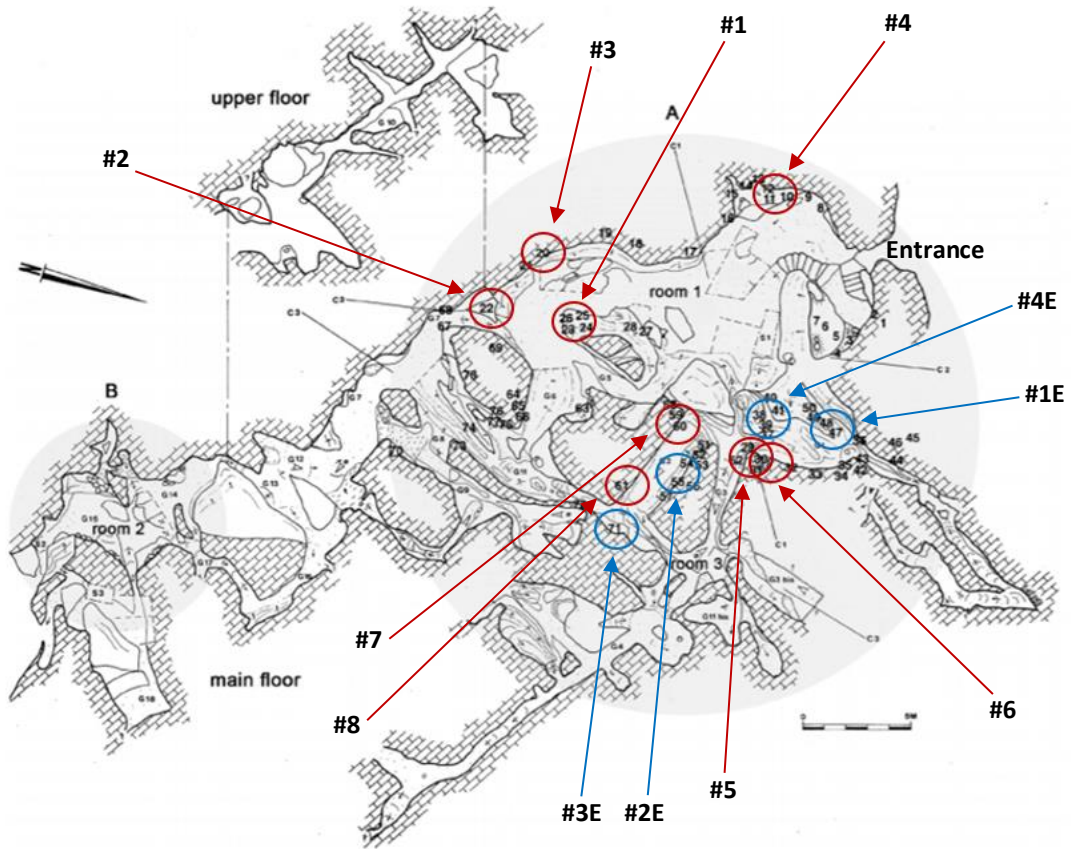
Figure 4: Map of Escoural Cave marking locations of each painting and engraving analyzed for this thesis. Red circles indicate paintings, blue circles indicate engravings (Adapted from Araújo C.A., Lejeune M., Gruta do Escoural: Necrópole Neolítica e Arte Rupest Paleolítica, 1995).

As displayed in the map above, new labels were given to the already existing numbered rock art at Escoural Cave. Shown below, in *figure 5-6*, are the original number(s) in brackets along with the new labels given for ease of the analysis of this thesis.

Figure 5: Paintings #1-4 analyzed at Escoural Cave.

Figure 6: Paintings #5-8 and engravings #1E-4E analyzed at Escoural Cave.

	Visible Light Photography	Raking Light Photography	IR photography (band-pass filters)	UVF photography	Photogrammetry	DStretch software	Hyperspectral Imaging	Vis-NIR FORS	EDXRF
Escoural Cave paintings									
#1	■		■	■	■	■	■	■	■
#2	■		■	■	■	■	■	■	■
#3	■		■	■	■	■	■		
#4	■		■	■	■	■			
#5	■		■	■	■	■	■		
#6	■		■	■	■	■	■		
#7	■		■	■	■	■	■		
#8	■		■	■	■	■	■		
Escoural Cave engravings									
#1E		■			■				
#2E		■			■				
#3E		■			■				
#4E		■			■				

Table 1: Imaging and multi-analytical techniques used on paintings and engravings at Escoural Cave.

2.1.1 VISIBLE AND RAKING LIGHT PHOTOGRAPHY

All rock art paintings were photographed using visible light photography, while all rock art engravings were photographed with raking light photography. Visible and raking light photography were implemented to document the paintings' visible features and surface irregularities, such as enhancing the cut marks in the engraved rock art. Visible light and raking light photography operate within the visible spectrum with wavelengths of 400-700 nm (see *figure 7*). Raking light photography requires light sources to illuminate the object – in this case the engravings – at an obtuse angle while the camera is placed perpendicular. The angle of light allows for surface irregularities to be exposed and enhanced.

A Nikon D3100 DSLR camera with AF-S DX NIKKOR 18-55MM F / 3.5-5.6G VR lens in manual mode was used on a tripod to capture the rock art photographs in visible and raking light. 1-

3 halogen lamps were placed accordingly in the cave in order to sufficiently illuminate the rock wall or to enhance the cut marks of the engraved rock art. All photos were taken with a scale marked off at 5cm increments. Angles of lighting and camera stations were dependent upon the accessibility of each engraving and painting.
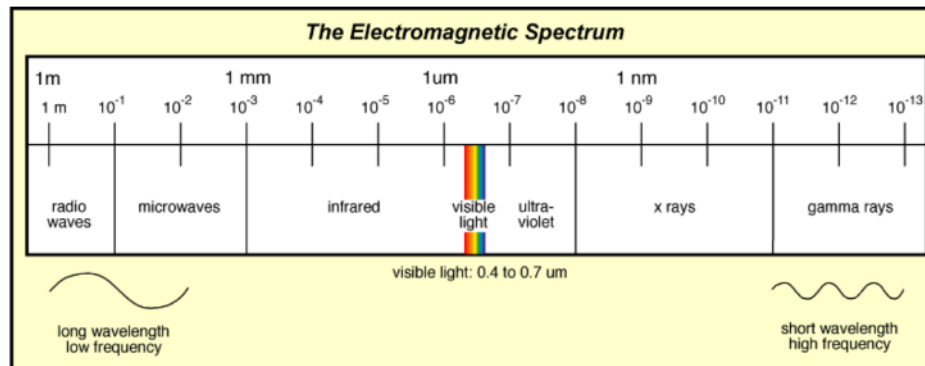

Figure 7: Diagram of the electromagnetic spectrum. (Adapted from Columbia University).

2.1.2 INFRARED PHOTOGRAPHY WITH BAND-PASS FILTERS

Infrared analysis of the rock art paintings in the 780-1300 nm range was collected using infrared photography with band-pass filters. All consumer-grade DSLR cameras are equipped to capture wavelengths from the UV to visible to NIR regions, however, factory set cameras are built with an IR blocking filter so to only produce visible light photographs (Williams & Shee, 2015). Through an affordable modification the IR cut filter can be removed and therefore transforming the camera for IR use with the appropriate band-pass filters attached and the use of halogen or incandescent light source (Williams & Shee, 2015). IR photography is useful in cultural heritage conservation for seeing the underdrawings of paintings made of charcoal or carbon-based inks; IR wavelengths are also able to pass under calcium carbonate crusts found in caves, allowing for the possibility of hidden charcoal paintings to be revealed in rock art sites.

A transformed, infrared sensitive Nikon D3100 was partnered with three band-pass filters; X-Nite780-850, X-Nite850-950nm, and X-Nite1000-13000 nm (LDP LLC MaxMax) for this thesis. Photographs were taken using 1-3 halogen lamps to properly illuminate the rock art surface. A tripod was used for camera stabilization. Distance of halogen lamps and infrared camera depend on the accessibility of paintings within the cave. Photoshop software was used to process all IR photos. Photoshop channel mixer was used to modify the IR photos in grayscale.

2.1.3 UVF PHOTOGRAPHY

Ultra-violet fluorescence photography was used throughout Escoural Cave to help document the degradation factors affecting the rock art. UVF is used as a surface identification method; through emitting wavelengths in the 350-360 nm range UVF can create a visible fluorescence in some minerals like calcite (Stuart, 2007).
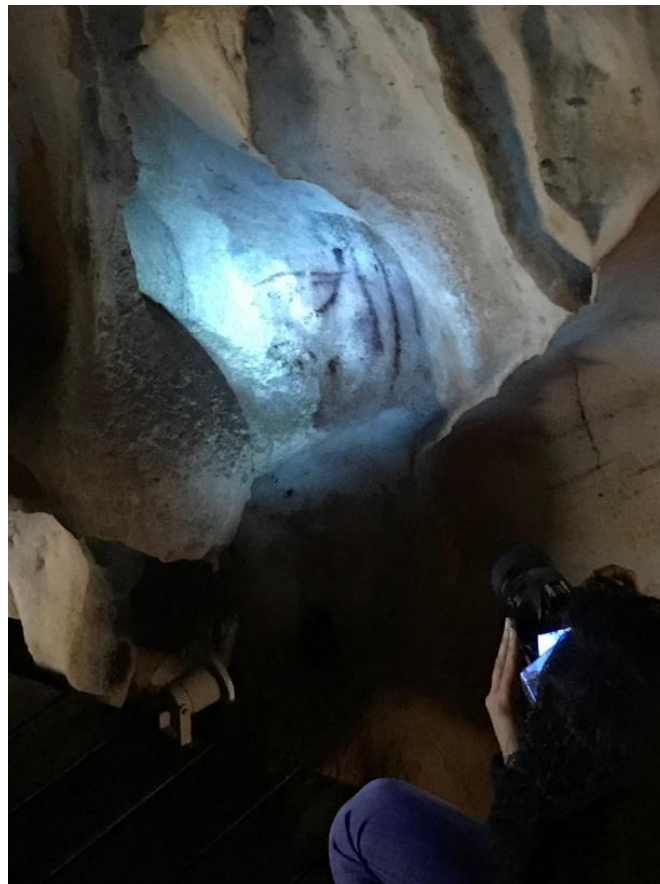
UVF photography of painting #5, Escoural Cave.

UVF can be achieved with a normal consumer-grade camera. This thesis was equipped with the same Nikon D3100 camera which was used for the visible and raking light photography. UVF photography requires completely dark surroundings to allow the camera to record as much UV fluorescence light as possible. For Escoural Cave, efforts were made to cover and turn off as many of the cave's artificially installed lighting as possible. The camera was placed on a tripod at varying distances depending again upon the accessibility of each painting and set to manual mode with shutter a speed of 5-10 seconds to capture maximum fluorescence. A Labino MPXL UV light was used in a sweeping motion on the rock surface as the camera captured the photograph. Protective glasses were worn during the photography.

2.1.4 PHOTOGRAMMETRY

3D photogrammetry is another technique which requires only a consumer-grade DSLR camera, proper lighting, and the appropriate computing software. 3D models of rock art not only encapsulate the current state of preservation of each painting or engraving, but also documents the rock art support allowing for conservators and documenters to see the stability and at-risk elements nearby to the rock art.

3D models of all rock art paintings and engravings were conducted using structure from motion (SFM) photogrammetry. Photographs were taken without tripod; however, due to minimal lighting in Escoural Cave, 1-3 halogen lamps were used for each painting and engraving for extra lighting. A minimum of 20 to a maximum of 100 photographs in sweeping arches from left to right were taken for each rock art panel, making sure each photo contained 30% overlap of the last photo taken. Again, closeness and angel of lighting of each rock art panel depended upon accessibility of each panel. Agisoft PhotoScan Professional software was used to align the photographs taken of each panel, create a dense cloud of matching points, tie points together with a mesh of triangles, and overlap with a texture to match that of the rock art surface.

2.1.5 DSTRETCH

Decorrelation stretch, DStretch, is a plugin for ImageJ software; using the Karhunen-Loève theorem (I Domingo, Carrión, Blanco, & Lerma, 2015), this software was created by Jon Harman in 2005 specifically for rock art. The plugin takes photographs and visually enhances them through the modification of hue and value and through manipulation of false colors (I Domingo et al., 2015; Harman, 2006; Quellec, Duquesnoy, & Defrasne, 2015). The software user is able to remove and correlate between spectral bands in order to optimized and highlight the differences in the photo, therefore enhancing deteriorated and faded pigments for better visualization (I Domingo et al., 2015).

Regular visible light photographs of each rock art painting were modified with the DStretch plugin. Relative to each painting's original attributes (e.g. pigment color) different scales and colorspace options were used to achieve maximum enhancement for each painting.

2.1.6 HYPERSPECTRAL IMAGING

Hyperspectral imaging is a non-invasive technique that allows for the acquisition of a full spectrum for each individually recorded pixel (Balas, Epitropou, Tsapras, & Hadjinicolaou, 2018; Bonifazi, Capobianco, Pelosi, & Serranti, 2019; Zucco, Pisani, & Cavaleri, 2017). This diagnostic tool was originally used for remote sensing conducted in military and remote space settings (Harman, 2006). Hyperspectral imaging can obtain high spatial and spectral resolution for each image captured (Balas et al., 2018). The Specim IQ portable hyperspectral camera was used for in-situ imaging at Escoural Cave. The Specim IQ hyperspectral camera records light intensity as a function of wavelength from the visible to NIR range of 400-1000 nm and as a function of location.

Hyperspectral camera being set up at Escoural Cave; painting #2. Lighting and white reference are being adjusted for optimal conditions.

The hyperspectral camera was placed as close as possible to each painting in order to fill the viewfinder with the image; however, due to lengthy integration time of a few seconds to a few minutes, a tripod is necessary for image acquisition, therefore limiting which paintings could be analyzed with this technique and how close the camera could be safely positioned. 2-3 halogen lamps were used to artificially illuminate the paintings inside Escoural Cave in order to achieve the maximum reflectance of light. The camera was used in default recording method (DRM) with simultaneous or custom white reference collection; after adjusting for focus and approving integration time, the spectral data is recorded, followed by the manual calibration of white reference and lighting approval, the image is captured and the spectral wavelengths are available. Following the acquisition of the hyperspectral images, the data is

imported to Specim IQ studio where a model and application are created for the detection of similar wavelengths throughout each photograph.

2.2 MULTI-ANALYTICAL APPROACHES

2.2.1 Vis-NIR FORS

Fiber optics reflectance spectra in the visible to near infra-red regions allows for rapid acquisition of data in a portable in-situ instrument (Cheilakou et al., 2014; Rosi, Daveri, Miliani, Verri, & Benedetti, 2009). The flexible optical fibers are used to convey electromagnetic radiation from the instrument to the target and vice versa, without sampling (Stuart, 2007). There are many applications of diffuse reflectance, the Vis-NIR FORS can effectively be used for colorimetric analysis, such as monitoring changes in color due to degradation; identification of chromophores and pigments; and identification of selected molecular groups such as organic binders (Cheilakou et al., 2014; Fischer & Kakoulli, 2013; Leona & Winter, 2019; Stuart, 2007). Depending upon the reflectance properties of a material the reflectance spectrum will show the ratio between the intensity of the incident light and that of the reflected light for each wavelength (Stuart, 2007).

The BWTEK i-Spec 25, a broadband portable spectrometer in combination with a handheld reflectance probe of trifurcated fiber optic bundle series integrated with a 5W tungsten halogen source with a focal aperture of 5mm and extended InGaAs array sensor, was used for analysis at Escoural Cave. The spectrometer measures across the UV-Vis-NIR range from 400-2500 nm, and the analysis is compiled through the supporting iSpec4 program.

After initial setup of the i-Spec 25 FORS with a portable field laptop, the 3 detectors (Detector 1: BRC711U-512 [345.6nm-1061.3nm]; Detector 2: BTC261P-512-OEM61 [883.0nm-1718.0nm]; Detector 3: BTC263E-256-OEM61 [1482.4nm-2654.9nm]) were set to the previously optimized settings of Detector 1: integration time 95ms, average 25, smoothing none; Detector 2: integration time 240µs, average 50, smoothing of Boxcar +1, detector mode of high sensitivity; Detector 3: integration time 332µs, average 100, smoothing of Boxcar +1, detector mode of high sensitivity. Detectors were calibrated based on standards made using traditional Palaeolithic pigments and binders; see *appendix 4*. The dark reference was collected as was the white reference with a barium sulfate disk. Next, the handheld probe was placed on the rock art pigment ensuring that the aperture was as flat as possible against

the rock art in order to reduce the interference of ambient light. The sample point was illuminated with a broad band radiation source, and the backscattered diffuse light was then collected by the detectors. For each pigment analyzed, 3-5 points were collected for reliable and representative results of each painting's pigment (see *appendix 5* for point analysis locations). All points were chosen based on the amount of visible pigment available and surface evenness. Calcite points were also taken for controls.

Following the collection of all data, the results were configured to TXT format and transferred to MATLAB for Principal Component Analysis for the creation of non-calibrated and calibrated models[1]. Spectral pre-0 was used to remove baseline drifts and unwanted light-scattering effects using MATLAB (version R2016a) and PLS toolbox (version 8.2.1) from Eigenvector Research Inc. The 62 FORS spectra of the Escoural cave paintings and lab standards were pre-processed with standard normal variate (SNV) scaling of samples (weighted normalization) followed by mean center for removing mean offset from each variable. PCA was applied to the Vis and NIR regions based on the three detector cut-offs of [400-1018 nm], [1031-1633 nm], [1655-2485 nm]. Spectra of the rock art painting samples were projected on a PCA model calibrated against spectra of pure binders subtracted from their background support of glass (parchment glue, Arabic gum, lime water, saliva, bone marrow, chicken blood, human blood, and urine).

2.2.2 EDXRF

The portable Energy dispersive x-ray fluorescence (EDXRF) instrument was used to compliment FORS analysis at the site of Escoural Cave. EDXRF is another in-situ instrument that allows for the non-invasive point analysis of rock art (Bonizzoni, Caglio, Galli, & Poldi, 2008; Liang, 2011). EDXRF is capable of elemental identification in elements with atomic numbers higher than sodium (Liang, 2011; Stuart, 2007). EDXRF obtains elemental information through x-ray fluorescence whereby electrons are displaced from their atomic orbital positions, and thereby releasing characteristic energy of a specific element allowing for the identification of said element (Stuart, 2007). As reflectance spectroscopy, EDXRF is able to detect main and trace elements used in rock art pigments (Liang, 2011). EDXRF is a

---

[1] PCA analysis was performed by Catarina Miguel PhD. of HERCULES Laboratory.

technique well suited for the preservation of rock art through the qualitative chemical analysis it can provide (Alberti, Fiorini, Guazzoni, Klatka, & Longoni, 2007; Gay et al., 2016).

A handheld Bruker Tracer III with silicon drift detector and rhodium x-ray source was used for the X-ray fluorescence analysis at Escoural Cave. Following instrument calibration of standards, the XRF Actual High Voltage and Actual Anode Current were set to kV 40.00/ µV 30.00 and 30 seconds for data acquisition at each point analysis. Point analysis locations were the same as those taken for the FORS in order to confirm results (see *appendix 4*).

2.3 MICROBIAL ANALYSIS

Microbial analyses were also conducted in Escoural Cave. A total of 8 locations throughout the cave were sampled for biofilms and microbial growth using sterile cotton swabs for culture-dependent and culture-independent methods of DNA sequencing for genera and species identification. Samples A; A1, B, C1, C2, D, and M were collected on 29 March on the first visit to Escoural Cave; while samples Y and G were collected during a return visit on 22 May 2019. No samples were taken directly from any paintings or engravings; however, samples A; A1 were taken nearby to painting #5. *Figure 8* shows the sample locations taken at Escoural cave, and *figure 9* shows each sample during the sampling process.

Microbial analysis was carried out in order to determine what biofilms were residing within Escoural Cave. As previously mentioned, hypogeal environments constitute extremely unique environmental niches, those that favor the development of many different microbes from bacteria, fungi, algae, and cyanobacteria (Mitova, Iliev, & Groudeva, 2015). As single microorganisms can form biofilms or colonies that then cause serious negative effects for rock art in hypogeal environments, it is necessary to analyze the type and number of microorganisms in order to create an effect preservation strategy to target these specific groups (Rosado et al., 2017; Stomeo et al., 2007; Stomeo, Portillo, Gonzalez, & Laiz, 2008).

Microorganism analysis at Escoural Cave was conducted with culture-dependent methods and culture-independent methods.
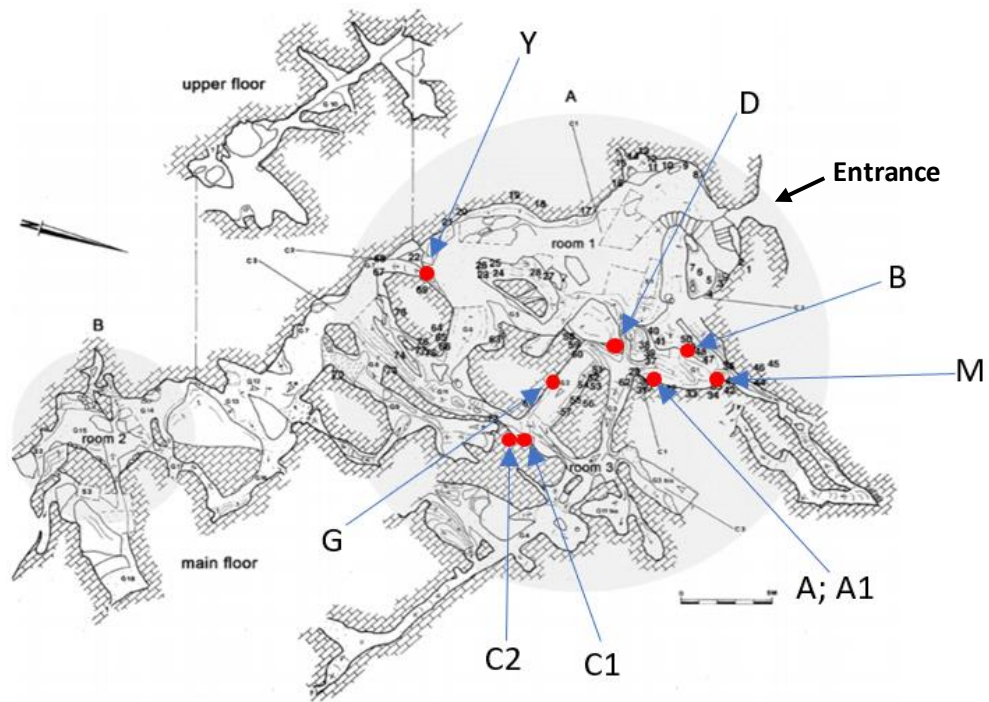
Figure 8: Map of Escoural Cave marking locations of microbial sampling and location of cave entrance. (Adapted from Araújo C.A., Lejeune M., Gruta do Escoural: Necrópole Neolítica e Arte Rupestre Paleolítica, 1995).
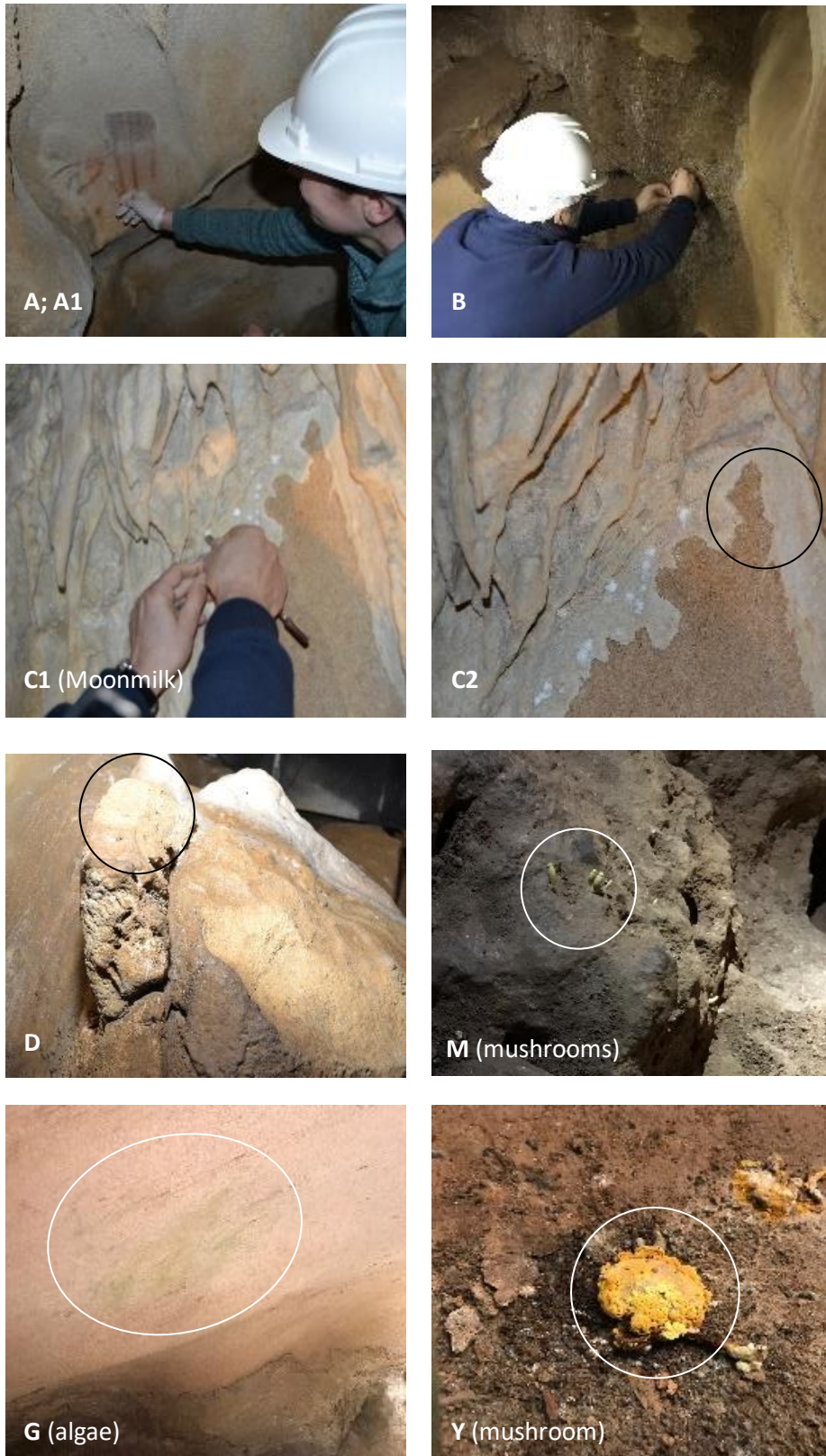
Figure 9: Sampling locations of microbial samples.

2.3.1 CULTURE-DEPENDENT METHODS

i) ISOLATION OF MICROORGANISMS

Following sample collection at Escoural Cave, samples A; A1, B, C1, C2, and D were immersed in 1 ml (sterile) solution of MRD (maximum recovery diluent) to promote the extraction of cells; samples were kept in IKA KS 4000 i Control agitation machine for 48 hours. Following agitation, samples A; A1, B, C1, C2, and D were inoculated. Each sample was divided into one pure sample and two samples 1/10 diluted with MRD. Pure and diluted samples were then inoculated on four different mediums; MEA (Malt Extract Agar), NA (Nutrient Agar), TSA (Trypticase Soy Agar), and CRB (Cook Rose Bengal). A total of 12 petri dishes for each sample were created. MEA and CRB dishes were placed in fungi incubator at 27 °C for 7 days; NA and TSA dishes were placed in bacteria incubator for 30 °C for 1-2 days.

After allotted incubation time, plates were analyzed for further isolation. After first inspection following incubation, all samples were again diluted with MRD to 1/100 in order to isolate more homogeneous results. Following full isolation of bacteria strains, samples were inoculated for the final time in ramps with NA medium and incubated at 30 °C for 48 hours for DNA extraction. A total of 43 bacteria stains were isolated from the 6 original samples for DNA extraction.

Sample M, a mushroom sample, was cut into 2mm pieces and placed inside four petri dishes with MEA medium and three petri dishes with CRB medium. M samples were incubated for 48 hours at 27 °C. After isolation of mushroom and fungi strains, samples were inoculated for final time in petri dishes with MEA medium and incubated for 5 days at 27 °C for DNA extraction. A total of 13 mushroom and fungi stains were isolated from the 7 original samples for DNA extraction.

All procedures described above were performed under aseptic conditions. Analysis of Y and G samples, collected at a later date, were conducted with culture-independent methods only.

ii) EXTRACTION OF BACTERIAL DNA

Bacterial colonies grown in new ramps with NA medium were used for DNA extraction. Cells were resuspended in 100 µl of buffer TE (Tris-10 mM, EDTA-1 mM, pH 8). Thereafter, 15 µl of 2 mg/ml lysozyme (in sterile H2O mil) was added to the cell suspension. The samples are gently vortexed and subsequently incubated at 37 °C for 40 min. 15 µl of 4 mg / ml α-

chymotrypsin was added in 10% SDS. The samples are shaken gently and incubated at 50 °C for 35 min. 100 µl of phenol/chloroform/isoamyl alcohol (25:24:1) was added to the aqueous phase. The samples were gently shaken manually and a spin was made. The supernatant was transferred to a new microtube, measuring the volume withdrawn. One volume of chloroform/iso-amyl alcohol (24:1) was added. The aqueous phase was transferred by measuring the volume withdrawn, and two volumes of absolute ethanol and 0.3 volumes of 3M sodium acetate were added. The samples were stored overnight at -20 °C. The following day, these were centrifuged at 11900 g for 25 min. The supernatant was discarded and the DNA was air dried (in the laminar flow chamber). Finally, the DNA pellets were resuspended with 100 µl sterile TE (Tris-10 mM, EDTA-1 mM, pH 8) and stored at -20 °C.

iii) EXTRACTION OF FUNGAL DNA

The previous fungi strains grown in MEA medium for five days at 27 °C were used for DNA extraction. For promotion of cell lysis, the cells were resuspended in 700 µl lysis buffer (Tris-HCl - 50 mM, NaCl - 250 mM, EDTA - 50 mM, SDS - 0.3%, pH = 8) in an Eppendorf tube of 2 ml, with the addition of 300 µl of microspheres in the suspension. Tubes were vortexed at full speed, in 30 second cycles on ice followed by 30 seconds in the vortex, for 3 minutes. The suspension was then incubated at 65 °C for 60 minutes. After incubation, suspension was vortexed again at full speed, in 30 second cycles on ice followed by 30 seconds in the vortex, for 3 minutes; then centrifuged at 14,000 rpm for 10 minutes at 4 °C. The maximum supernatant was collected into a new 2 ml Eppendorf tube in which 700 µl of TE (Tris-10 mM, EDTA-1 mM, pH = 8) buffer containing RNase (50 µg / ml) was added. Microtubes were then incubated again at 37 °C for 60 minutes in order to solubilize the nucleic acids. 500 µl of the chloroform/isoamyl alcohol solution (24:1) was then added to the mixture by mixing the phases by inversion.

After centrifugation at 4 °C at 10,000 rpm for 10 minutes, the supernatant was collected into another 2 ml Eppendorf tube and cold 3M sodium acetate buffer (pH = 5.2) was added, at the ratio of 1/10 volume obtained and mixed by inversion. Next, 2.5 volumes of cold absolute ethanol (-20 °C) were added, promoting the mixing of the phases by inversion. The mixture was centrifuged at 4 °C at 13,000 rpm for 15 minutes with subsequent decantation of the supernatant. The obtained pellet was washed with 1 ml of 70% (v/v) ethanol by slowly adding the ethanol to the Eppendorf wall, again centrifuging at 4 °C at 10,000 rpm for 10 minutes.

The supernatant maximum was removed and a spin was then performed to remove excess supernatant. The obtained pellet was air dried at room temperature for 30-60 minutes (in the laminar flow chamber). DNA was solubilized in 100 μl of TE buffer solution and stored at -4 °C.

iv) DNA QUANTIFICATION BY MOLECULAR ABSORPTION SPECTROMETRY

The extracted DNA was quantified by molecular absorption spectrometry on a Thermo Scientific μDrop Plate MultiScan Go spectrophotometer coupled to a SkanTY for MultiScan 3.2 software. 2 μl of each DNA sample and a TE buffer (blank) sample were applied with absorbance readings at 230, 260 and 280 nm. The concentration of DNA was calculated by the expression: [DNA] (μg/ml) = Abs260 nm x 50 μg/ml/cm x (10/0.51) cm.

At 50 μg/ml/cm the inverse of the molar absorptivity coefficient for double-stranded DNA and 10/0.51 cm is the inverse of the optical path characteristic of the equipment. The ratios given for the purity of the samples were also calculated:

$$\frac{\text{Abs}_{260}}{\text{Abs}_{280}} \quad e \quad \frac{\text{Abs}_{260}}{\text{Abs}_{230}}$$

v) DNA AMPLIFICATION OF BACTERIA AND FUNGI STANDS

Bacteria DNA samples were amplified by the polymerase chain reaction (PCR) method, using a set of primers (518F/785R) encoding of the 16s rDNA region (see *table 2*). Fungi DNA samples were also amplified by the same PCR technique, however using a different set of primers (ITS1/ITS4) encoding the 18s rDNA region (see *table 2*).

	Primer	Sequence 5'-3'
Bacterial Analysis	518F	CCA GCA GCC GCG GTA ATA CG
	785R	CTA CCA GGG TAT CTA ATC C
Fungal Analysis	ITS1(F)	TCC GTA GGT GAA CCT GCG G
	ITS4(R)	TCC TCC GCT TAT TGA TATGC

Table 2: Primers used for the amplification of bacterial and fungal DNA.

Reaction mixtures were prepared for DNA amplification with the composition shown in *table 3*.

Volume (µl)		
	Blank	Microtube sample
H$_2$O RNAse free	19.6	18.6
Buffer reaction 10x with MgCl$_2$ (25mM)	2.5	2.5
dNTPs (2mM)	2.5	2.5
Primer F	0.1	0.1
Primer R	0.1	0.1
Taq DNA Polymerase	0.2	0.2
Sample DNA	-	1.0
Vf=25 µl		

Table 3: Preparation of mixture for PCR.

A microtube was prepared by replacing the DNA with 1 µl of H2O and used as a negative control. The samples were then centrifuged and placed in the MJ Mini Bio-Rad thermocycler with the PCR amplification program according to the following procedures. For PCA analysis of Bacteria in the 16S rDNA the program was set to 3 minutes at 95 °C (initial denaturation), followed by 36 cycles of denaturation from 50 seconds at 94 °C, annealing from 50 seconds at 56 °C, and extension of 1 minute at 72 °C. The final 10-minute extension was made at 72 °C. For fungi, the region of interest was the ITS region with the PCR program set at 5 minutes at 94 °C (initial denaturation), followed by 40 cycles of denaturation of 1 minute at 94 °C, annealing for 1 minute at 50 °C, and extension of 2 minutes at 72 °C. The final extension of 6 minutes was made at 72 °C.

vi) DNA DETECTION

Analysis of the PCR amplification products was performed by 1.5% agarose gel electrophoresis, which confirms the amplification, integrity of the DNA as well as the presence of contaminants.

A 1.5% agarose gel in 0.5x TBE solution was prepared with the addition of 5 µl of GreenSafe Premium (MB13201, NZYTech), allowing polymerization for 15 minutes at room temperature. The gel was placed in the electrophoresis tub, containing 0.5x TBE buffer. Samples were applied to each well of the gel; 2 µl of Loading buffer 1x and 5 µl of the DNA marker NZYDNA Ladder VII (0.5 µg.µl-1, MB06101 NZYTech) was applied to the first well of the gel followed by 5 µl of sample with 2 µl of Loading buffer 6x (15081, NZYTech) applied to the remaining

wells. Electrophoretic separation was carried out by applying a potential difference of 75 V. Finally, the analysis of the bands was carried out in an Ultraviolet (Molecular Imager, Gel-XR + Imaging System, Bio-Rad) chamber with the use of the software Image Lab 5.0.

vii) QUANTIFICATION OF DNA AMPLIFICATION FROM PCR

PCR products were quantified by spectrofluorimetry using the Quantus Fluorometer (E6150, Promega). The DNA quantification kit, QuantiFluor One dsDNA (E487, Promega) was used.

Samples were prepared with 199 µl QuantiFluor One dsDNA and 1 µl of sample, incubated for 5 minutes at room temperature in the dark. The concentration of the samples was determined by calibration with blank of 199 µl QuantiFluor One dsDNA and 1 µl if TE, and a standard prepared with 199 µl QuantiFluor One dsDNA and 1 µl of Lambda DNA.

vii) SEQUENCING OF DNA SAMPLES

PCR products were sequenced through an external service by capillary electrophoresis with the ABI PRISM 3730 xl sequencer (Applied Biosystems) using the BDT v1.1 Kit (Applied Biosystems). The sequences obtained were then analyzed and aligned with GenBank deposited sequences (NCBI) for homology analysis via the BLAST search engine. Construction of dendrograms was done through the MEGA software (Version 7.0.25), through the Neighbor-Joining grouping method.

2.3.2 CULTURE-INDEPENDENT METHOD: NGS[2]

i) EXTRACTION OF DNA

The DNA from samples A; A1, B, C1, C2, D, M, Y, and G were extracted through the EZNA Stool DNA Kit (OMEGA bio-tek). 100 mg of each sample, 200 mg of Glass Beads X and SLX-Mlus Buffer were added to a microfuge tube. Mixture was vortexed for 10 minutes at full speed until completely homogeneous. DS Buffer and 20 µl of Proteinase K were then added, mixed, and incubated at 70 °C for 1 hour. Next, the SP2 buffer was added, vortexed, and stood at room temperature for 5 minutes, followed by centrifugation at 13500 rpm for 5 minutes. After centrifugation, the supernatant was transferred to a new microtube, the cHTR Reagent added, vortexed, and the mixture centrifuged again, and the supernatant was collected in a

---

[2] NGS was performed by Professor Ana Teresa Caldeira, Cátia Salvador PhD., and Sriradha Bhattacharya PhD. candidate.

new microtube. BL Buffer and 100% Ethanol are added to the microtube and centrifuged. Next, the HiBind DNA Mini Column is inserted with the previous solution into a new 2 ml Collection Tube; centrifuged for 1 minute at full speed, the filtrate and tube are discarded. The HiBind DNA Mini Column is transferred to a new Collection Tube with VHB Buffer. After centrifuging the tube, the filtrate is discarded and 700 µl of Washer Buffer DNA is added. The tube is centrifuged again and filtrate is discarded (repeat this step 2x). HiBind DNA Mini Column is centrifuged empty at room temperature for 2 minutes (to dry the column before elution), column is transferred to a microfuge tube and preheated elution buffer of 65 °C is added to the center of the HiBind matrix. Finally, the column is centrifuged at full speed for 1 minute and the DNA is stored at -20 °C.

ii) PCR AMPLIFICATION

Extracted DNA was amplified through Polymerase Chain Reaction. PCR reaction mixture consists of 2.5µl extracted DNA, a pair of Forward and Reverse primers (*table 4*) and a 2x KAPA HiFi HotStart ReadyMix buffer. Amplification was performed in the MJ Mini (Bio-Rad) thermal cycler under precise conditions; denaturation for 3 minutes at 95 °C, 25 cycles of 30 seconds (at 95 °C, 55 °C and 72 °C) and finally 5 minutes at 72 °C. The amplified DNA was stored at 4 °C.

	Primer	Sequence 5'-3'
Prokaryotic	Bakt_341F	CCT ACG GGN GGC WGC AG
	Bakt_805R	GAC TAC HVG GGT ATC TAA TCC
	Amplicon PCR Forward Primer (Illumina Protocol)	
	Amplicon PCR Reverse Primer (Illumina Protocol)	

Table 4: Primers used for the amplification of prokaryotic DNA.

iii) GEL ELECTROPHORESIS

Confirmation of PCR amplification was conducted with gel electrophoresis. 1% agarose gel electrophoresis with Green Safe DNA dye was performed. Samples were applied to the gel well and electrophoretic run was performed at 75 V. DNA marker at 100 bp. After electrophoresis completion, gel analysis was performed with Bio-RAD system.

iv) PURIFICATION OF PCR AMPLIFICATION

Following amplification analysis, the PCR amplification was purified by the total Mag-Bind Pure NGS Protocol. Magnetic beads were placed at room temperature for 5 minutes, then

vortexed. 27.6 μl of magnetic beads were placed in each sample Eppendorf and were then shaken and re-incubated for 5 minutes at room temperature. Following the incubation time, tubes were placed in the Magnetic Separation Device; the supernatant was cleared and removed. The same process was completed for the two required washes with 80% Ethanol (freshly prepared with H2O RNase free). Tubes were then kept on the Magnetic Device holder for approximately 15 minutes; residual liquid was then discarded after the tubes were removed from the carrier. 35 μl of 10mM Tris pH 8.5 was added to tubes and stirred and incubated at room temperature for 5 minutes. Tubes were places upon the Magnetic Device again until the supernatant became clear. 25 μl of supernatant was transferred to new tubes and stored at 2-8 °C (for short-term storage) or at 4 °C (for long-term storage).

v) QUANTIFICATION OF PCR AMPLIFICATION

The purified PCR amplification was quantified by fluorescence through QuantiFluor® ONE DNA (Promega) in the Quantus Fluorometer quantification equipment (Promega).

vi) INDEX PCR AND PRODUCT ANALYSIS

Following quantification, the Index PCR was done in order to label each of the samples in the study.

Reaction mixture used for PCR contained 5 μl of each purified sample, one pair of primers - Nextera XT Index Primer 1 (N7xx) and Nextera XT Index Primer 2 (S5xx) and the 2x KAPA HiFi HotStart ReadyMix enzyme. Amplification was performed through the following conditions: 3 minutes at 95 °C, 8 cycles of 30 seconds (at 95 °C, 55 °C and 72 °C), and finally 5 minutes at 72 °C. Products stored at 4 °C.

Index PCR products were analyzed by 1% agarose gel electrophoresis (according to 2.4.1 c) Followed by the purification procedure of Index PCR products (as described in 2.4.1 d, with 56 μl of magnetic beads) and the quantification of Index PCR products with the Quantus Fluorometer quantification equipment, as described in 2.4.1 e.

vii) BUILDING OF LIBRARY (POOL) AND DENATURATION

Prepared libraries were normalized to 4 nM, followed by the preparation of Pool of libraries (4 nM). Simultaneously, 4 nm Phix was prepared; functioning as an internal control. Pool and Phix were denatured with 0.2 N NaOH and incubated for 5 minutes at room temperature. Denatured Pool and Phix were diluted with HT1 (10 pM), pooled (Pool library + 5% Phix) and

incubated for 2 minutes at 96 °C to terminate the denaturation process. Mixture was then kept on ice for 5 minutes.

viii) ANALYSIS OF LIBRARIES BY NGS

Previously prepared libraries were analyzed by NGS using MiSeq, Illumina equipment with the Nano Kit V2. Following the finished sequencing, data analysis was conducted through the MiSeq Reporter Software (classification based on the Greengenes database).

III. RESULTS AND DISCUSSION

This chapter aims to present the results from the various imaging techniques, multi-analytical approaches, and microbial analysis methods conducted at Escoural Cave, and to discuss the interpretations of the findings. The results and discussion shown are laid out in order according to the aims presented in the introduction of this thesis, section 1.4.1.

3.1 CURRENT STATE OF PRESERVATION

This section describes the results of the first aim of this thesis - to document the current state of preservation of the rock art found inside Escoural Cave. To properly study the rock art at Escoural Cave, it was necessary to document the current state of preservation as of spring/summer 2019, in order for future research to determine if any substantial new deterioration or damage has occurred since the time of this thesis. Almost all methods contributed to this goal. Visually, the imaging techniques were able to provide a digital database for the rock art's current state. The methods pertaining to microorganism analysis were useful for understanding which biotas were thriving inside the cave at the time of this thesis and if they were responsible for contributing to further degradation of the rock art.

Photogrammetry was useful for viewing not only the rock art itself, but also the surrounding context of the rock art support in the natural three-dimensional form. *Figures 10-11* are two examples of the photogrammetric models created of the rock art in Escoural Cave. Image (A) is of engraving #1E, and image (B) is of painting #1; size, orientation, and location are also displayed.[3] *Figure 10* shows an example of an engraved panel that has remained relatively undisturbed from heavy degradational processes, in this case an engraving of horse heads. The location of this engraving is relatively well protected and has yet to be severely impacted by calcite coverage as compared to other paintings and engravings inside the cave. In *figure 11*, it is possible to see large calcite vein formations covering the upper region of the rock art panel and continuing down. Water stains are also visible where the limestone appears to have been heavily saturated with percolating water.

---

[3] The remaining complete photogrammetric models can be viewed in virtual format at the sharing platform, Sketchfab. Follow the link provided to view complete models in a virtual setting: https://sketchfab.com/shruban/models.
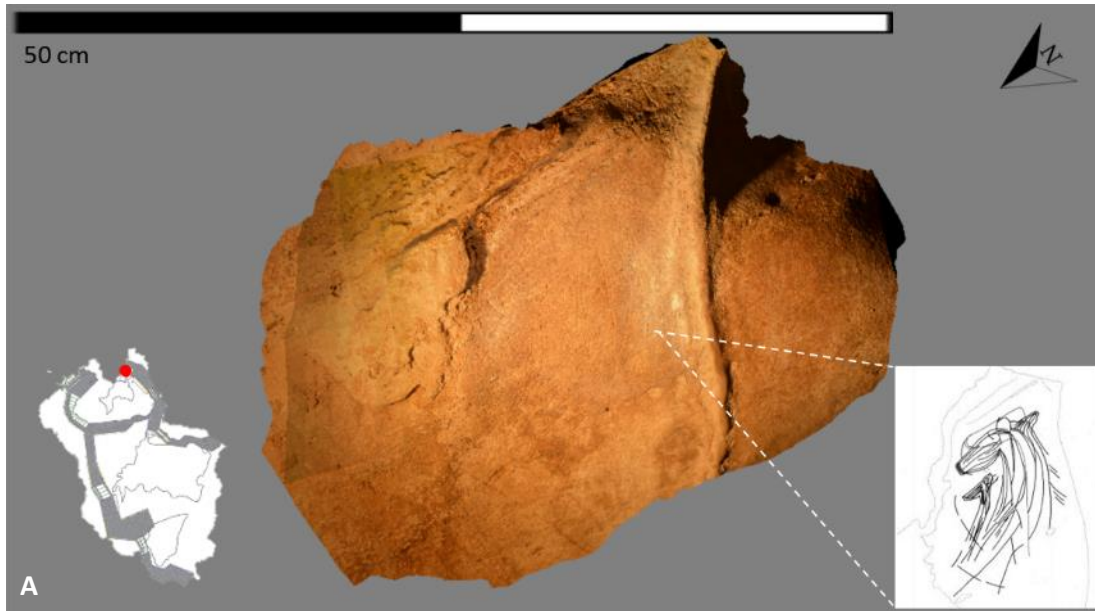
Figure 10: Screenshot of 3D model of engraving #1E at Escoural Cave. Size, orientation, location and sketch are also displayed.

Figure 11: Screenshot of 3D model of painting #1 at Escoural Cave. Size, orientation, and location are also displayed.

UVF photography also contributed to documenting the current state of preservation of the paintings in Escoural Cave. Below, in *figure 12,* the extensive leaching stains and drip lines can be seen in full extent due to the fluorescence of calcite along with the corresponding visible light photograph showing what painting #4 currently looks like. As described by archaeologists, painting #4 depicts an Equidae figure (Araújo & Gomes, n.d.).
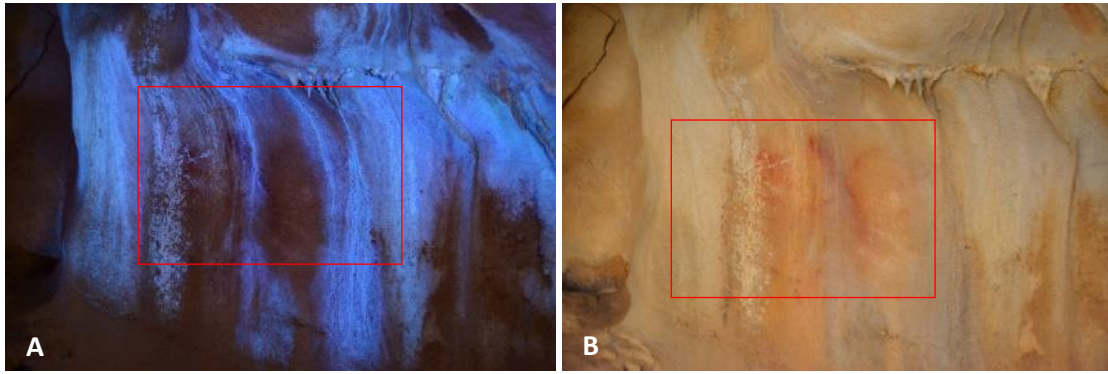
Figure 12: UVF and visible light photographs of Escoural Cave painting #4.

Lastly, all visible light and raking light photographs taken at Escoural Cave, as those shown in *figure 13*, helped to record the state of preservation the paintings and engravings at Escoural Cave are currently maintaining. Limited visibility of painting #3 can be seen in image (A), while image (B) shows engraving #2E with a calcite formation deposited in the middle of the rock art. Not all photographs that contributed to documenting Escoural Cave's current state of preservation are included in this results section, however, all the relevant photographs have been compiled and given to the Escoural Cave Interpretation Center in the village of Santiago do Escoural to be stored with their records for future reference.
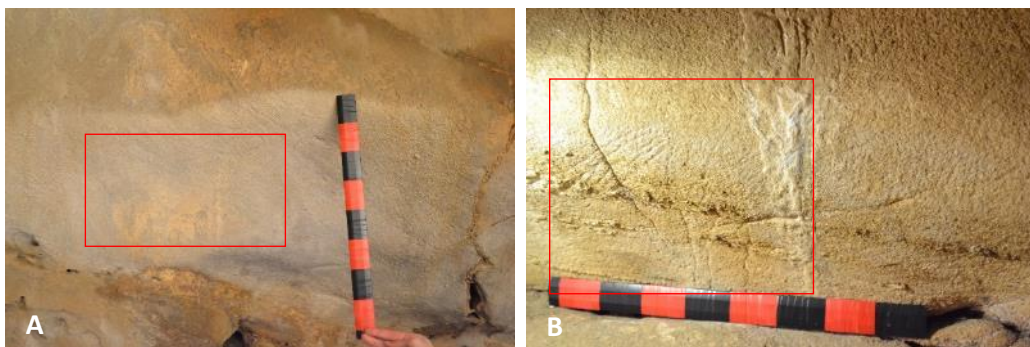
Figure 13: In painting #3 (A), the lower body and legs of a bovine or horse can slightly be seen. In engraving #2E (B), the tail and hind legs of a horse can be seen.

The importance of conservation work involving cultural heritage cannot be trivialized; even though Escoural Cave has previously been subject to many analysis campaigns before, it is necessary with all cultural heritage objects especially those most at risk, to make a record of how these objects are changing throughout time in order to determine their degradation processes and learn how to best protect them from further deterioration. As reviewed in section 1.3, rock art is particularly prone to degradation usually out of the control of those who monitor and protect it. Natural mechanical and chemical weathering processes and

external anthropogenic impacts are often beyond the scope of control when it comes to protecting most rock art; therefore, the record keeping of theses site can be instrumental in the fight for their preservation.

3.2 THROUGH THE USE OF VARIOUS TECHNIQUES WERE ANY PREVIOUSLY UNKNOWN ROCK ART PAINTINGS UNCOVERED OR MADE MORE VISIBLE?

All imaging techniques were employed to answer this research question; although, no new panels or paintings were uncovered, a number of existing panels did benefit from the various techniques used, as new hidden details began to emerge in the paintings. Shown below in *figures 14-17*, are two of the more difficult panels to interpret in Escoural Cave. Reasons for uncertainty in their interpretation are due to the state of their condition and the degradation they have undergone for thousands of years.

PAINTING #2
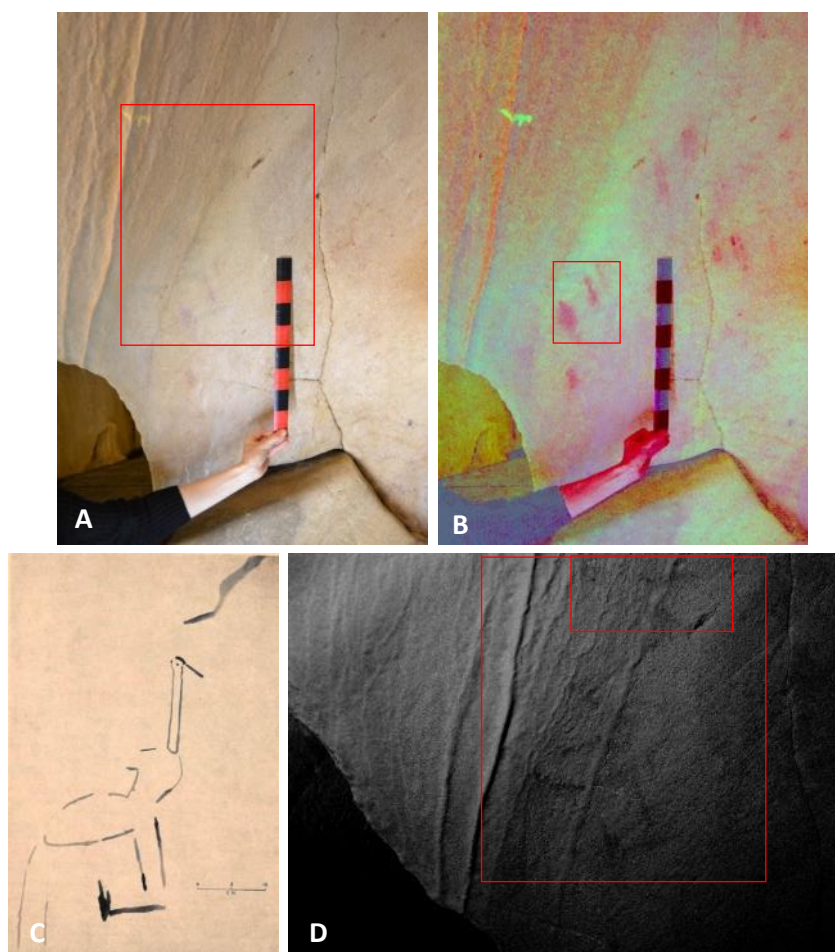
Figure 14: Letters A-F represent the complete panel of painting #2. (A) Visible light photography; (B) Visible photo with DStretch software colorspace LRE applied at 20% scale; (C) Original sketch of panel by Manuel Farinha dos Santos in 1963 (Adapted from Araújo C.A., Lejeune M., Gruta do Escoural: Necrópole Neolítica e Arte Rupestre Paleolítica, 1995); (D) IR photography with 780nm filter.
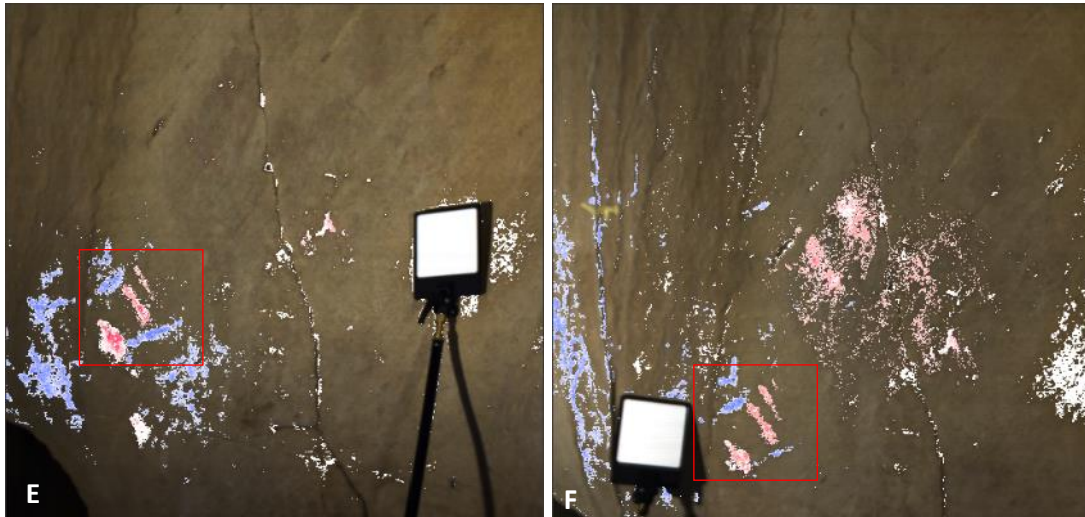
Figure 15: Continued panel of painting #2. (E-F) Hyperspectral images from Specim IQ studio (Painting #2).

Displayed above in *figure 14-15* are the various imaging techniques employed on painting #2 in Escoural Cave. In photograph (A), the visible light photo shows how degraded the rock art currently is with the majority of the painting barely visible; (B) the corresponding DStretch altered photo reveals many pairs of red parallel lines across the panel. (C) is a depiction by the original archaeologist, Manuel Farinha dos Santos, of a bird like figure he believed the panel represented. (D) using IR photography, we can see that Santos' depiction of a bird is slightly similar, however still controversial as the IR image reveals more details. (E-F) are final outputs from the Specim IQ studio - the results were formulated by picking individual pixels with the same wavelengths, identifying them with a color marker, and selecting a range of sensitivity. Red pigment wavelengths are shown in red, while black pigment wavelengths are shown in blue. The darker the pixel the more similar the wavelength is to the original pixel selected.

PAINTING #3
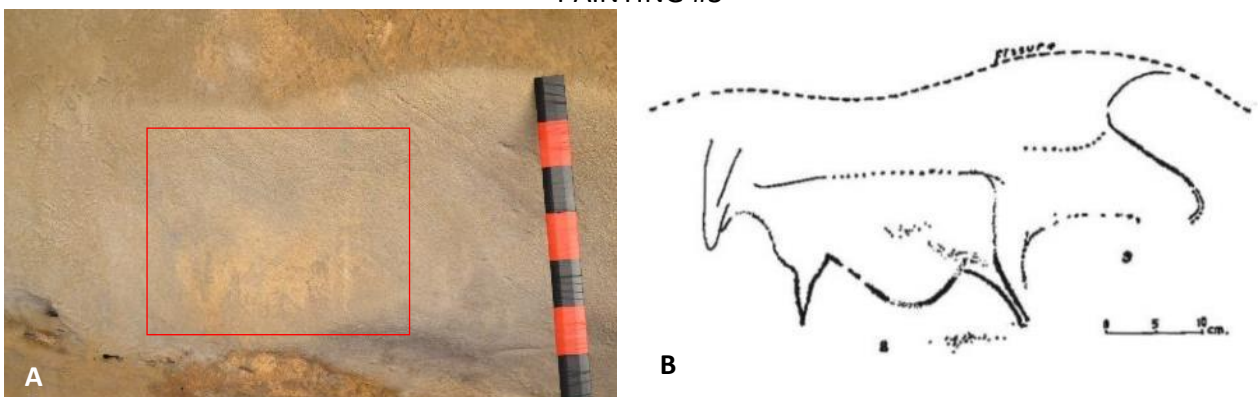
Figure 16: Letters A-D represent the complete panel of painting #3. (A) Visible light photography; (B) Original sketch of panel by André Glory in 1965 (Adapted from Araújo C.A., Lejeune M., Gruta do Escoural: Necrópole Neolítica e Arte Rupestre Paleolítica, 1995).

44
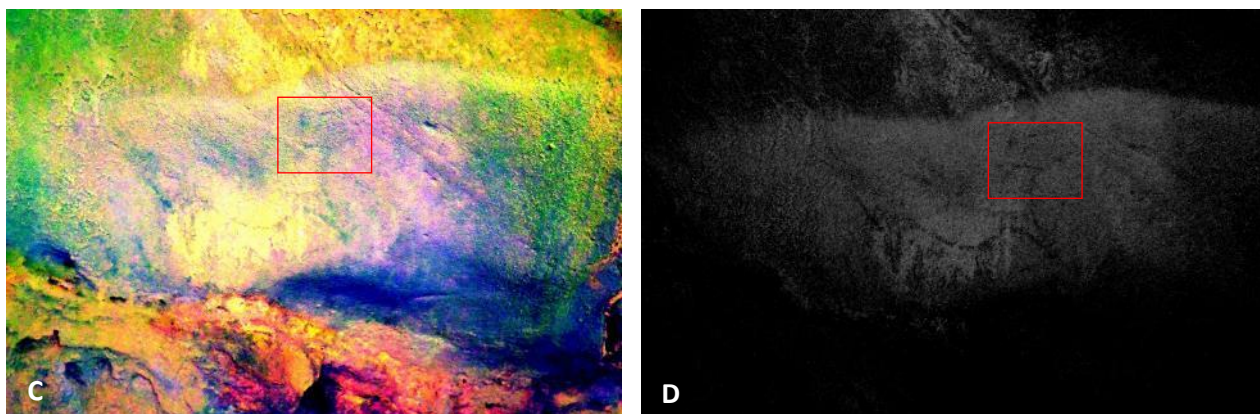
Figure 17: Continued panel of painting #3. (C) DStretch software applied with colorspace YBK at 30% scale; (D) IR photography with 780 nm filter (Painting #3).

Above in *figures 16-17* we can see the various imaging techniques employed on painting #3 in Escoural Cave. Although photograph (A) is taken in visible light, it is extremely difficult to make out the figure in the panel. (B) is the original sketch by rock art specialist, André Glory, depicting an animal in the Bovidae family, similar looking to a modern-day goat perhaps. Lastly, (C-D), although one photograph is altered with DStretch and the other taken with IR photography, both reveal similar results. (C-D) seem to depict a head on the right side of the body and possibly to include horns, which directly contradict the original sketch from Glory. The hyperspectral camera was not used due to the distance of the painting from a stable location which was needed to acquire the image.

All of the imaging techniques used for this thesis were relatively affordable and easy to learn. 3D photogrammetry is an affordable technique which requires only a consumer grade camera, proper lighting, and a processing software. 3D photogrammetry is valuable for the 3D images they acquire instead of limiting the recording to a 2D image, allowing for a complete and detailed documentation of the position of the rock art on the substrate. IR photography, another affordable technique, can be extremely useful in penetrating calcite crusts and exposing superimposed carbon-based pigments such as charcoal. DStretch plug-in is another affordable, fast, and user-friendly technique. DStretch results can improve user objectivity of rock art interpretations and can allow for higher rates of precision as the alteration choices are fixed settings (Quellec et al., 2015).

However, with all these techniques, the accompanying limitations are also necessary to acknowledge. Imaging results were highly dependent upon the conditions inside Escoural

Cave. The location of each painting and their relative distance from the stable walking platform limited which techniques could be used on which paintings; while lighting conditions also had to be taken into account, not only for visibility of certain techniques (e.g. IR photography), but also for their continued use, which is known to increase the presence of various phototrophic microorganisms that thrive in the presence of direct light (Mulec & Kosi, 2009; Saiz-Jimenez, 2014).

Overall, the usefulness of non-invasive analysis is key for this research question. Due to the extreme fragile nature of rock art, non-invasive methods are the only examples of acceptable techniques to use when trying to reveal hidden rock art. Calcite penetrating IR methods and other pigment enhancing imaging techniques were enormously useful for the enhancement of the extremely degraded rock art found at Escoural Cave, some of which is no longer fully visible to the naked eye. Although other invasive techniques do exist, e.g. physical calcite removal from rock art substrate, they are not typically recommended due to the potential harm they can cause in the process. Many papers site the destructiveness that calcite removal can cause despite the original intentions to save the art risk rock art (Whitley, 2001). Damages can range from unintentional removal of pigment alongside the calcite, and opening up new, more vulnerable substrate for bio-colonization of unknown microbials.

3.3 ARE THE SPECIM IQ HYPERSPECTRAL CAMERA AND BWTEK i-SPEC 25 VIS-NIR FORS USEFUL FOR ROCK ART ANALYSIS?

3.3.1 HYPERSPECTRAL CAMERA RESULTS

The Specim IQ hyperspectral camera was attempted on paintings #1-2 and #5-8, at Escoural Cave; painting #3-4 were not analyzed with the hyperspectral camera due to the distance of the rock art from the camera. Out of these six paintings at least three hyperspectral photos were taken of each with varying angles and positioning of the camera and lighting. Only four of the six painted panels achieved limited results, the other two failing to match the various pixels with corresponding wavelengths. The paintings that were able to achieve results with the Specim IQ studio were paintings #2, #5, #7, and #8; the hyperspectral images can be seen in corresponding sections within *appendix 3*. As mentioned, the majority of the hyperspectral imaging results did not reveal any more details of the degraded paintings than other, simpler and more affordable imaging techniques. The exception was painting #2. Below in *figure 18*, is a compilation of nine hyperspectral images taken of painting #2 with the use of PhotoShop software.
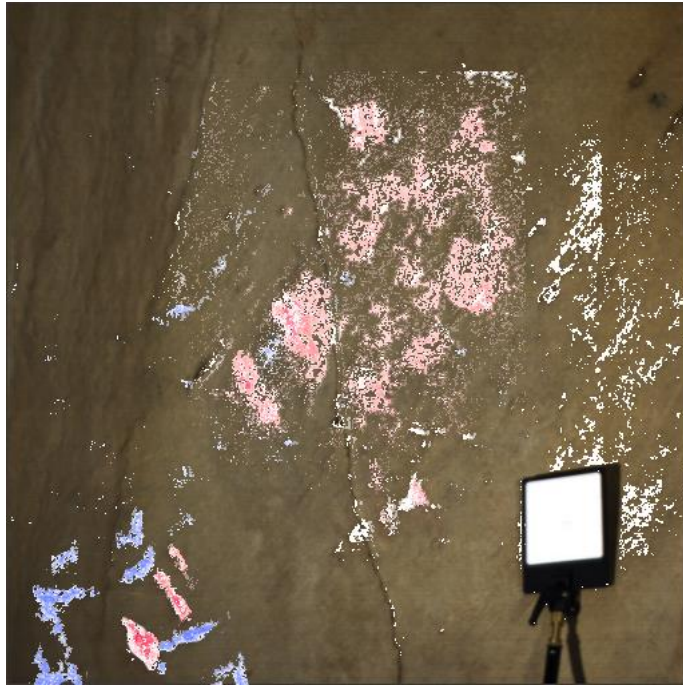
Figure 18: Compilation of hyperspectral camera results from painting #2. Compiled using Photoshop.

Each of the nine photographs taken for the compilation of *figure 18* focused on a different section of the panel with white reference and lighting moved to accommodate the camera location. Out of the 9 photographs, 27 AOIs were selected with a total of 7 classes, 5 red and 2 black; sensitivity of the classmark ranged from 0.9986 to 0.9998.

Although painting #2 was one of the more difficult panels to view in visible light (see *figure 14)*, the hyperspectral camera was able to capture higher quality results when compared to the other painted panels; this is believed to be a result of the flatter, more homogeneous surface of the panel's rock substrate and the ideal location which allowed for a reasonable distance for camera and lighting setup.

Hyperspectral imaging is also able to identify pigment material based on wavelengths acquired for each pixel of the photograph. Ranging from 420.4-1000.5 nm, the wavelengths can determine characteristic pigment spectra in the visible region, while not encompassing enough of the NIR region to determine additional pigment components such as organic binders. The Specim IQ hyperspectral camera was able to successfully collect the spectra of pigments in a limited number of photographs taken, most likely due to the unevenness of the limestone substrate, the unfortunate irregularity of the lighting, the undesirable distance of the camera from the panels, and the extreme degradation of many of the paintings due to

the calcite coverage. The spectra collected from selected points of Painting #5 , *figure 19*, represented by geometric lines, was successfully identified as red ochre due to the characteristic shape of the spectra and bands seen at 615 nm and 740 nm (Cosentino, 2014; Daniel & Mounier, 2016). These results were further confirmed with EDXRF and Vis-NIR FORS. No black pigments were able to be identified due to the high absorbance of the color, leaving the spectra difficult to ascribe to charcoal, bone black, or manganese oxide.
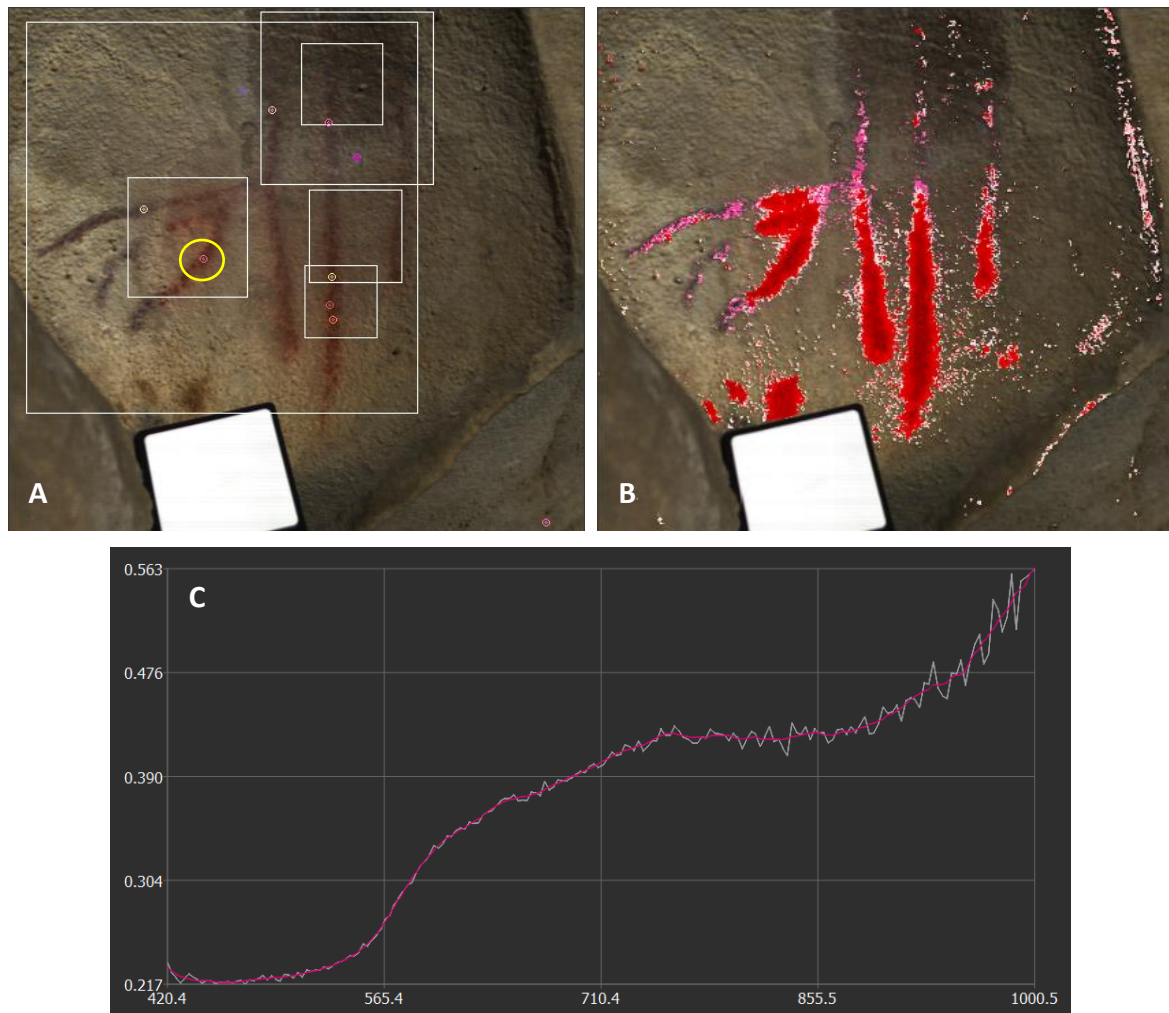
Figure 19: Hyperspectral imaging results from Painting #5. (A) Hyperspectral photograph taken with selected areas of interested indicated with squares, yellow circle indicates pixel wavelength in image (C). (B) Mask created using 1 photograph, 6 AOIs with a total of 5 classes, all red points, sensitivity of the classmark ranged from 0.9920 to 0.9993. (C) Spectra of red pigment pixel using Savitzky–Golay smoothing with polynomial order of 2.

Overall, the portable hyperspectral camera from Specim IQ had varying results throughout Escoural Cave. Many variables factored into the acquisition of each photograph. Due to the nature of the hyperspectral camera, a focal length of 1.8, i.e. a distance of 12 cm is recommended for capturing wavelengths. Multiple halogen lamps are also required for obtaining proper levels of illumination on the rock art panels. Finally, a tripod is necessary for

stabilization of the portable camera as the integration time for capturing data is dependent upon lighting and distance – ranging from seconds to minutes for data capture. Unfortunately, as mentioned in previous sections, many of the rock art panels analyzed for this thesis were located in difficult to reach locations and furthermore, not only were many of the panels extremely degraded and facing severe calcite coverage, they also were not located on ideally flat substrates. All of these factors influenced not only the position of the camera, halogen lamps, and white reference, but also the ability for precision and accuracy of data acquisition. Although the recommended focal distance is 12 cm, none of the rock art panels were able to be photographed at that close of a distance, and two panels were not able to be photographed at all due to poor resolution of pixels.

This method allows for the acquisition of wavelengths for each pixel ranging from 400 nm to 1,000nm. However, due to the image capturing process and the photograph alteration software, Specim IQ studio, the procedure for selecting wavelengths is highly subjective to the user, allowing for a range of results for the final output depending on which pixel was chosen and the level of sensitivity applied. Although the portable hyperspectral camera allows for insitu use, dependent upon each individual case a tradeoff has to be made. Either a priority is made to focus on the pixel size (spatial sampling) of your sample or on the width of the spectral sampling (Delaney et al., 2015). Overall, although Escoural Cave suffers from severely degraded rock art, the portable hyperspectral camera showed the capability of conducting promising results, however, this is believed to be highly dependent upon the rock art itself. This hyperspectral camera may be useful on other rock art locations where the conditions for setting up the equipment and acquiring the photographs are more favorable.

3.3.2 Vis-NIR FORS RESULTS

Optimization of the BWTEK i-Spec 25 Vis-NIR FORS along with creation of standards for replication of traditional Palaeolithic pigments and binders was conducted in order to acquire a database for comparison against spectra acquired from the paintings in Escoural Cave. EDXRF was also performed in order to confirm the results given by the FORS. See *appendix 4* for optimization of FORS, creation of standards, and database; see *appendix 5* for sample location of FORS and EDXRF points.

i) SPECTRA OF ESCOURAL CAVE

Below in *figures 20-22,* are all spectra collected from Escoural Cave using the Vis-NIR FORS. The Spectra have been separated based on pigment sample; *figures 20-22* shows all red spectra collected from Escoural Cave, followed by all black spectra collected, and all limestone blank spectra collected. All spectra displayed are shown to include full range of the Vis-NIR FORS detectors, from 350-2500 nm in transmission mode.
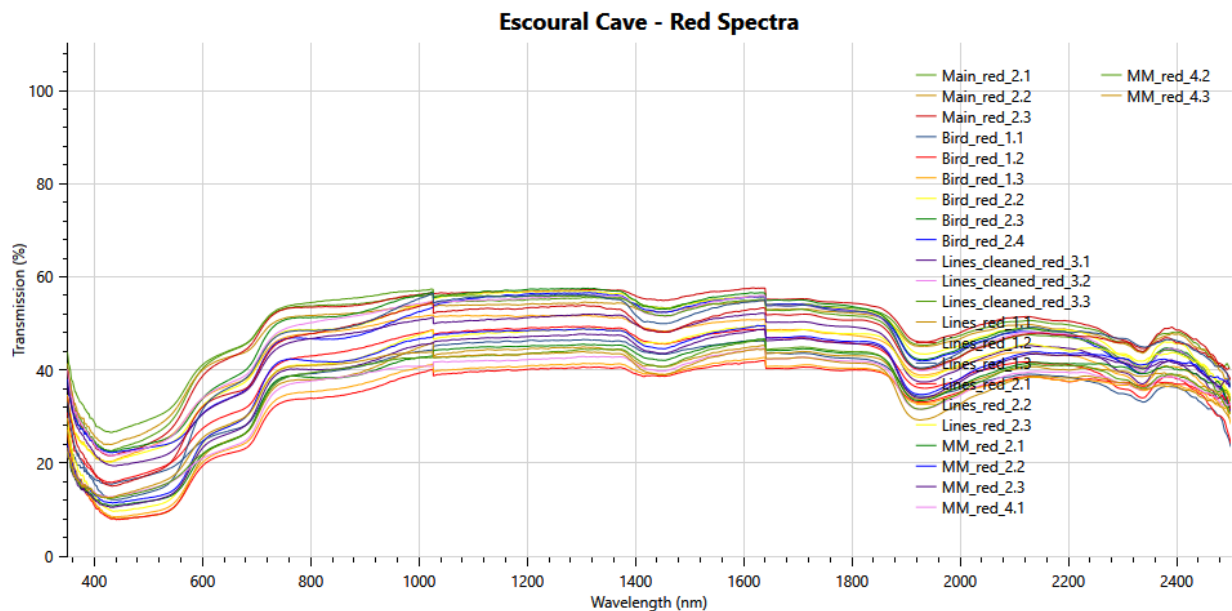
Figure 20: FORS spectra of all red pigments from Escoural Cave. Main= Painting #1, Bird= Painting #2, Lines= Painting #5, MM= Painting #6, 3 Horses= Painting #7, Unknown= Painting #8.

The spectra shown in *figure 20*, a total of 24 spectra from four different paintings, identify the red point locations to be red ochre, an extremely common source for red pigment in Palaeolithic rock art (Smith, 2014). The reflected visible region from 400-800 nm is extremely useful in identification of pigment. Prominent bands displayed in spectrum of pure red ochre include predictable broad reflectance bands at 615 nm and 740 nm (Cosentino, 2014; Daniel & Mounier, 2016). Identification of these speaks were found in both the standards taken of known red ochre and the spectra of the red points as seen above in *figure 20*. EDXRF analysis acquired on the same points were able to corroborate the results as each red location contained high quantities of iron, as those found in hematite – a common iron oxide mineral in red ocher to which the red chromophore is obtained from. Organic binder materials are known to absorb in the NIR region, however the high noise ratio seen in the far NIR region of 1600-2500 nm was impossible to detect any characteristic binders that could have been possibly used the in Palaeolithic rock art.
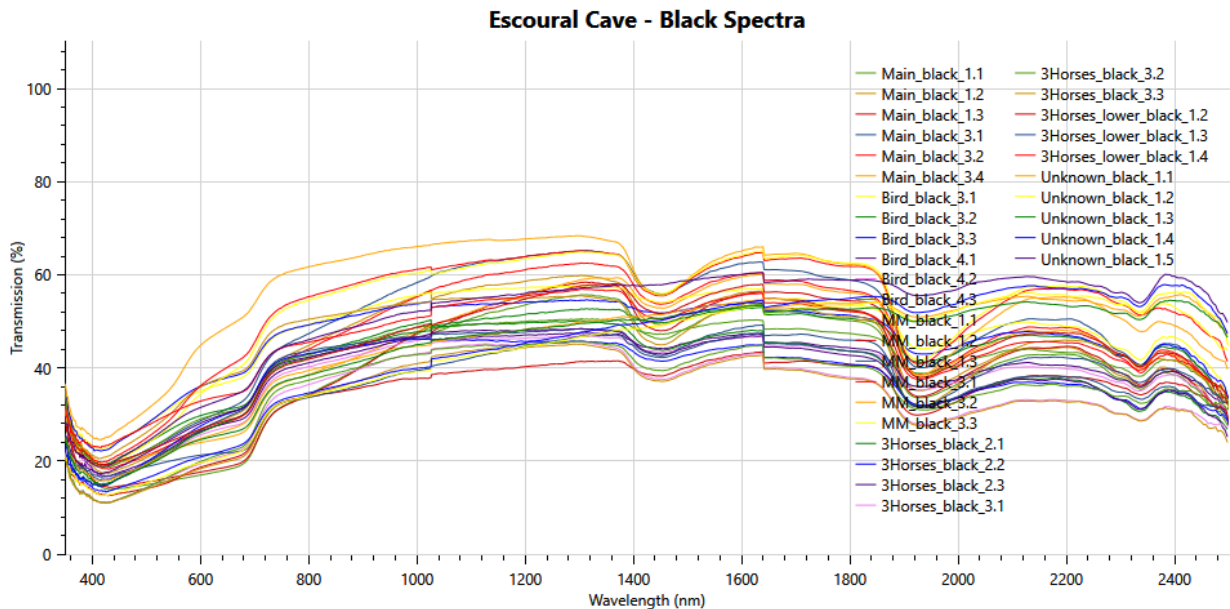
Figure 21: FORS spectra of all black pigments from Escoural Cave. Main= Painting #1, Bird= Painting #2, Lines= Painting #5, MM= Painting #6, 3 Horses= Painting #7, Unknown= Painting #8.

The spectra shown in *figure 21* are a compilation of a total of 32 spectra from five different paintings in Escoural Cave. As found in research and through the analysis done of the standards created (Cosentino, 2014; Daniel & Mounier, 2016), the traditional black Palaeolithic pigments of charcoal, bone black, and manganese oxide have high absorption rates and are unable to reflect light back to create characteristic bands in the visible region, therefore it is impossible to identify them based solely on the spectra between 350-800 nm. Although the pigments samples were considered black pigment, there was a considerable amount of interference in the spectra due to the reflection of the nearby limestone and or calcium carbonate; as seen in *figure 21*, the bands are shown to elevate diagonally from 400 nm to 700 nm. One interesting result obtained from the black pigments was that of painting #8, otherwise known as painting 'unknown'. Spectrum seen in *figure 21* display five relatively flat bands between 1050 nm and 650 nm. Although inconclusive at first, EDXRF was able to take samples of in the same location as those taken for the FORS analysis and provide information that the pigment composition in painting #8 contained higher levels of Manganese than any other pigment samples analyzed; therefore, leading to the conclusion that the blank pigment found on painting #8 is from Manganese Oxide. Again, similar to the spectra collected for the red points, no clear absorption bands belonging to binders can be determined from the spectra *in figure 21* due to the extensive interference of noise.
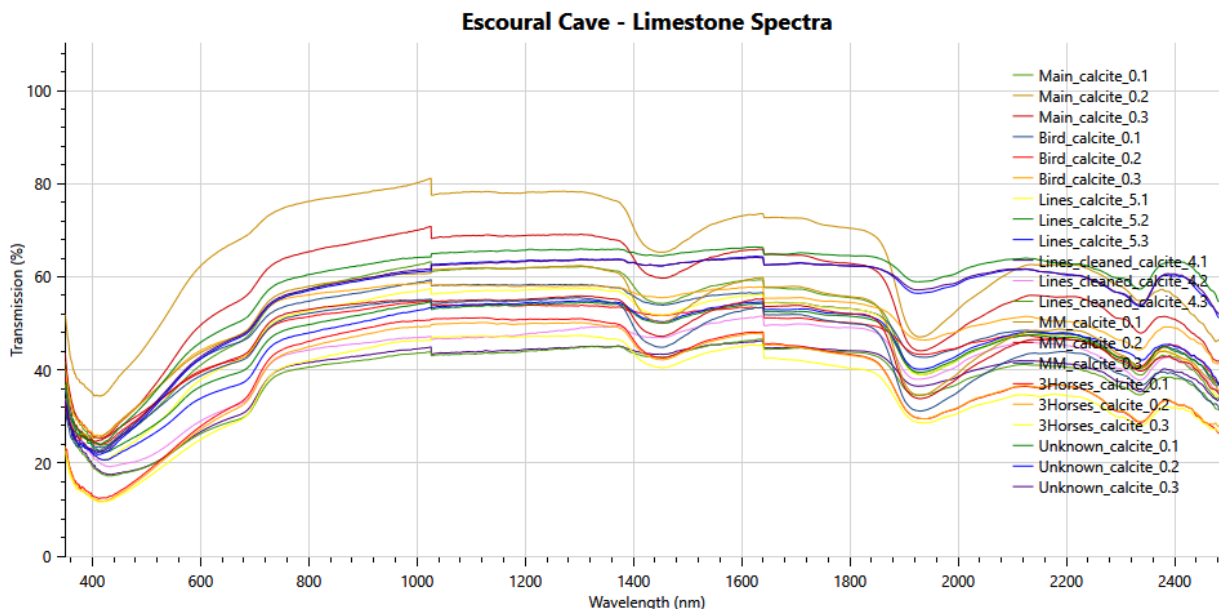
Figure 22: FORS spectra of all limestone blanks from Escoural Cave. Main= Painting #1, Bird= Painting #2, Lines= Painting #5, MM= Painting #6, 3 Horses= Painting #7, Unknown= Painting #8.

As shown in *appendix 4,* and due to many factors such as thin and degraded painted pigments, unevenness of the limestone surface structure, extreme calcite formations nearby or on top of sampling locations, and size of aperture used on the FORS of 5mm, it is recognized that the spectra collected in Escoural Cave were heavily influenced by the nearby surroundings; therefore, limestone blanks spectra were also taken to determine how similar the results obtained were to the collected red and black pigments spectra.

As seen above in *figure 22,* the reflectance of the limestone blank spectra were quite reflective, and somewhat similar in nature to the black spectra points complied in *figure 21*. However, interestingly, the NIR regions of 800-2500 nm appear relatively the same in all spectra taken from Escoural Cave – most likely attributed to interference when trying to collect only red and black sample locations near calcite. Interference of background material can be supported through the EDXRF results which indicate all samples locations in Escoural Cave to contain high levels of calcium.

Three prominent defining bands of absorption are seen at roughly 1450 nm, 1900 nm, and 2350 nm in nearly all spectra from Escoural Cave. These three bands differ slightly, but are believed to be attributed to the saturation of the limestone support. NIR spectroscopy conducted on limestone in a South Korean mine were able to determine CaO content in limestone dependent upon wet and dry conditions of the rock (Oh, Hyun, & Park, 2017). Oh

et al. demonstrated in dry limestone that the characteristic calcite absorption bands can be seen at 1850 nm, 2000 nm, 2350 nm, and 2500 nm while the intensity of the CaO can affect the absorption features; however, if the limestone is saturated with water, broad water features can be observed at 1900 nm and limit the calcite absorption bands to only 2350 nm and 2500 nm. Therefore, due to the water feature found at 1900 nm in all spectra from Escoural Cave, it is reasonable to conclude that the limestone surface was heavily inundated with water during the FORS analysis. Another factor to bear in mind, that short wavelength infrared light is very penetrating, and therefore could display higher amounts of the limestone background if the penetration was able to pass through the paint layer with ease.

Overall, due to the highly sensitive nature of the Vis-NIR-FORS, the instrument was able to successfully relay characteristic red ochre spectra despite the high interference from the background limestone. Unfortunately, the instrument was less successful in attempts to identify the addition of possible organic binders. The lack of characteristic binder bands could be attributed to a wide variety of influences; is it possible that the high noise-to-signal ratio, despite optimization efforts to minimize noise, could have made identification of possible binders impossible to interpret; it is quite possible that the original binders have partially or completely degraded or bio-deteriorated over time; even the mixture of various pigment, filler, and binder could have caused a chemical reaction in which the original spectral behavior could be modified, and even the heterogenous nature of the limestone surface could have caused the diffuse light to interact in an irregular manner (Cavaleri et al., 2013; Clark, 1999; Dooley et al., 2013; Oh et al., 2017; Yivlialin et al., 2019). Overall, due to the high sensitivity of NIR spectroscopy, the complexity of the spectra proved to be quite intricate for interpretation (Clark, 1999; Dooley et al., 2013; Yivlialin et al., 2019). Therefore, principal component analysis was used in order to determine if the NIR region did in fact register the presence of binders in the paintings at Escoural Cave.

ii) PCA RESULTS OF ESCOURAL CAVE SPECTRA

62 Vis-NIR-FORS spectra from Escoural Cave's rock art paintings were used with principal component analysis to determine the presence of possible binders. The PCA was separated into various regions of interests. Regions of interest included the Vis-NIR region from 400-1018 nm, the NIR region from 1031-1633 nm, and the far NIR region of 1655-2485 nm. While optimal calibration of the FORS instrument was set to the conditions of various parameters,

cutoffs for each of the three detectors still occurred; therefore, the three regions of interest were set to avoid the cutoffs in order for them to not interfere with the PCA results; refer to section 2.2.1 for PCA methodology. Below, *figure 23* shows all 62 spectra collected from Escoural Cave and the regions selected for PCA analysis based on the cutoffs of the three detectors.
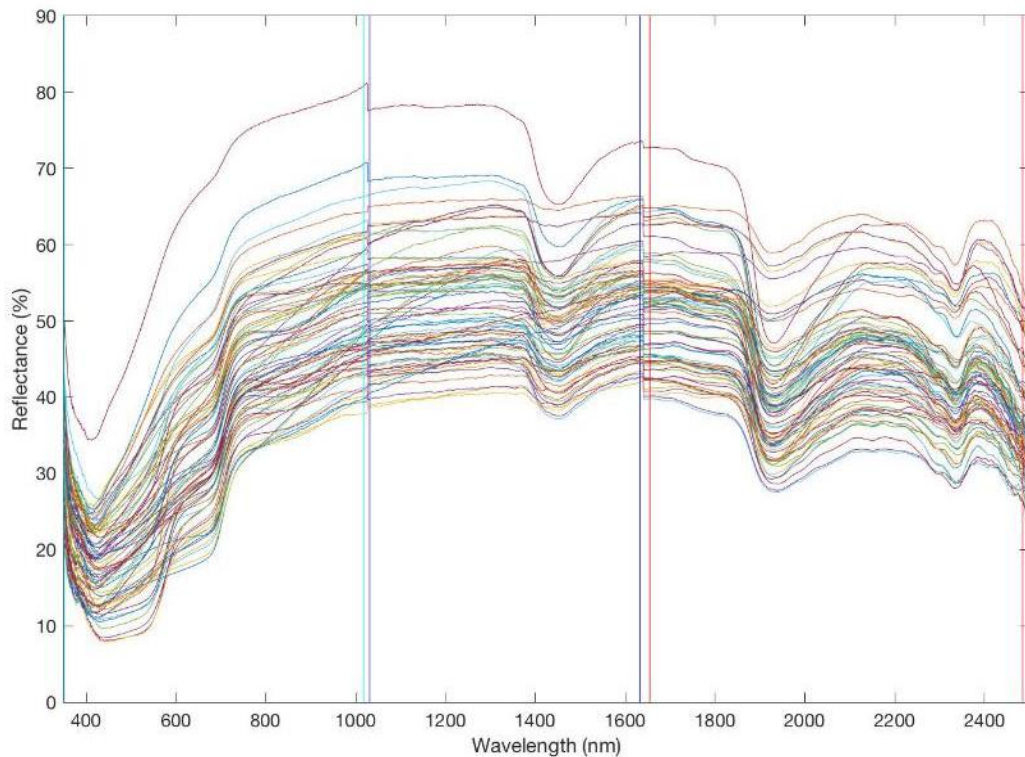
Figure 23: All 62 spectra collected from Escoural Cave. Different analyzed regions indicated by the three different rectangles (turquoise, violet, and red).

Uncalibrated PCA analysis of Escoural Cave Spectra

Uncalibrated PCA analysis of the turquoise region (400-1018 nm) is shown in *figure 24*. Clusters have formed according to pigment chromophores of black, red, and limestone/calcite. Outliers are seen in the corresponding yellow circle and in the overlapped region between the black and gray circles. Based on EDXRF results, the outliers circled in yellow – three limestone/calcite samples taken from painting #5 – are shown to contain larger amounts of iron than all other limestone/calcite points taken in the cave. These outliers can be easily explained, the region in which they were analyzed had previously undergone calcite removal in attempts to make the painting more visible (see *appendix 2)* – perhaps remaining iron rich pigment was distributed during the cleaning, or the cleaning process accidentally removed the iron pigment from the location. Overlapping of the black and gray circles can be

clarified due to interference of limestone/calcite background when trying to sample the limited black pigment locations on some paintings.
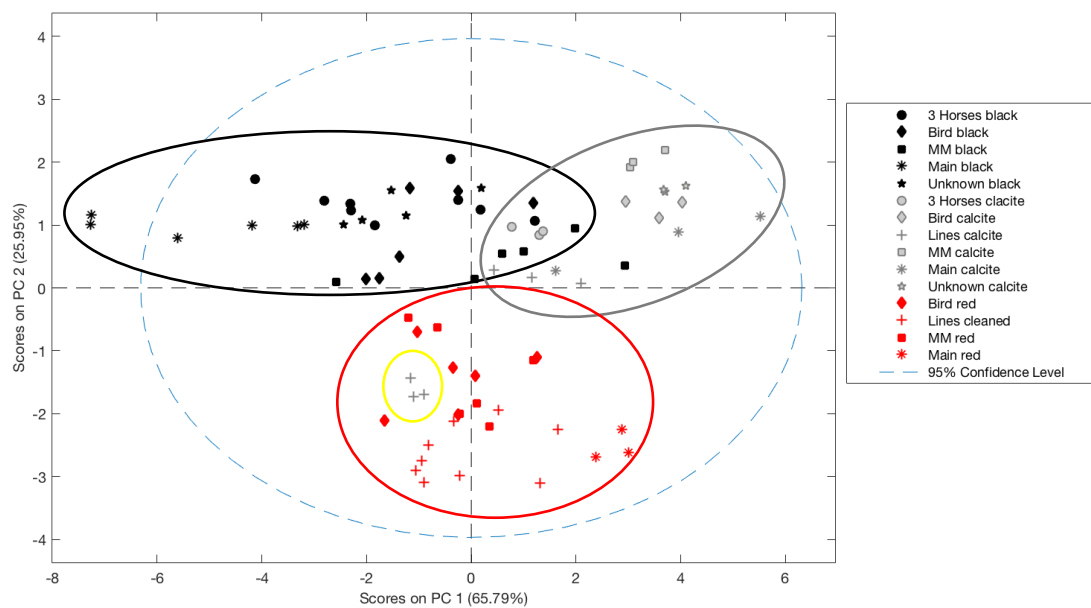
Figure 24: Score plot of uncalibrated 351-1018 nm region from Escoural Cave spectra. Colored circles indicating clustered groups and outliers; black circle indicates black pigments, red circle indicates red pigment, gray circle indicated limestone/calcite, and yellow circle indicates outliers. Main= Painting #1, Bird= Painting #2, Lines= Painting #5, MM= Painting #6, 3 Horses= Painting #7, Unknown= Painting #8.

Shown in *figure 25*, are the loading plots used for the PCA of the turquoise region (400-1018 nm). Loading plots indicate which wavelength regions contain the most variance (Varmuza & Filzmoser, n.d.). Principal component 1 (PC1) contains 65.79% of the variance, while PC2 is 25.95%; for an overall total of 91.74%.
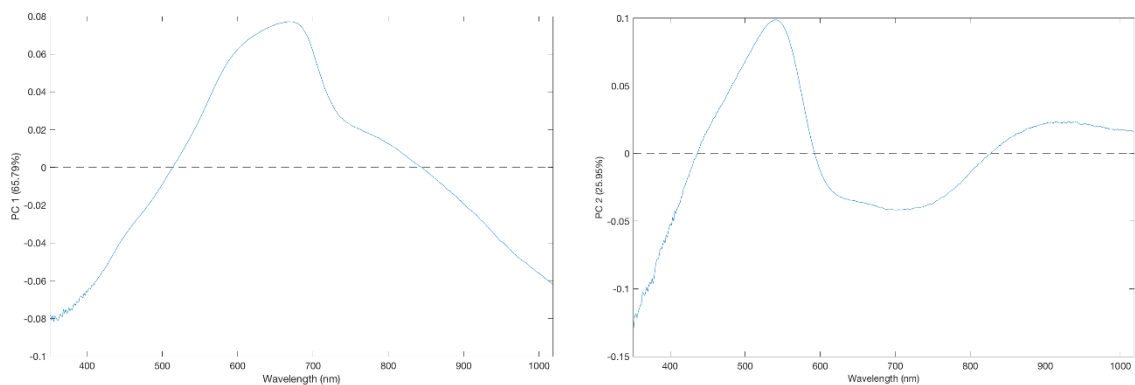
Figure 25: Loadings plots left to right of PC1 (65.79%) and PC2 (25.95%).

Uncalibrated PCA analysis of the violet region (1032-1633 nm) is shown in *figure 26.* Clusters are believed to have formed according to either varying amounts of calcite detected in each sample and/or the water saturation of the limestone background of each sample. While outliers in the yellow circle are indicative of large amounts of manganese oxide in the sample location of painting #8, which is confirmed with EDXRF results as well. Painting #8 is the only painting found in Escoural Cave with substantial amounts of manganese oxide. The spectra samples with the most limestone/calcite samples determined through EDXRF and FORS results are found in the red square indicating that the PC2 loading (*figure 27)* is discriminating based on amount of limestone/calcite, specifically the band found at 1450 nm on almost all spectra expect those from painting #8 containing manganese oxide.
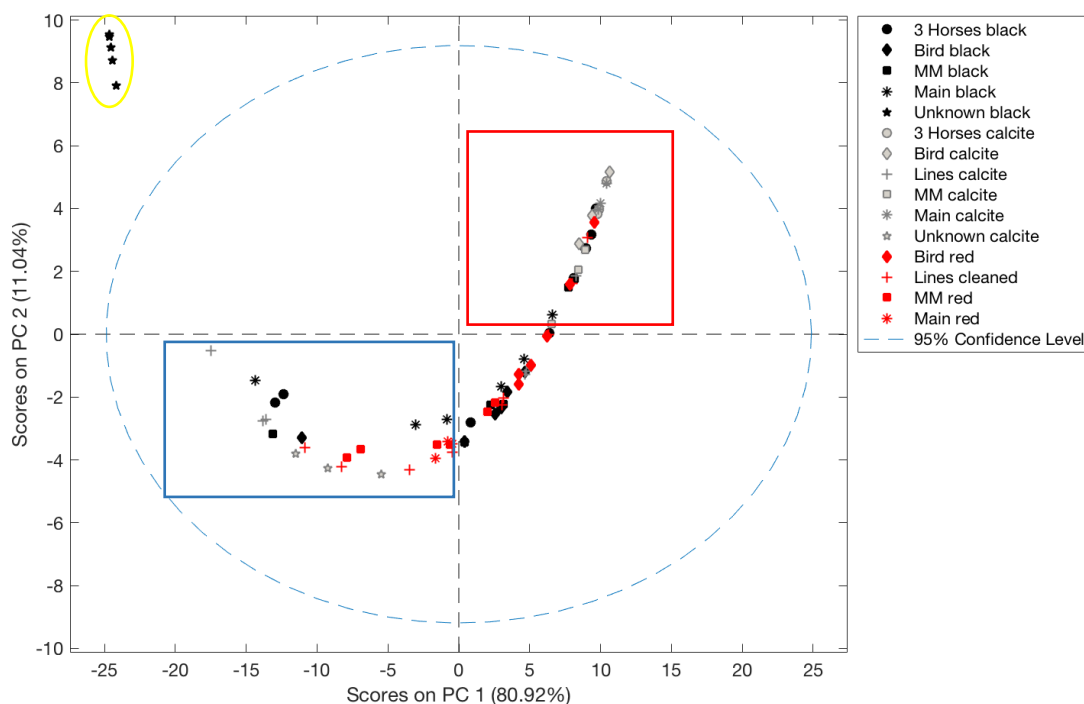
Figure 26: Score plot of 1031-1633 nm region. Colored circles indicating clustered groups, colored squares indicating similar regions. Main= Painting #1, Bird= Painting #2, Lines= Painting #5, MM= Painting #6, 3 Horses= Painting #7, Unknown= Painting #8.

Shown in *figure 27*, are the loading plots used for the PCA of the violet region (1032-1633 nm). PC1 contains 80.92% of the variance, while PC2 is 11.04%; totally to a combined score of 91.96%.
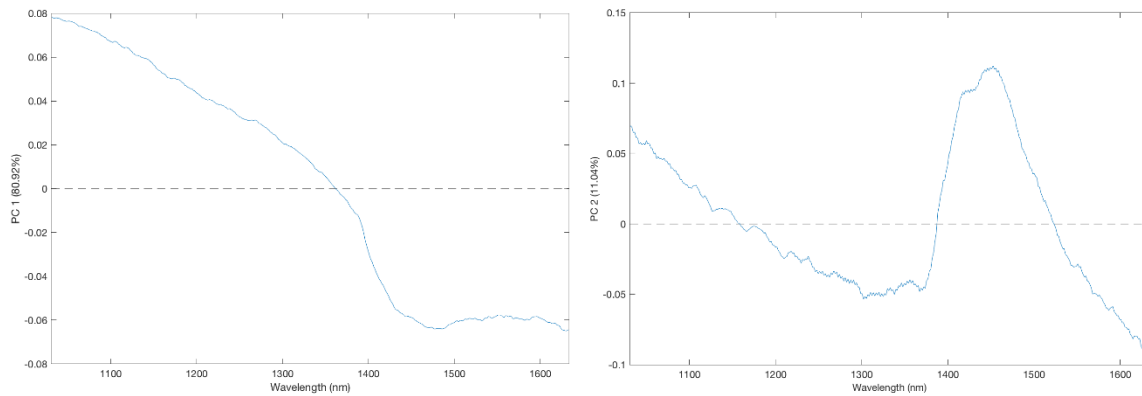
Figure 27: Loadings plots left to right of PC1 (80.92%) and PC2 (11.04%).

Uncalibrated PCA analysis of the red region (1655-2485 nm) is shown in *figure 28*. Clusters are believed to have formed according to varying amounts of calcite detected in each sample. While outliers in the yellow circle are indicative of large amounts of manganese oxide in the sample locations from painting #8. Clusters seen in the green circle are revealing of samples containing higher amounts of iron, manganese oxide, and calcite, according to XRF results. Clustering could potentially be occurring based on binder; however, in order to determine this the PCA from Escoural Cave needs to be calibrated against the Palaeolithic database created using traditional Palaeolithic binders.

Shown in *figure 29*, are the loading plots used for the PCA of the red region (1655-2485 nm). PC1 contains 62.37% of the variance, while PC2 is 31.67%; with an overall amount of 94.04% indicating high discrimination.
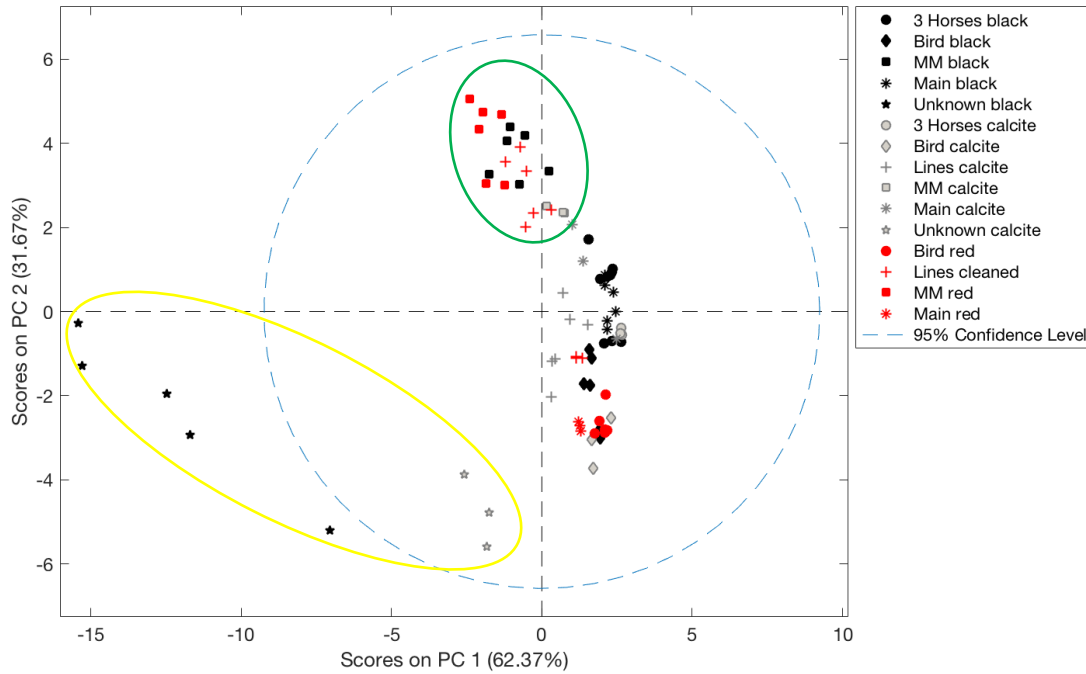
Figure 28: Score plot of 1655-2485 nm region. Colored circles indicating clustered groups. Main= Painting #1, Bird= Painting #2, Lines= Painting #5, MM= Painting #6, 3 Horses= Painting #7, Unknown= Painting #8.
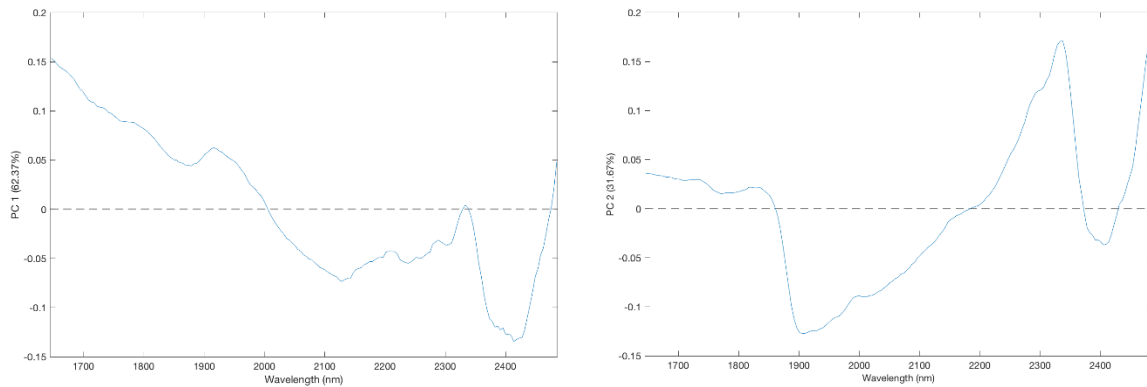
Figure 29: Loadings plots left to right of PC1 (62.37%) and PC2 (31.67%).

Calibrated PCA analysis of Escoural Cave spectra vs. Palaeolithic binders' spectra

As previously stated, through creation of a FORS pigment and binder database and the spectra results from Escoural Cave it was clear that the background support from the sampling process heavily influenced the resulting spectra. Therefore, it was decided that a calibrated PCA analysis should be completed where results from Escoural Cave were calibrated against the Palaeolithic binder database in order to determine if binders are in fact discernable in the spectra from the rock art paintings.

As characteristic bands are only found in the NIR region, a calibrated PCA of the Vis region is not included in the results. Calibrated PCA analysis of the violet region (1031-1633 nm) is shown in *figure 30*. In general, the results formed indicate that the majority of the cave samples are similar in nature once the detection leaves the visible range; however, as indicated by the blue arrow, the black samples taken at painting #8 remain outliers from the rest of the Escoural Cave samples. The red circle indicated in *figure 30* is highlighted to show the main clustering of samples from Escoural Cave; additionally, the yellow circle indicates the grouped cluster of the urine binder.

Shown in *figure 31*, are the loading plots used for the calibrated PCA of the violet region. PC1 contains 63.31% of the variance, while PC2 is 15.73%; with an overall amount of 79.04%.
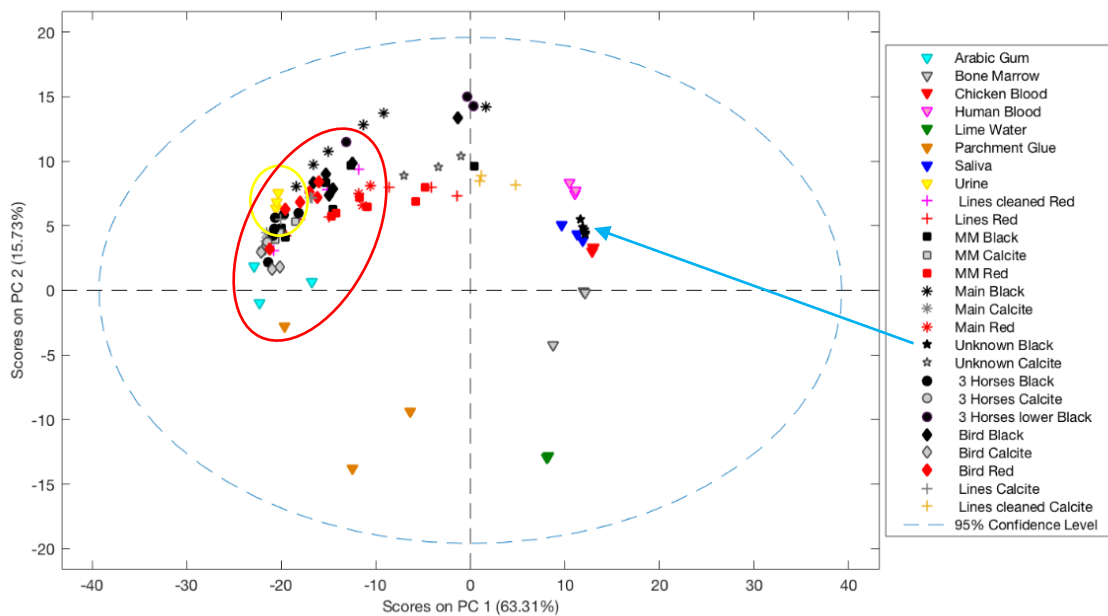
Figure 30: Calibrated PCA of Escoural Cave samples against Palaeolithic binders with glass background subtracted. Score plot of 1031-1633 nm region. Main= Painting #1, Bird= Painting #2, Lines= Painting #5, MM= Painting #6, 3 Horses= Painting #7, Unknown= Painting #8.
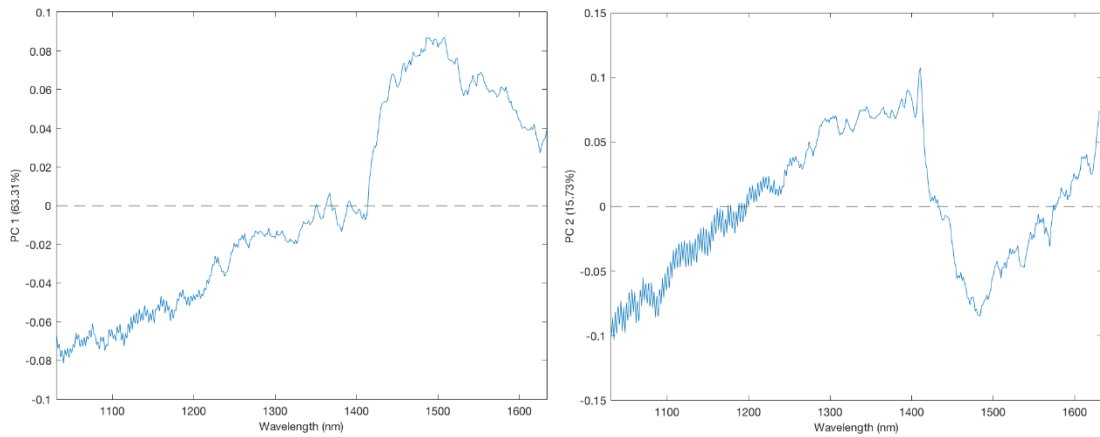
Figure 31: Loadings plots left to right of PC1 (63.31%) and PC2 (15.73%).

Calibrated PCA analysis of the red region (1655-2485 nm) is shown in *figure 32*. Two main clusters seem to stand out; the yellow circle is again highlighting the unique outlier samples of painting #8 from the rest of the samples taken at Escoural. While the red circle expresses the grouping of the majority of samples from Escoural Cave along with the nearby inclusion of the urine binder once again.

Shown in *figure 33*, are the loading plots used for the calibrated PCA of the red region. PC1 contains 37.35% of the variance, while PC2 is 30.23%; with an overall amount of 67.58%.
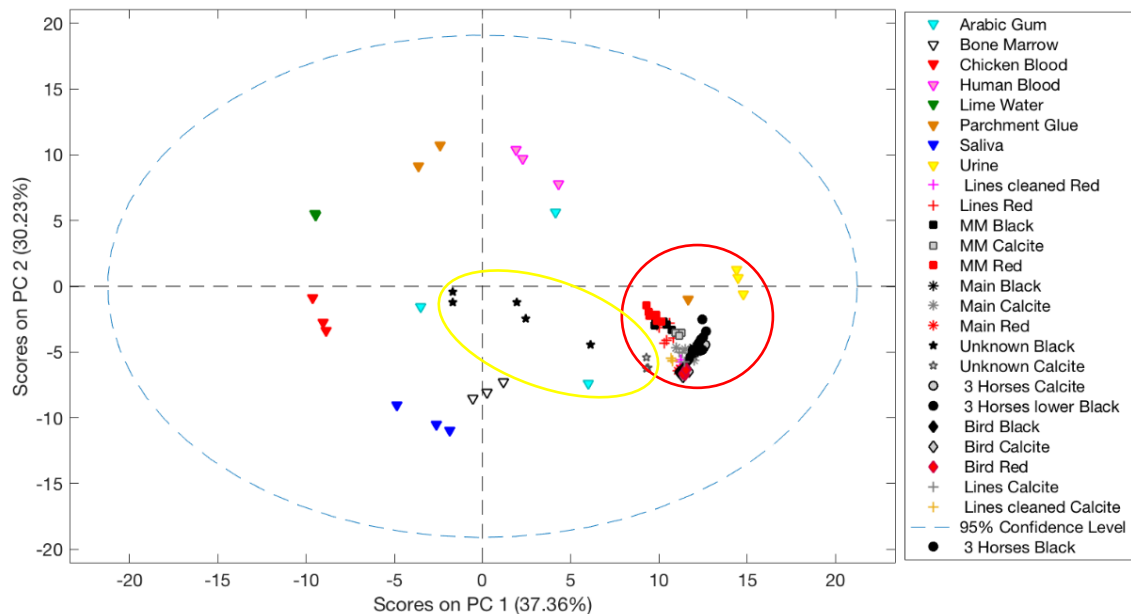
Figure 32: Calibrated PCA of Escoural Cave samples against Palaeolithic binders with glass background subtracted. Score plot of 1655-2485 nm region. Main= Painting #1, Bird= Painting #2, Lines= Painting #5, MM= Painting #6, 3 Horses= Painting #7, Unknown= Painting #8.
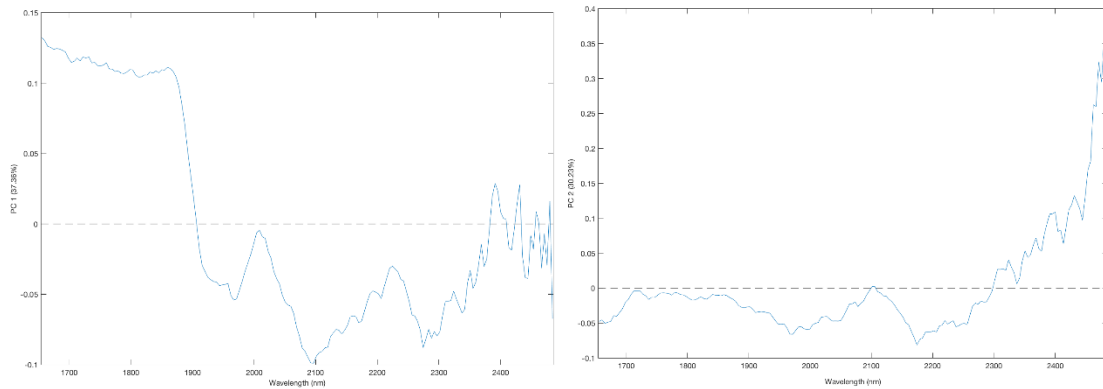
Figure 33: Loadings plots left to right of PC1 (37.35%) and PC2 (30.23%).

Interesting results were obtained through the calibration PCA of the Escoural Cave samples against the Palaeolithic binders. Merely from looking at the clustering effects, one may be persuaded that urine is the most likely binder used in the paintings at Escoural Cave. Although, this could be true, the correlation that is shown in the PCA does not take all factors into account and cannot be used as definitive evidence that urine was used as a binder in Escoural Cave. Further work needs to be conducted in order to confirm or deny the correlation seen in the PCA scatter plots of *figure 30 and 32*. A possible next step could be the chemical analysis of the components of not only urine, but all the possible Palaeolithic binders, through analytical methods such as GC-MS. These methods would reveal the chemical components such as functional groups found in the binders while a comparison of the results could be further investigated through, after exhausting all the possible non-invasive methods, the destructive method of micro sampling the paintings at Escoural Cave. However, finding viable pigment samples is more easily said than done.

Finally, it may be concluded that the Vis-NIR FORS is an extremely sensitive technique that easily allows for the identification of pigments through short wave infrared spectroscopy. This technique however, is limited and extremely difficult to use when analyzing binders in rock art paintings. As shown in *appendix 4*, even the creation of a database in laboratory conditions proved to be difficult when trying to interpret the results, let alone efforts to read the NIR region in samples from the field.

Although the idea of a portable, fast, and non-invasive yet highly sensitive NIR spectrometer seemed ideal, the limitations and conditions faced during the procedure in Escoural Cave could be partially to blame for the results achieve specifically inside Escoural. That being said, this technique could be more useful and applicable for identifying binders in rock art that face

better preservation conditions and are not highly influenced by calcium crusts. Below in figure 34, a close-up image can be seen of the current condition of the rock art pigments, in this case a black pigment is surrounded and is extremely at risk from the overlapping calcite crusts found throughout the cave.
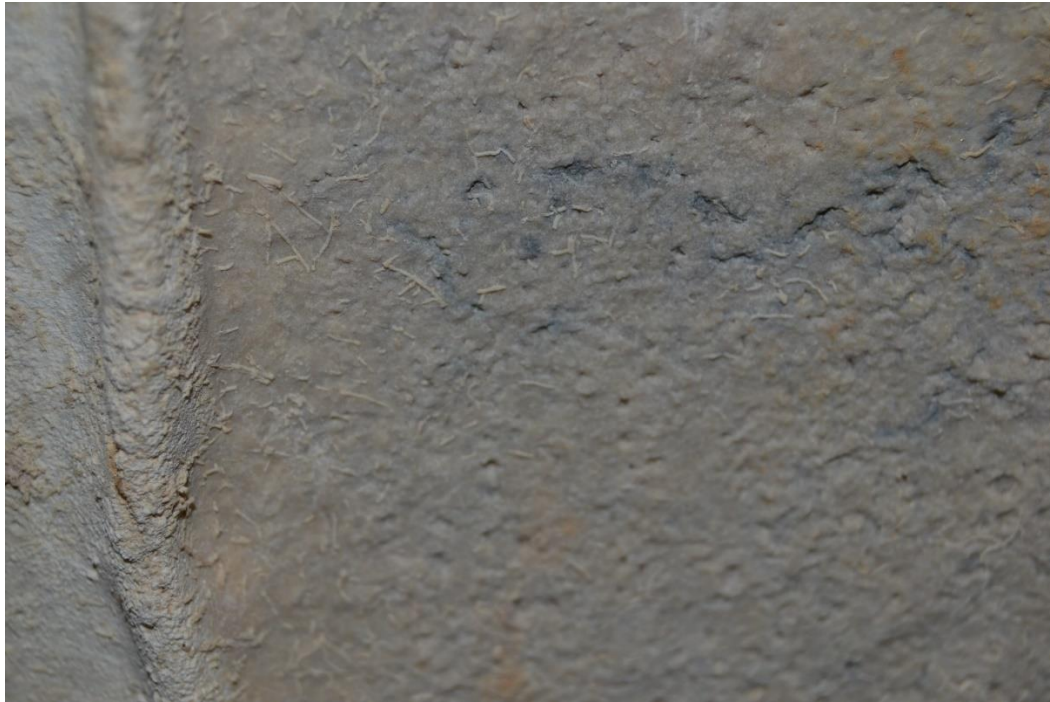
Figure 34: Close up photography of painting #1. In the upper half of the photograph the black pigment is barely visible due to the calcite intrusion.

3.4 WHICH BIOTA ARE THRIVING INSIDE ESCOURAL CAVE, AND ARE THEY CONTRIBUTING TO THE BIODETERIORATION OF THE PAINTINGS AT ESCOURAL CAVE?

As reviewed in section 1.3.1, the growth and study of microorganisms and biofilms residing on and near rock art found in hypogeal environments can reveal important insights into the deterioration and degradation of that rock art and can be enormously useful in future mitigation strategies for the preservation of at-risk rock art.

Lascaux Cave has one of the most well-known instances of biological outbreak inside a show cave; after the sealed off hypogeal environment was rediscovered in 1940 for tourism, a rapid biodeterioration process began with the accidental introduction of new nutrient sources that allowed for harmful biofilms to spread and damage the Palaeolithic rock art inside. These biofilms are now well known in the rock art community and have been a source of fear among those intent on protecting rock art sites; these extremely harmful fungi include *Fusarium*, *Bracteacoccus minor,* and *Ochroconis lascauxensis* (Saiz-Jimenez, 2014). As this thesis pertains to rock art found inside Escoural Cave, a cave, that similar to Lascaux was sealed off for a

majority of its existence from the Neolithic period to the 20th century, the sampling and identification of the microbial populations residing inside Escoural Cave is imperative. Microbial identification can help protect the rock art and those who visit it by giving insight into the natural environment; through microbial analysis this thesis will be able to reveal if any microorganisms are causing rapid deterioration of the paintings, and potentially expose the presence of any microorganisms which are pathogenic to those who visit the show caves.

3.4.1 CULTURE-DEPENDENT METHODS
i) CHARACTERIZATION OF THE MICROBIAL ISOLATES
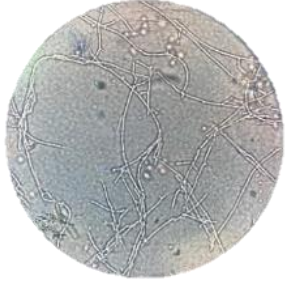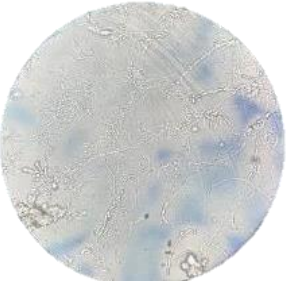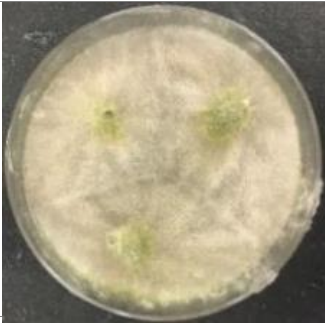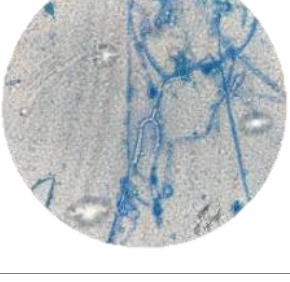
In total, 40 colonies of bacteria were isolated through culturing processes, whose DNA was extracted and then quantified. Based on further examination, 28 bacteria strains were then selected for DNA sequencing (isolation charts represented in full in *appendix 6),* in which all 28 bacterial strains were identified. *Table 5* is the bacterial isolation chart showing the most abundant bacterial genus found inside Escoural Cave, *Bacillus.*

In total, 13 different fungi colonies were also isolated. Based on their microscopic and macroscopic appearance only 8 fungi strains were selected for DNA sequencing and identified. *Table 6* is the fungi isolation chart. Through the use of culture-dependent methods, there was no one fungi genus that was found to be more abundant in the samples taken from Escoural Cave. (Underlined letters indicate original sample location, see *section 2.3* for sampling locations).

Sample	Strain Genus	Macroscopic features	Microscopic features (100x)
<u>C$_1$</u>.4-2	*Bacillus sp.15*		

Table 5: Bacterial isolates. See appendix 6 for rest of bacterial isolates.

Sample	Strain Genus	Macroscopic features	Microscopic features (100x)
M	*Cladosporium sp.1*		
M1-1	*Paecilomyces marquandii*		
M1-3B	*Mortierella sp.1*		
M2-1	*Bionectria sp.1*		
A$_{100}$-1	*Trichoderma sp. 1*		
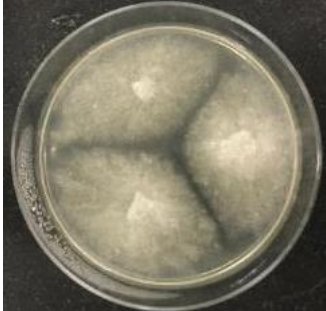
A₁-1 (**A₁₀**.2-1*)	*Lecanicillium sp. 1*		
C₁.1-1	*Polyporus sp.1*		

*Table 6: Fungal isolates. * Sample A10.2-1 was not extracted for DNA sequencing as the macroscopic and microscopic features were identical to those of sample A1-1.*

ii) DNA ANALYSIS OF ISOLATED STRAINS

After extraction of DNA from the pure isolates, quantification using molecular absorption spectrometry was performed on each sample. *Table 7* shows the mean values obtained as well as the relation Abs260 / Abs280 for the bacterial isolates, and *table 8* shows the mean values obtained as well as the ratio Abs260 / Abs280 for the fungal isolates. Purity values lower than 1.7 indicate a contamination of proteins, due to the cleaning process not fully removing the proteins from the sample. Phenols, unless properly removed during cleaning processes, are another common contaminate that absorb in the same region (260-280 nm).

Sample	Mean ± Standard Deviation	Purity		C1.4-1	727.58 ± 21.87	1.78
A1-1	456.62 ± 17.13	1.64		C1.4-1*	620.92 ± 10.98	1.71
A1-1*	513.87 ± 10.75	1.70		C1.5-1	257.99 ± 10.10	1.34
A1-2	489.75 ± 19.93	1.62		C1.5-1*	207.76 ± 6.62	1.64
A1-2*	367.27 ± 15.77	1.52		C1.5-2	746.70 ± 35.64	1.47
A1-2--2	1129.98 ± 9.08	1.85		C1.5-2*	335.07 ± 8.05	1.36
A1-2--2*	1756.09 ± 33.86	1.59		C1.100-1	297.61 ± 4.29	1.38
A2-1	520.34 ± 12.16	1.63		C1.100-1*	297.55 ± 15.22	1.49
A2-1*	667.99 ± 10.15	1.66		C2.1-1	367.04 ± 12.15	1.71
A-3	958.09 ± 15.90	1.46		C2.1-1*	360.42 ± 11.13	1.73
A-3*	1283.42 ± 16.55	1.56		C2.2-1	437.19 ± 11.65	1.58
A3-1	274.69 ± 6.42	1.74		C2.2-1*	627.45 ± 9.73	1.64
A3-1*	395.70 ± 16.71	1.52		C2.3-1	232.53 ± 6.08	1.53
A100-1	112.45 ± 5.78	1.57		C2.3-1*	411.59 ± 5.61	1.46
A100-1*	130.13 ± 12.22	1.35		C2.4-1	483.81 ± 28.46	1.51
A100-2	650.20 ± 24.79	1.61		C2.4-1*	847.86 ± 40.11	1.51
A100-2*	429.75 ± 7.45	1.63		C2.5-1	342.45 ± 14.88	1.51
A1.1-1	677.09 ± 24.22	1.61		C2.5-1*	328.35 ± 22.52	1.52
A1.1-1*	604.22 ± 16.05	1.56		C2.100-1	582.27 ± 13.30	1.73
A1.100-1	692.57 ± 16.96	1.70		C2.100-1*	901.09 ± 15.45	1.54
A1.100-1*	87.79 ± 1.11	1.59		D1-1	771.24 ± 30.34	1.63
A1.100-2	740.29 ± 28.07	1.40		D1-1*	1265.36 ± 5.93	1.73
A1.100-2*	647.39 ± 25.44	1.69		D1-2	114.00 ± 2.55	1.72
B1-1	703.19 ± 16.34	1.74		D1-2*	217.11 ± 2.75	1.69
B1-1*	1200.18 ± 102.41	1.79		D2-1	953.27 ± 20.93	1.40
B2-1	431.32 ± 7.61	1.51		D2-1*	808.58 ± 0.68	1.43
B2-1*	358.01 ± 9.06	1.40		D2-2	966.09 ± 16.60	1.65
B3-1	308.28 ± 16.04	1.39		D2-2*	1167.60 ± 13.16	1.44
B3-1*	444.89 ± 24.96	1.54		D3-1-1	405.15 ± 9.45	1.58
B100-1-2	177.09 ± 8.35	1.53		D3-1-1*	350.05 ± 16.87	1.64
B100-1-2*	153.17 ± 6.00	1.42		D3-1-2	277.83 ± 11.02	1.72
C1.1-1	687.52 ± 2.36	1.83		D3-1-2*	978.12 ± 31.14	1.59
C1.1-1*	476.49 ± 3.67	1.83		D3-2	526.23 ± 34.73	1.66
C1.2-1	261.08 ± 20.70	1.77		D3-2*	763.19 ± 11.44	1.57
C1.2-1*	546.34 ± 32.07	1.56		D4-1	382.50 ± 85.01	1.26
C1.3-1-1	411.06 ± 22.47	1.72		D4-1*	1058.38 ± 15.05	1.69
C1.3-1-1*	371.21 ± 8.21	1.67		D100-1	1427.17 ± 45.83	1.80
C1.3-1-2	387.32 ± 72.81	1.77		D100-1*	1033.77 ± 42.01	1.87
C1.3-1-2*	488.95 ± 5.11	1.81		D100-2	1517.16 ± 51.40	1.65
C1.4-1	939.80 ± 25.99	1.38		D100-2*	1888.92 ± 27.05	2.02
C1.4-1*	882.06 ± 22.95	1.50				

Table 7: DNA quantification of bacterial isolates with molecular absorption spectrometry.

Sample	Mean ± Standard Deviation	Purity
A1-1	394.05 ± 18.29	1.70
A1-1*	200.64 ± 4.85	1.71
A1.1-1	228.46 ± 11.10	1.20
A1.1-1*	156.83 ± 6.66	1.20
A1.1-2	135.78 ± 1.27	1.09
A1.1-2*	108.95 ± 0.83	1.05
A100-1	168.91 ± 3.06	1.13
A100-1*	189.56 ± 12.89	1.17
C1.1-1	311.49 ± 16.37	1.23
C1.1-1*	293.06 ± 5.75	1.23
C2.1-1	95.93 ± 1.41	1.03
C2.1-1*	147.92 ± 7.60	1.08

Sample	Mean ± Standard Deviation	Purity
M	73.99 ± 3.36	1.09
M*	78.43 ± 4.97	1.12
M1-1	232.71 ± 13.11	1.39
M1-1*	202.17 ± 7.40	1.41
M1-3B	163.87 ± 44.59	1.13
M1-3B*	264.40 ± 11.91	1.13
M2-1	94.77 ± 3.93	1.39
M2-1*	109.31 ± 5.42	1.36
M3-1	185.78 ± 1.19	1.10
M3-1*	161.31 ± 10.93	1.11
M4-1	180.44 ± 2.78	1.21
M4-1*	278.22 ± 7.29	1.37

Table 8: DNA quantification of fungal isolates with molecular absorption spectrometry.

iii) AMPLIFICATION OF THE 16S REGION

DNA of bacterial colonies were amplified during PCR using primers 518F/785R and further analyzed by agarose gel electrophoresis. *Figure 35*, displays the resulting bands obtained from the electrophoresis for the bacterial colonies.

Quantification of final PCR products which successfully displayed bands in electrophoresis was performed by fluorimetry; see *table 9*. Based on the results of quantification of the PCR products, only the duplicates with the highest amount of DNA were sent on for sequencing.

Sequencing results allowed for the identification of the bacterial isolates. The results are shown in *table 10*. Furthermore, the sequencing results of the 28 bacterial isolates were used to create a phylogenetic tree using the neighbor-joining method; see *figure 36.*
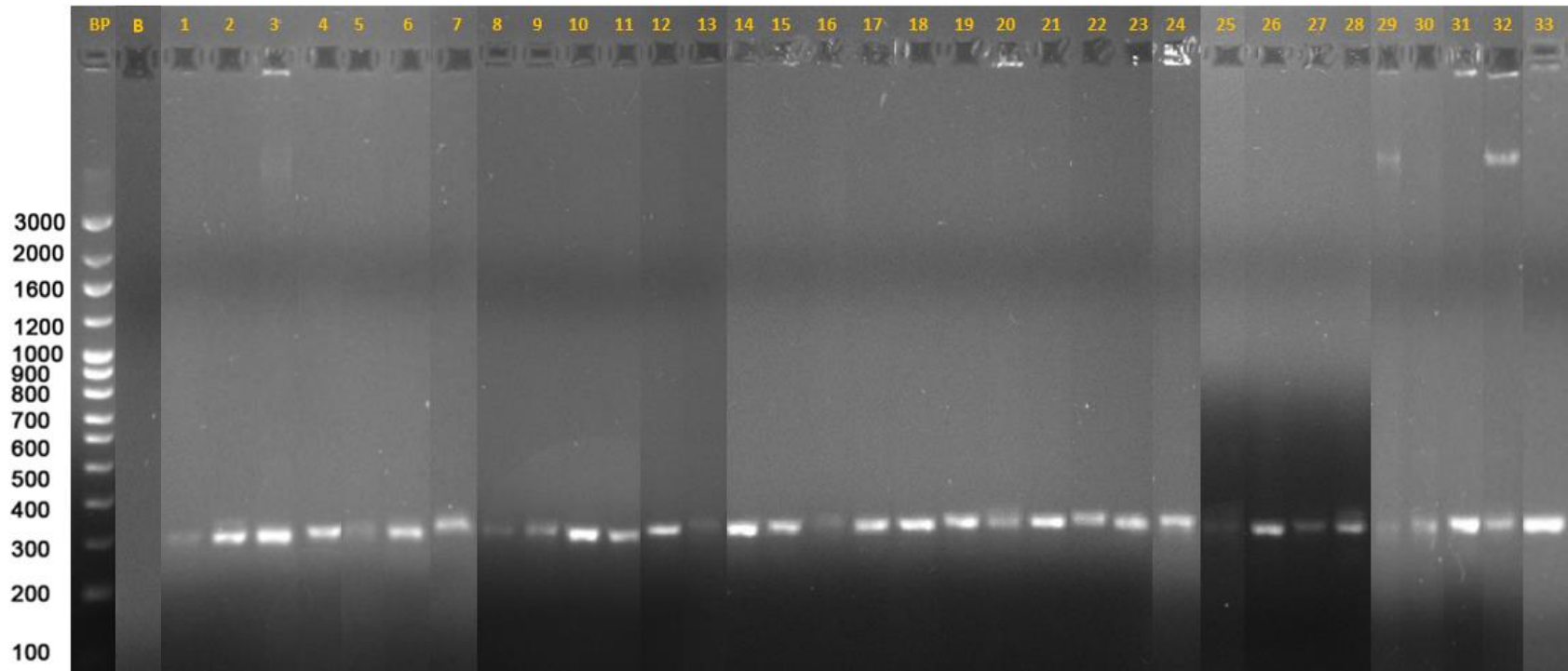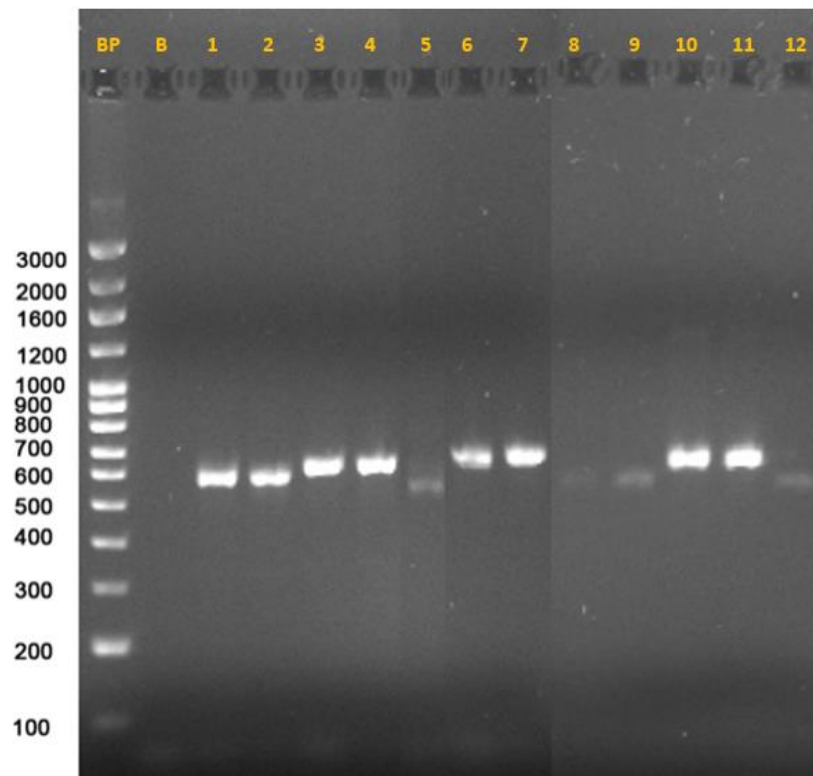
Figure 35: Gel electrophoresis for amplification of 16S region in bacterial colonies (Legend = BP: DNA NZYDNA Ladder VII; B: blank; 1: D100-1; 2: D1-1; 3: A1. 100-1; 4: A100-2; 5: B100-1-2; 6: A1-2--2; 7: B1-1; 8: D1-1*; 9: A1.100-1*; 10: C2.3-1*; 11: A100-2*; 12: $C_{1}.4$-2*; 13: B1-1*; 14: $C_{2}.1$-1; 15: $C_{2}.100$-1; 16: $C_{1}.2$-1; 17: A3-1; 18: $C_{2}.2$-1; 19: $C_{1}.1$-1; 20: D_{100}-2; 21: $C_{1}.3$-1-2; 22: $C_{1}.3$-1-1; 23: A1-1; 24: $C_{1}.2$-1*; 25: A1-2; 26: $C_{1.100}$-1; 27: D3-2; 28: A_{100}-1; 29: D2-2*; 30: D1-2*; 31: D3-1-1*; 32: A_{100}-1*; 33: $C_{1}.4$-2).

Bacteria Sample	Quantification
C_2.1-1	21.00
C_2.100-1	13.00
C_1.2-1	4.95
C_1.2-1*	15.00
A3-1	11.00
C_2.2-1	13.00
C_1.1-1	9.50
D_{100}-2	10.00
C_1.3-1-2	9.80
C_1.3-1-1	8.80
A1-1	10.00
D_{100}-1	3.98
D1-1	8.70
D1-1*	2.28
$A_{1.100}$-1	20.00
$A_{1.100}$-1*	5.90
C_2.3-1	20.00
A_{100}-2	10.00
A_{100}-2*	10.00

Bacteria Sample	Quantification
B_{100}-1-2	3.18
A1-2--2	11.00
C_1.4-2*	12.00
B1-1	11.00
B1-1*	6.30
B3-1	4.49
D1-2*	7.30
A1-2	13.00
D3-1-1*	12.00
$C_{1.100}$-1	18.00
D3-2	6.80
A_{100}-1	13.00
A_{100}-1*	11.00
C_1.4-2	13.00

Table 9: Quantification results of bacterial DNA by fluorimetry. Quantification measured in ng/µl. Duplicates with highest quantity of DNA were sent to sequencing.

Sample Name	Isolated Strain	Most similar species	Identity	*GenBank* access number
A$_{1 \cdot 100}$-1	*Enterobacter sp.1*	*Enterobacter hormaechei*	98.77%	JQ832555.1
		Enterobacter cloacae		JQ832546.1
		Enterobacter asburiae		JQ830553.1
A$_{100}$-2	*Bacillus sp.1*	*Bacillus simplex*	99.58%	JQ834713.1
A$_1$-2--2	*Stenotrophomonas sp.1*	*Stenotrophomonas rhizophila*	99.60%	MF111399.1
A3-1	*Bacillus sp.2*	*Bacillus simplex*	99.21%	MF965139.1
A1-1	*Bacillus sp.3*	*Bacillus simplex*	98.81%	MF965139.1
A$_1$-2	*Bacillus sp.13*	*Bacillus simplex*	100.00%	JQ834713.1
A$_{100}$-1	*Solibacillus sp.1*	*Solibacillus silvestris*	98.81%	MK830724.1
		Solibacillus isronesnsis		MK484463.1
B1-1	*Enterobacter sp.2*	*Enterobacter cloacae*	96.28%	JQ830680.1
B$_{100}$-1-2	*Citrobacter sp.1*	*Citrobacter farmeri*	95.87%	JQ830050.1
B3-1	*Enterobacter sp.3*	*Enterobacter cloacae*	93.72%	JQ832864.1
C$_1$.4-1	*Bacillus sp.4*	*Bacillus simplex*	99.21%	MF965139.1
C$_2$.3-1	*Bacillus sp.5*	*Bacillus simplex*	99.19%	MF965139.1

C$_2$.1-1	*Bacillus sp.6*	*Bacillus simplex*	99.21%	MF965139.1
C$_2$.$_{100}$-1	*Bacillus sp.7*	*Bacillus muralis*	98.42%	MK823372.1
		Bacillus simplex		MK229043.1
C$_1$.2-1	*Bacillus sp.8*	*Bacillus nealsonii*	100.00%	JQ833487.1
		Bacillus circulans		JQ319541.1
C$_2$.2-1	*Bacillus sp.9*	*Bacillus muralis*	99.80%	MH630010.1
		Bacillus simplex		MK229043.1
C$_1$.1-1	*Bacillus sp.10*	*Bacillus nealsonii*	98.80%	KY126832.1
C$_1$.3-1-2	*Bacillus sp.11*	*Bacillus simplex*	99.19%	MF965139.1
C$_1$.3-1-1	*Bacillus sp.12*	*Bacillus nealsonii*	100.00%	JQ833487.1
		Bacillus circulans		JQ833511.1
		Bacillus flexus		JQ835119.1
C$_1$.$_{100}$-1	*Bacillus sp.14*	*Bacillus simplex*	99.60%	MF965139.1
C$_1$.4-2	*Bacillus sp.15*	*Bacillus muralis*	98.80%	MH630010.1
		Bacillus simplex		MK229043.1
D1-1	*Acinetobacter sp.1*	*Acinetobacter calcoaceticus*	99.60%	KF374680.1
D$_{100}$-1	*Pseudomonas sp.1*	*Pseudomonas kilonensis*	100.00%	MF111295.1
		Pseudomonas putida		MF111822.1
D$_{100}$-2	*Pseudomonas sp.2*	*Pseudomonas fluorescens*	93.78%	KJ194131.1
D3-2	*Pseudomonas sp.3*	*Pseudomonas putida*	100.00%	MF111272.1
D2-2	*Stenotrophomonas sp.2*	*Stenotrophomonas maltophilia*	98.74%	AM421782.1

D1-2	*Stenotrophomonas sp.3*	*Stenotrophomonas maltophilia*	99.16%	AM421782.1
D3-1-1	*Lysinibacillus sp.1*	*Lysinibacillus fusiformis*	100.00%	KT757231.1
		Lysinibacillus sphaericus		HQ334982.1

Table 10: Sequencing results of bacterial colonies.
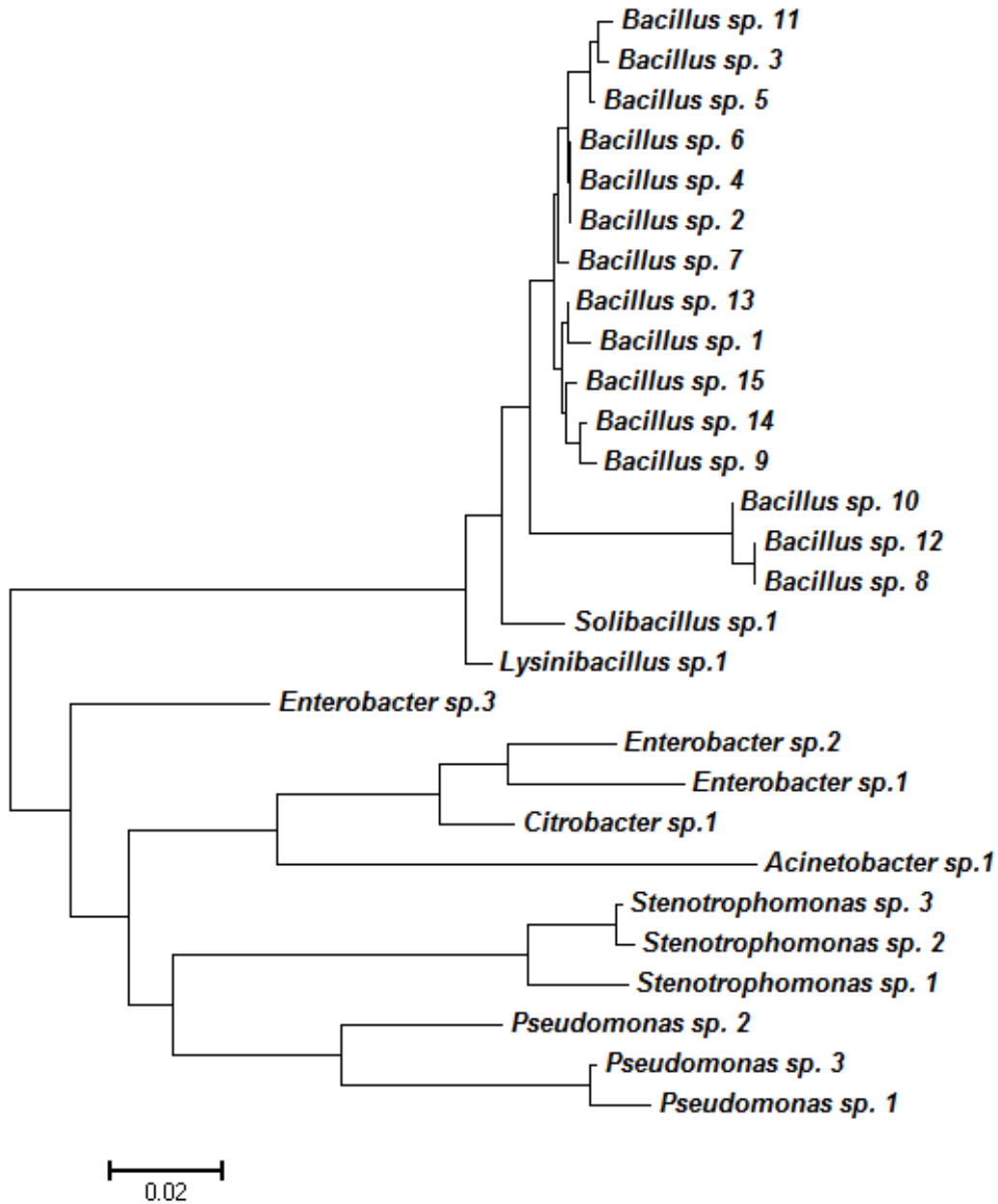
Figure 36: Evolutionary relationships of taxa inferred using the Neighbor-Joining method. The optimal tree with the sum of branch length = 0.68579748 is shown. The tree is drawn to scale, with branch lengths in the same units as those of the evolutionary distance used to infer the phylogenetic tree. Analysis involved 28 nucleotide sequences. There was a total of 245 positions in the final dataset.

Out of 40 isolated bacterial cultures, 28 isolates were successfully identified for a total of 70%.

The most prominent bacterial genus identified from culture-dependent methods was *Bacillus* followed by *Enterobacter*, *Stenotrophomonas*, and *Pseudomonas*.

DNA of fungal colonies were amplified during PCR using primers ITS1F/ITS4R and further analyzed by agarose gel electrophoresis. *Figure 37*, displays the resulting bands obtained from the electrophoresis for the fungal colonies.

Quantification of final PCR products which successfully displayed bands in electrophoresis was performed by fluorimetry; see *table 11*. Based on the results of quantification of the PCR products, only the duplicates with the highest amount of DNA were sent on for sequencing.

Sequencing results allowed for the identification of the fungal isolates. The results are shown in *table 12*. Furthermore, the sequencing results of the 8 fungal isolates were used to create a phylogenetic tree using the neighbor-joining method. See *figure 38.*

Figure 37: Gel electrophoresis for amplification of ITS/18S region in fungal colonies (Legend = BP: DNA NZYDNA Ladder VII; B: blank; 1: A1-1; 2: A1-1*; 3: A100-1; 4: A100-1*; 5: M*; 6: C1.1-1; 7: C1.1-1*; 8: M1-1*; 9: M1-3B; 10: M1-3B*; 11: M2-1; 12: M1-1).

Fungi Sample	Quantification
A1-1	23.00
A1-1*	22.00
A_{100}-1	25.00
A_{100}-1*	27.00
M*	7.60
C_1.1-1	20.00
C_1.1-1*	26.00
M1-1	1.30
M1-1*	2.66
M1-3B	16.00
M1-3B	12.00
M2-1	1.99

Table 11: Quantification results of fungal DNA by fluorimetry. Quantification measured in ng/µl. Duplicates with highest quantity of DNA were sent to sequencing.

Sample Name	Isolated Strain	Most similar species	Identity	*GenBank* access number
A1-1	*Lecanicillium sp. 1*	*Lecanicillium coprophilum*	99.62%	MH177615.1
A_{100}-1	*Trichoderma sp. 1*	*Trichoderma harzianum*	99.66%	KY750444.1
M	*Cladosporium sp.1*	*Cladosporium allicinum*	99.80%	MK460808.1
		Cladosporium herbarum		MK211240.1
C_1.1-1	*Polyporus sp.1*	*Polyporus arcularius*	99.50%	KU863052.1
M1-1*	*Paecilomyces marquandii*	- - -	100%	JQ013003.1
M1-3B	*Mortierella sp.1*	*Mortierella alpina*	99.37%	KY465758.1
M2-1	*Bionectria sp. 1*	*Bionectria ochroleuca*	99.62%	HM113485.1

Table 12: Sequencing results of fungal colonies.
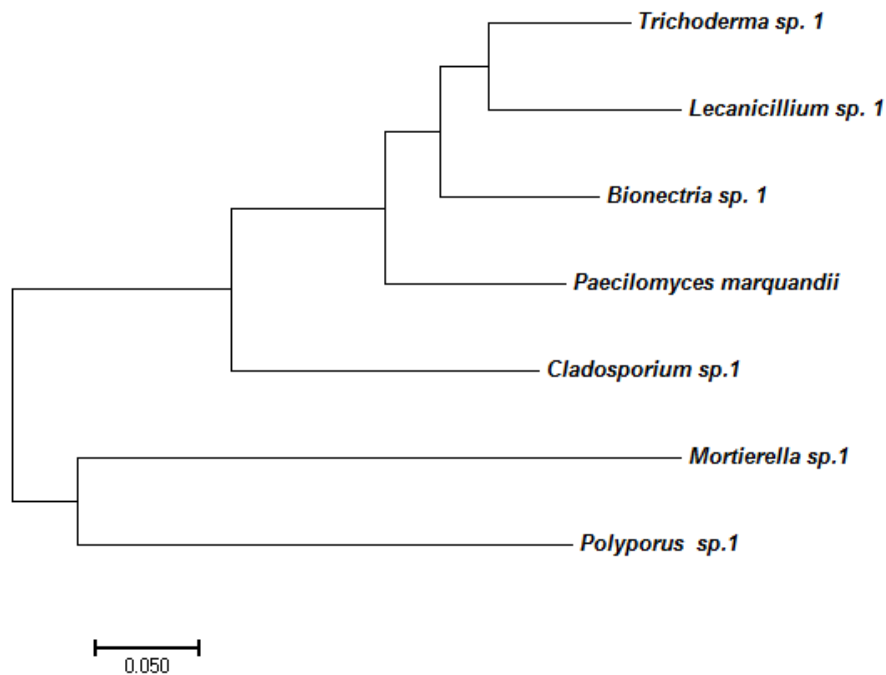
Figure 38: Evolutionary relationships of taxa inferred using the Neighbor-Joining method. The optimal tree with the sum of branch length = 1.27848468 is shown. The tree is drawn to scale, with branch lengths in the same units as those of the evolutionary distance used to infer the phylogenetic tree. Analysis involved 7 nucleotide sequences. There was a total of 423 positions in the final dataset.

Out of 13 isolated fungal cultures, 8 isolates were successfully identified for a total of 62%. All species and genera groups identified were different with no majority genus or species found.

3.4.2 CULTURE-INDEPENDENT METHOD: NGS

NGS analysis using prokaryotic primers of Bakt_341F, Bakt_805R, Amplicon PCR Forward Primer (Illumina Protocol), and Amplicon PCR Reverse Primer (Illumina Protocol) was performed on 8 of the samples taken from Escoural Cave; A, B, C_1, D divided into two samples of D(1) and D(12), M, G, and Y (see section 2.3 for sample locations). 656 different genera and 1,612 species were identified for all samples listed; however, only the top 40 genera and species are shown in the results section.

Shown in *figures 39-40* are phylogenetic trees depicting which samples contained the most similar genera and species results and their abundance of each. Samples C_1, A, and G are closely aligned, as are D(1), B, and D(12), samples Y and M show similar results as well. A PCA graph, *figure 41,* also indicating correlation between samples confirms the results displayed in the phylogenetic tree.

76
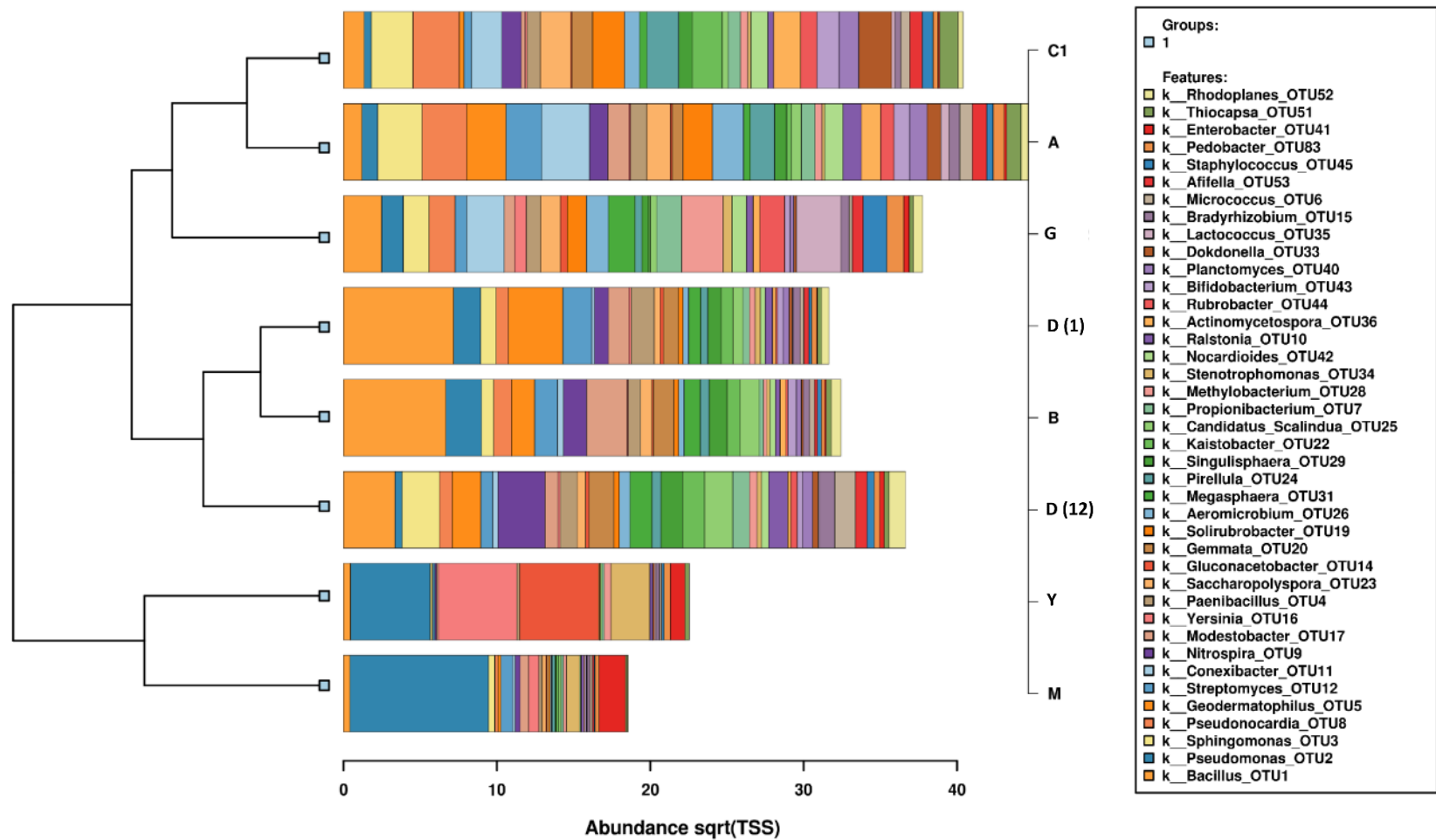
Figure 39: Phylogenetic tree of most abundant genera from NGS analysis of Escoural Cave samples A, B, C1, D(1), D(12), M, G, and Y.
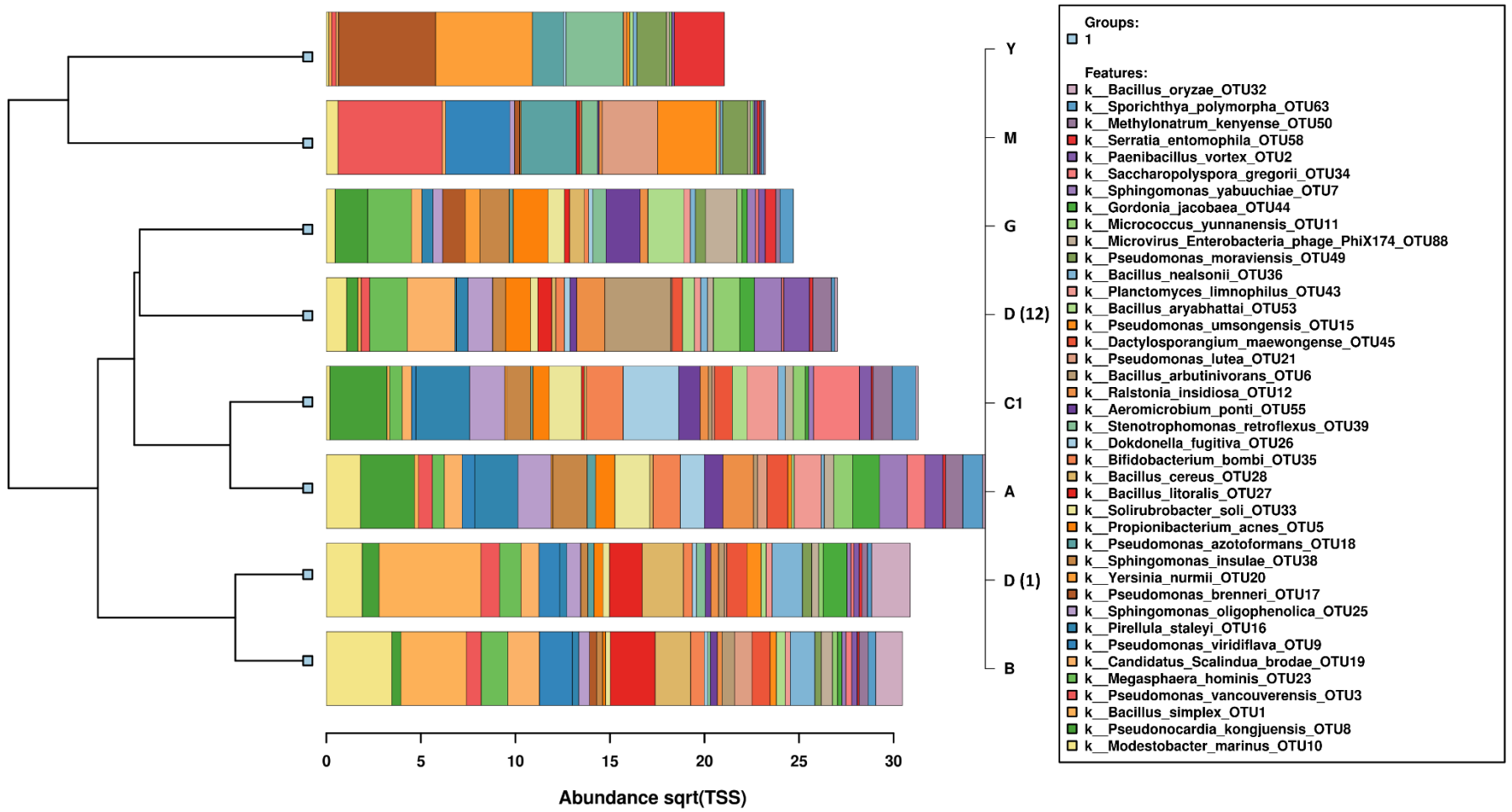
Figure 40: Phylogenetic tree of most abundant species from NGS analysis of Escoural Cave samples A, B, C1, D(1), D(12), M, G, and Y.
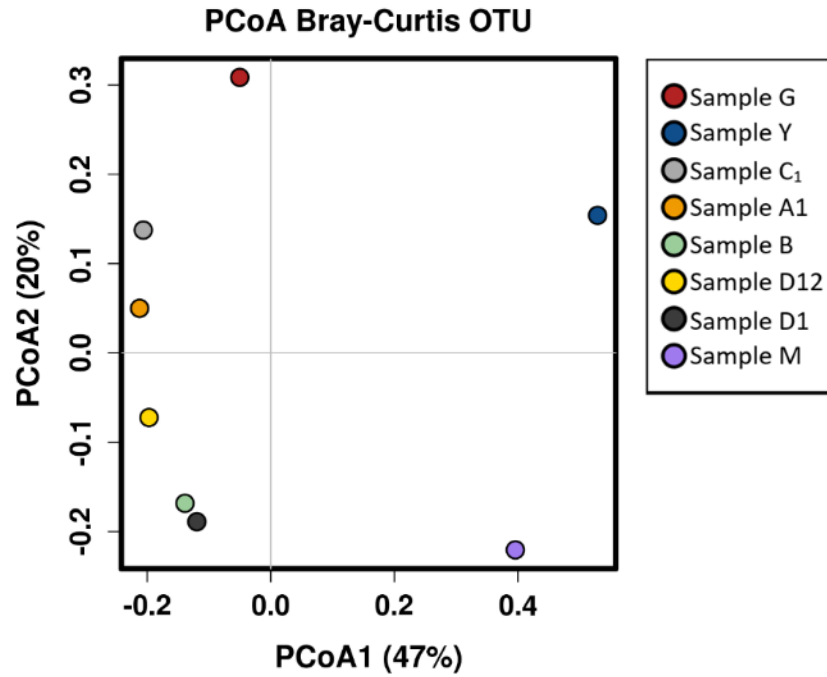
Figure 41: PCA graph of samples A, B, C1, D(1), D(12), M, G, and Y from Escoural Cave.

Indicated in the graphs shown in *figure 42*, *Bacillus* and *Pseudomonas* were the most prevalent genera found in the Escoural Cave samples. Samples D(1), B, and D(12) contained a majority of the *Bacillus* seen. Samples Y and M contain a majority of the *Pseudomonas* seen.

Figure 43, *Bacillus* sp.*, Paenibacillus vortex,* and *Pseudomonas vancouverensis* are shown as some of the most prevalent species found in the Escoural Cave samples.
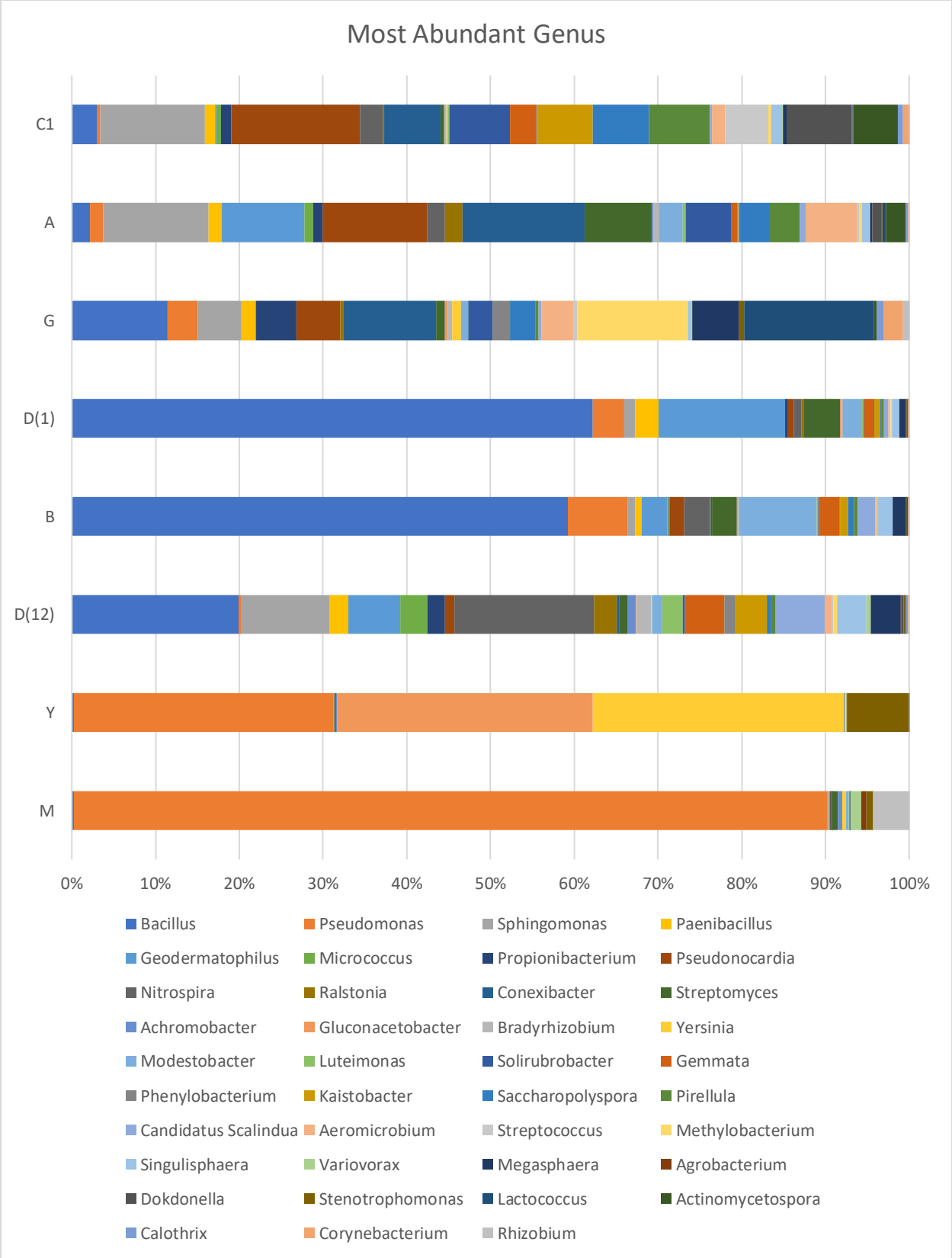
Figure 42: Most abundant genus determined by NGS in Escoural Cave samples A, B, C1, D(1), D(12), M, G, and Y.
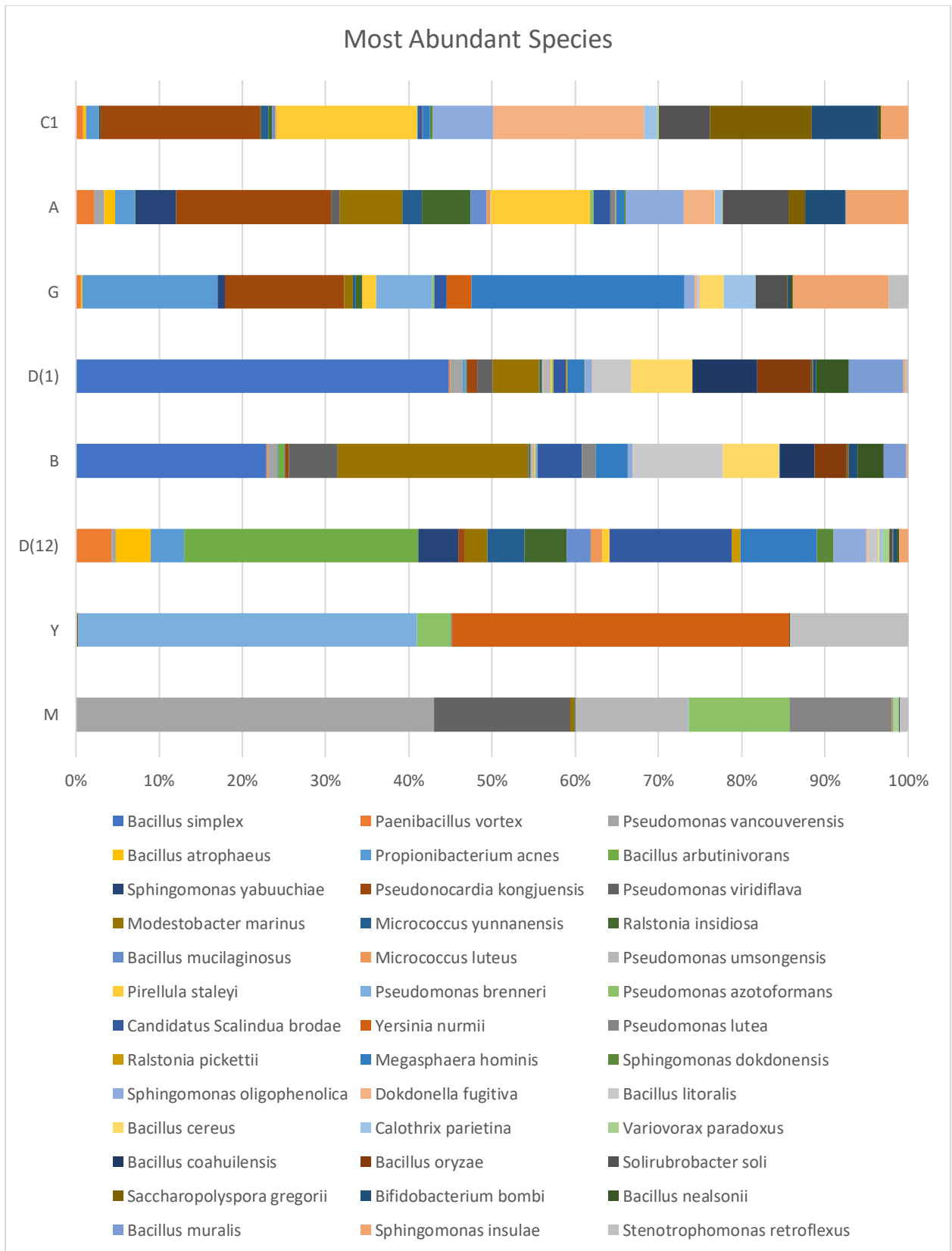
Figure 43: Most abundant species determined by NGS in Escoural Cave samples A, B, C1, D(1), D(12), M, G, and Y.

3.4.3 MICROBIAL RESULTS DISCUSSION

The majority of bacterial isolates identified through culture-dependent methods included the genera of *Bacillus*, *Enterobacter*, and *Pseudomonas;* while the most cultured bacteria species was *Bacillus* sp. All isolates are commonly found in soil and are able to find a natural habitat in hypogeal environments (Gaálová, Donauerová, Seman, & Bujdáková, 2014; Mitova et al., 2015; Yasir, 2017). The *Bacillus* genus is able to form endospores and remain dormant for a long time if suitable nutrients are lacking (Mitova et al., 2015). *Enterobacter* genus are able to survive on wet and dry surfaces and can be a sign of fecal contamination; specifically, the *cloacae* species can be a source of human disease and can cause infections like pneumonia (Hennings, Baumann, Sobottka, Schmiedel, & Klose, 2009) Gaálová et al. (2014) found, while studying microbiota in the Slovakia cave of Domica, that *E. cloacae* is questionable when found in cave environments and can be traced to sources of fecal contamination due to possible bat guano found or infiltration of contaminated livestock fecal runoff from nearby farmland. Lastly, *Pseudomonas* genus are also able to colonize and survive in a wide range of niches due to their metabolic diversity; and again, are commonly found within soil environments (Gaálová et al., 2014). The various cultured fungi isolated from Escoural Cave are also readily found within the soil and rhizosphere environments and can be expected within karstic environments.

Culturing bacteria and fungi is an affordable, however time-consuming method useful for creating isolate samples of certain species found inside Escoural Cave; these isolates can be further stored and placed in cryopreservation for future analysis. Mitigation strategies can be developed and tested on these pure isolates if deemed necessary and then used to further protect the cultural heritage inside Escoural Cave. However, there are also limitations for traditional culturing methods. It is commonly known that only a small fraction of bacteria and fungi are able to be cultured from the original existing diverse ecosystem that the samples originated from (Amann, Ludwig, & Schleifer, 1995; Groth & Saiz-Jimenez, 2010). There are a number of reasons why a species cannot be grown within laboratory settings - possibly the bacteria or fungi are not grown in suitable conditions, or it is possible they have entered into a non-culturable state (Amann et al., 1995). Therefore, it can be assumed that the real amount of biodiversity found inside Escoural Cave or any cultural heritage site is much greater than what was originally identified through traditional culturing methods. As shown above in sections 3.41 and 3.4.2., the total amount of bacterial isolates identified through culture-

dependent methods was only eight distinct genera, while the culture-independent method of NGS was able to sequences 656 different genera from the same samples within Escoural Cave. NGS method is a powerful, extremely fast, however expensive method allowing for the sequencing of large amounts of microbial communities from relatively small sample amounts (Ster et al., 2018).

NGS primers used for sequencing were prokaryotic identifiers and therefore are only used for identification of bacteria and cyanobacteria. Similar to the cultured isolates, the main genera of *Bacillus* and *Pseudomonas* were identified. Other more prevalent genera identified through NGS, that were not isolated through culturing procedures include S*hingomonas* – found in various environments and able to survive under low nutrient conditions (Leys et al., 2004); and *Paenibacillus* – an anaerobic, endospore forming bacteria which is found in soil environments, with the ability to promote biofertilization and act as biopesticides (Grady, MacDonald, Liu, Richman, & Yuan, 2016). The majority phylum of all the samples taken from Escoural Cave and analyzed with NGS were *Actinobacteria* – commonly found in soil and usually unrepresented in cultures, however typically represent a larger total amount of bacteria in samples (Valme Jurado et al., 2010); and *Proteobacteria* – a phylum of bacteria that is typical of nitrogen fixing and contains common pathogenic bacteria, while also processing the ability to thrive at low nutrient levels (Yasir, 2017) (see *appendix 7* for charts depicting different taxonomic regions of each sample analyzed with NGS).

Through the analyses completed at Escoural Cave, from observations of biological outbreaks and results determined from the culture-dependent and culture-independent methods, a few recommendations can be given for the continued promotion of safety – for the rock art itself and the visitors touring the cave – within Escoural Cave. A safety recommendation due to the presence of certain species and genera found inside Escoural Cave, especially due to the presence of *Enterobacter cloacae*, it is recommended to limit hand contact with any objects inside the cave, to avoid contact with the face and mouth, and to wash hands immediately following each visit. For those with compromised immune systems whom are prone to respiratory problems, the wearing of protective face masks is also advised. Furthermore, for protection regarding the rock art inside Escoural Cave, it is recommended that more precautions are taken to reduce human induced organic nutrients that are easily transported by tourists throughout the cave. Safety precautions include the verbal restriction for visitors

not to touch the rock surfaces inside the cave, to limit contact to only handrails when necessary, and a safety precaution of necessary shoe covers for all visitors inside the cave to reduce the transportation of surface nutrients into the cave.

V. CONCLUSION

This research aimed to document the current state of preservation of the 20,000-year-old rock art found inside Escoural Cave, while using only non-invasive methods. The thesis also aimed to determine if two new to rock art analysis instruments, the Specim IQ hyperspectral camera and the Vis-NIR FORS are useful techniques when performing analyses on rock art. Lastly, this research used culture-dependent and culture-independent methods to determine which microbial populations are living inside Escoural Cave and if those microbes were potentially harmful to the rock art inside the cave.

Through the use of multiple imaging techniques, the foremost rock art paintings and engravings in Escoural Cave were successfully documented in their current state of preservation; these imaging techniques were also able to reveal and uncover some of the images in paintings #2, 3, and 7 which are currently hidden to the naked eye due to extreme deterioration and degradation.

Based on optimization of both the Specim IQ hyperspectral camera and Vis-NIR FORS, alongside the creation of specific standards and rock art replications for the construction of a representative database of Palaeolithic pigments and potential binders to supplement the FORS analysis, this research was able to determine that both these instruments are extremely sensitive in nature and require near perfect laboratory conditions for optimal operation; therefore, these methods cannot be fully recommended for use on all rock art research. Those sites with high visibility, limited deterioration or damage, and preferred smooth surfaces may be able to achieve more desirable results.

The Specim IQ hyperspectral camera was able to improve visibility of one highly degraded painting inside Escoural Cave, painting #2. Additionally, results from the Vis-NIR FORS were able to identify pigment chromophores in the visible region and predict correlation between the Escoural Cave paintings and a potential Palaeolithic binder of urine. Important factors to consider when using these instruments include distance from the hyperspectral camera and adequate lighting conditions in order to acquire suitable data of wavelengths. Important factors for the Vis-NIR FORS include consideration of the evenness of the rock support surface, thickness and evenness of painted lines due to the extreme penetrating ability of the IR light source, creation of accurate Palaeolithic databases for comparison of results, and optimal integration time of the instrument in order to obtain the best results.

Results from the microbiological analyses preformed on eight sample locations from Escoural Cave indicate the presence of characteristic soil and subterranean microbial genera and species; however, analyses also uncovered the presence of potential disease carrying microbes i.e. *Enterobacter cloacae* and harmful to rock art biofilms of lampenflora in relatively close proximity to nearby rock art.

Overall, the results from this thesis were significant and enlightening into the extent of deterioration and damage the rock art at Escoural Cave is facing. The research was also able to explore the use of only non-invasive methods in documentation and analysis efforts and the implementation of two instruments that never before have been used for the examination of rock art. The work completed for this thesis will also be able to inform future works at Escoural Cave, especially those aimed at preventive conservation efforts. Lastly, the efforts and results of this thesis will hopefully provide inspiration and encouragement for other researchers and archaeologists to continue the use of non-invasive and non-destructive techniques when they document and analyze rock art in the future.

5.1 FUTURE WORK

As mentioned in the previous section of 1.2.1, many campaigns and analyses have been previously completed in regards to the rock art at Escoural Cave, therefore, future work should continue to maintain innovative and original research. Possible future work could involve the use of newly developed methodology to gain further insight into the cultural heritage at Escoural Cave. Preferably in the future, as this thesis has done, each new campaign held at Escoural Cave would also include allotted time to document the current state of preservation found inside the cave in order to maintain a continuous documentation of any deterioration or damage found on the rock art.

Currently, it is believed that the rock art inside Escoural Cave has been analysed and documented thoroughly since it's rediscovery in 1963 and that any future work on Escoural Cave should aim towards preventive conservation of the rock art. Preventive conservation could range from long term monitoring of temperature, relative humidity, and CO_2 levels inside and outside the cave, to the implementation of stricter regulations for tourists entering the cave. Further work regarding analysis of Palaeolithic binders at Escoural Cave could involve micro-sampling of various paintings in order to chemically analyze the components

and to perform chemical analyses on sample binders, such as urine, to determine if in fact urine was a binding material used on the rock art.

Future work involving microbial analysis could include interest in completing NGS analysis on the same eight sample locations taken for this thesis while using Eukaryotic primers in order to sequence fungi species. Other areas of interest for future work could include fungi air spore analysis in order to determine how fungal strains are spreading throughout the cave. Lastly, future work could include projects to mitigate harmful microfilms that are flourishing inside Escoural Cave; particular interest would be in preventing the growth of the lampenflora found at sample location 'G' in Escoural Cave. The algae growth is a clear result of the artificial illumination residing nearby to the rock's substrate. Possibly mitigation strategies could involve removing the nearby lighting fixture or investigating the use of varying wavelengths for the reduction or elimination of the lampenflora found there; for example, blue light emission at 460 nm has been found to successfully limit the growth of phototrophs (Mulec & Kosi, 2009; Saiz-Jimenez, 2014).
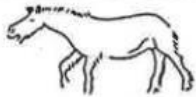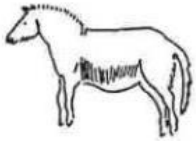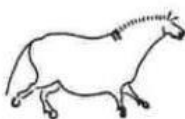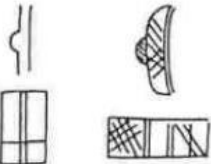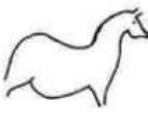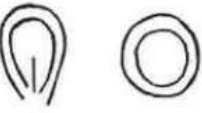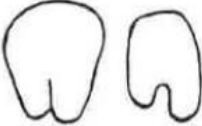
Overall, there is much potential for future analyses to be carried out in Escoural Cave, whether efforts are intended to mitigate harmful biofilms or efforts to deeper understand the artistic techniques behind the binders and pigments used in Escoural Cave.

APPENDICES

View from original southeast facing entrance of Escoural Cave where evidence of a Neolithic settlement remains.

PERIODE	STYLE	CHEVAUX	FIG. HUM^{nes}	SIGNES

The stylistic evolution of Palaeolithic rock art. (Adapted from Gourhan A. L. in Roteiros da Arqueologia Portuguesa 4; Gruta do Escoural, 1995). The chart shown above depicts the stylistic progression of the chronology of rock art in Palaeolithic Europe. Rock art begins in the earliest Aurignacian period 30,000 BCE where depictions of simplistic animal figures appear alongside symbolistic abstract forms. Next, during the Gravettian period of 25,000 BCE, the figures have evolved to include anthropomorphic representations with more detail. The illustrations continue to the Solutrean art of 20,000 BCE where illustrations are more details and representative of the figures, while also introducing geometric designs. Lastly Magdalenian period of 15,000 BCE achieves the most realistic depictions of animal and human forms.

(Scale is in 5cm increments.)

Images (A) and (B) were taken prior to 2010 when a campaign was undertaken through a partnership between the Directorate Regional Culture of Alentejo and the Cabinet of Archaeology and Heritage Management Culture (GAEM) to improve the state of conservation at Escoural Cave, while also working to improve the visualization of the paintings found within the cave (Barquín, 2015). Image (C) represents the geometric motif today. There is a strong debate whether cleaning calcite crusts from rock art do more harm than good ("Documentation and Conservation of Rock Art," n.d.; Whitley, 2001). Although the complete paintings can be revealed by removing calcite crusts, the potential to remove fragile pigments attached to the said crusts is also very high. Coatings that form over paintings, whether calcium carbonate, lichens, or fungi can sometimes act as a protective layer for the rock art; although they are slightly covered, a crust can help stabilize a deteriorating surface of the supporting rock.
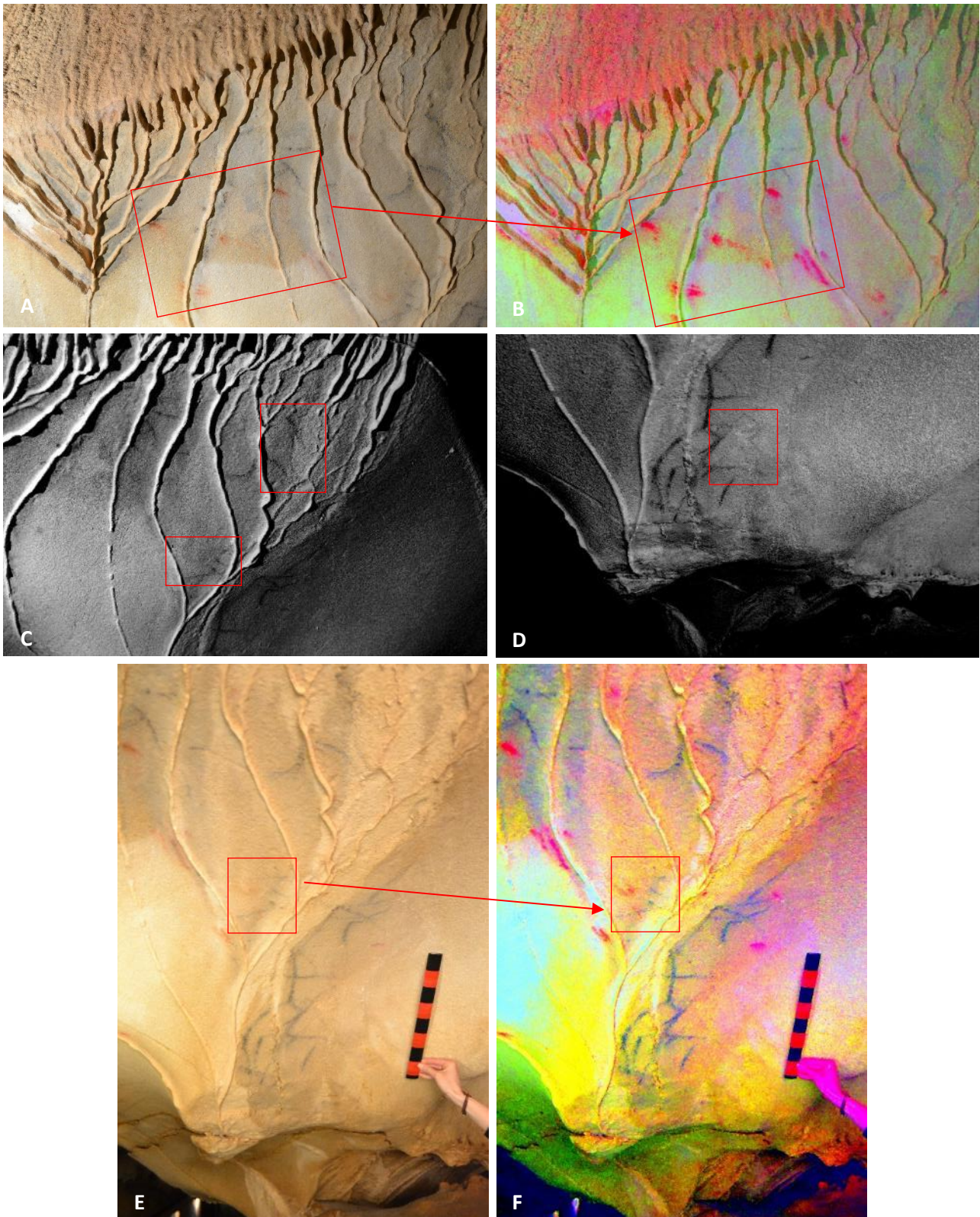
PAINTING #1

Figure 1: Letters A-F represent the complete panel of painting #1.(A) Visible light photograph compared with (B) matching DStretch photograph using colorspace YBR applied at 10% scale; (C-D) IR photography with 780nm filter; (E) visible light photograph compared with (F), matching DStretch photograph using colorspace YDS at 25% scale.

Displayed above in figure 1 of this appendix, are the various imaging techniques employed on painting #1 in Escoural Cave. (A) is the visible light photograph of the upper part of the panel, while in image (B) we have the same photo altered with DStretch software using the YRB colorspace at 10% scale; visible is potentially the underbelly, front, and back leg of a mammal. Therefore, it is possible to suggest a red Bovidae or Equidae figure was once painted in this location, however is no longer visible due to the loss of pigment from the leaching processes occurring and the calcite vein formation on top of it. In photos (C-D), IR photography helped establish hidden features painted with carbon-based pigments that are difficult to see with the naked eye. In (C), the tail and rear end of the Equidae figure can be seen and a new shape is also seen in the lower half of the panel; while in (D) another possible figure emerges. Lastly, photos (E-F) show the visible light and corresponding photo altered with DStretch to enhance not only the black pigments but also the red pigments within the panel. See *figure 11* for full photogrammetry view of painting #1. Additionally, the Specim IQ hyperspectral camera was used on this painting, however, the resulting hyperspectral image did not produce any valuable results.

PAINTING #4

Figure 2: Letters A-C represent the complete panel of painting #4. (A) Visible light photography; (B) DStretch software applied with colorspace LDS at 10% scale; (C) Original sketch of panel by by Manuel Farinha dos Santos in 1963 (Adapted from Araújo C.A., Lejeune M., Gruta do Escoural: Necrópole Neolítica e Arte Rupestre Paleolítica, 1995).

The above photographs in figure 2, are from the panel of painting #4. Due to the location of this painting, only a few imaging techniques could be applied. Not only is the painting large, roughly 1 meter in length, the rock wall containing the painting is about 2.5 meters from the stable walkway. Photograph (A), again shows the extremely limited appearance of the painting due to the calcite that is forming on the rock's surface; (B) is the DStretch altered photograph in which the Equidae figure can be made out, along with other red pigments that appear. However, two large red pigment spots appear to have spread down the painting as a result of the calcite leaching; (C) is the original sketch depicted by the archaeologist, André Glory. The hyperspectral camera was placed too far away and the resulting photographs could not identify pixels with much accuracy. IR photography could not reveal any additional information either.

PAINTING #5
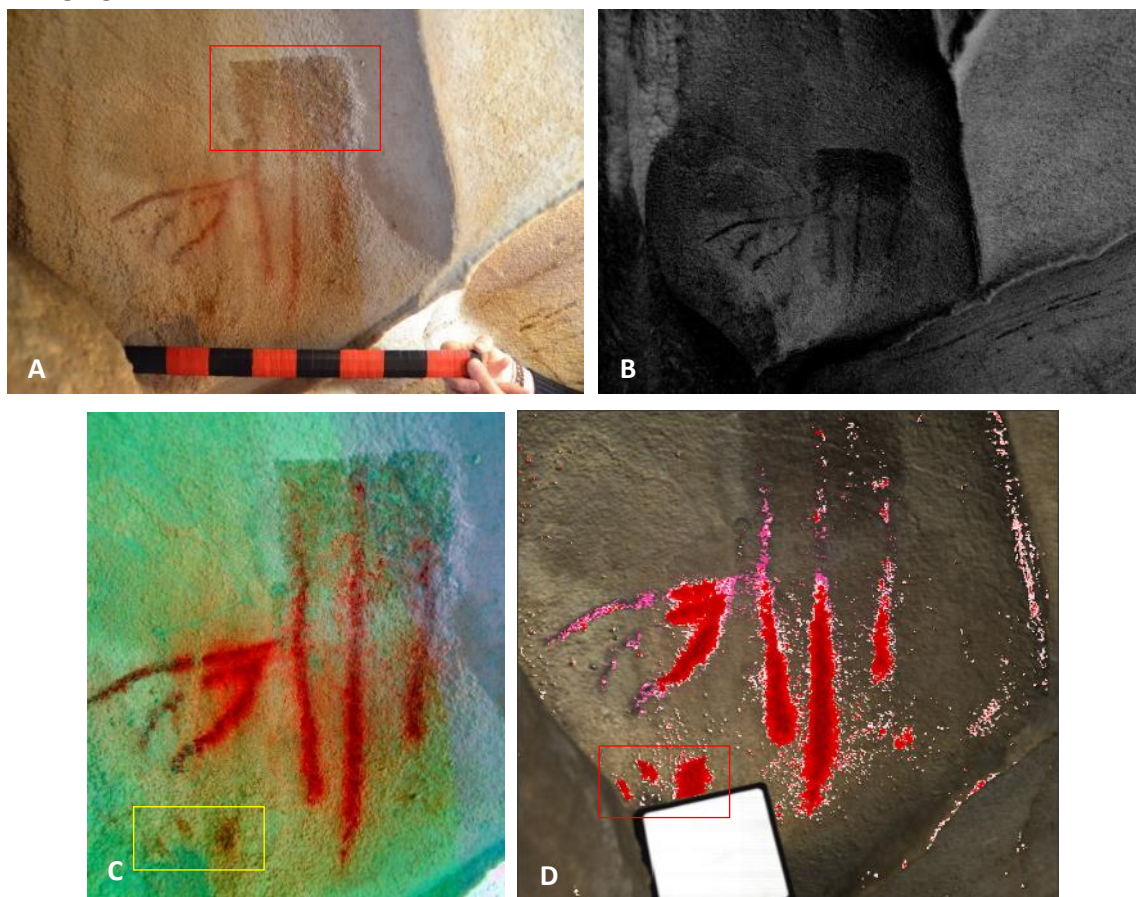
Figure 3: Letters A-D represent the complete panel of painting #5. (A) Visible light photography; (B) IR photography with 780nm filter; (C) DStretch software applied with colorspace LRB, auto color balance, and auto contrast at 7.5% scale; (D) Hyperspectral image from Specim IQ studio.

Shown above in figure 3, is the panel representing painting #5. This painting is unique within Escoural Cave as it is the only painting with attempted calcite removal; as mentioned in

appendix 2, during a previous campaign in 2010-2012, efforts were made to clean a portion of the calcite covering this geometric painting. Photograph (A) is a visible light photograph, marked with a red box is the location of the calcite removal. (B) is an IR photo in which the painting can be seen, however it does not reveal any more than the visible photo. (C) is a photograph altered by DStretch in which the three vertical lines can be seen continuing into the cleaned calcite region; (C) has also enhanced the three red dots found in the lower left corner of the painting. Lastly, (D) is the hyperspectral results from the Specim IQ studio, however, the results do not reveal any more than those seen from the DStretch photograph.

PAINTING #6
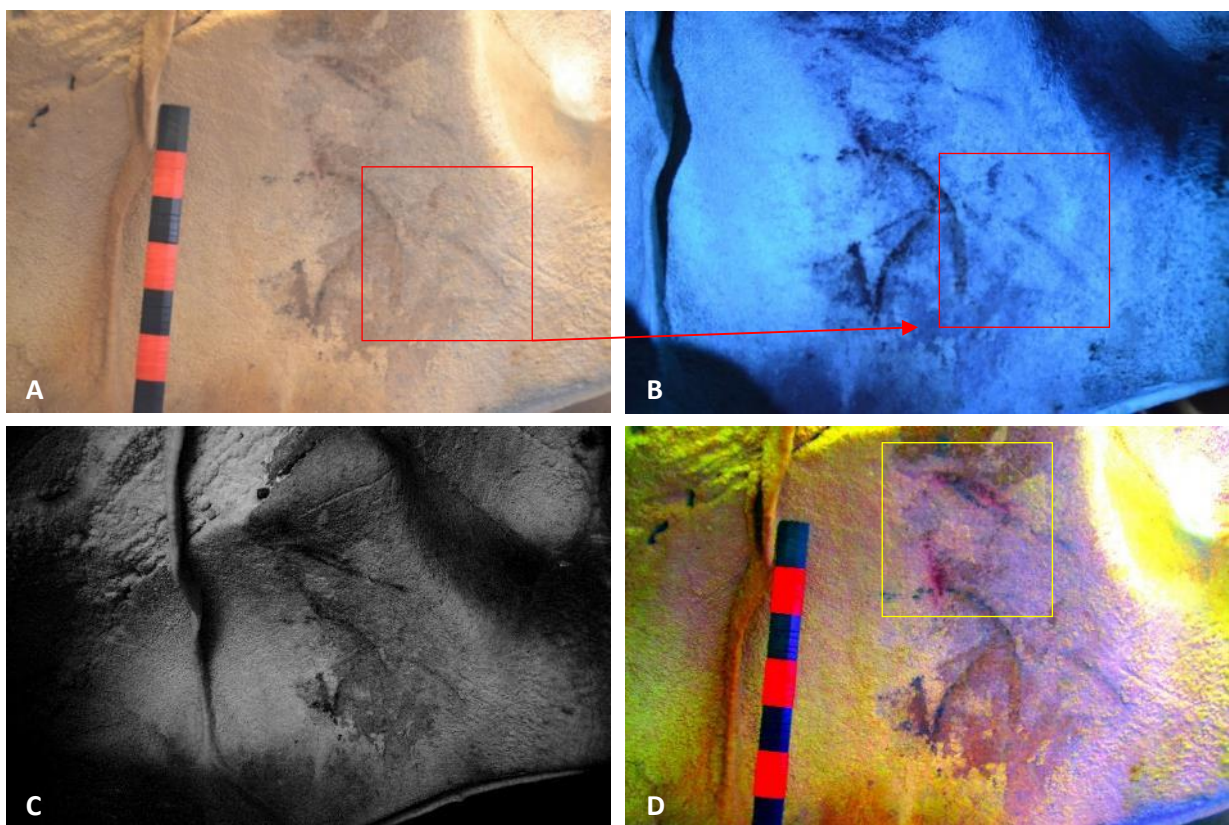
Figure 4: Letters A-D represent the complete panel of painting #6. (A) Visible light photography; (B) UVF photography; (C) IR photography with 780nm filter; (D) DStretch software applied with colorspace YRB, auto color balance, and auto contrast at 20% scale.

Above in figure 4, are the various imaging techniques employed on painting #6 in Escoural Cave. Photograph (A) is taken in visible light where three figures, possibly the rear end of an Equidae animal, the upper torso and neck of a Bovidae, and the head of another Bovidae can be made out depending upon the lighting and the precipitation within the cave. A prominent, well covering calcite crust can be seen covering parts of the painted panel. (B) is a photograph in using UVF - although not fluorescing, the third figure can be seen more clearly as a head of

a Bovidae. (C) a photograph in IR was not able to see under the thickly laid calcite crust. (D) is a photo altered with DStretch software in which the third figure of the Bovidae head is again, more clearly seen, while the top most figure is nicely enhanced. Hyperspectral imaging was not able to produce a quality image based on matching wavelengths.

PAINTING #7
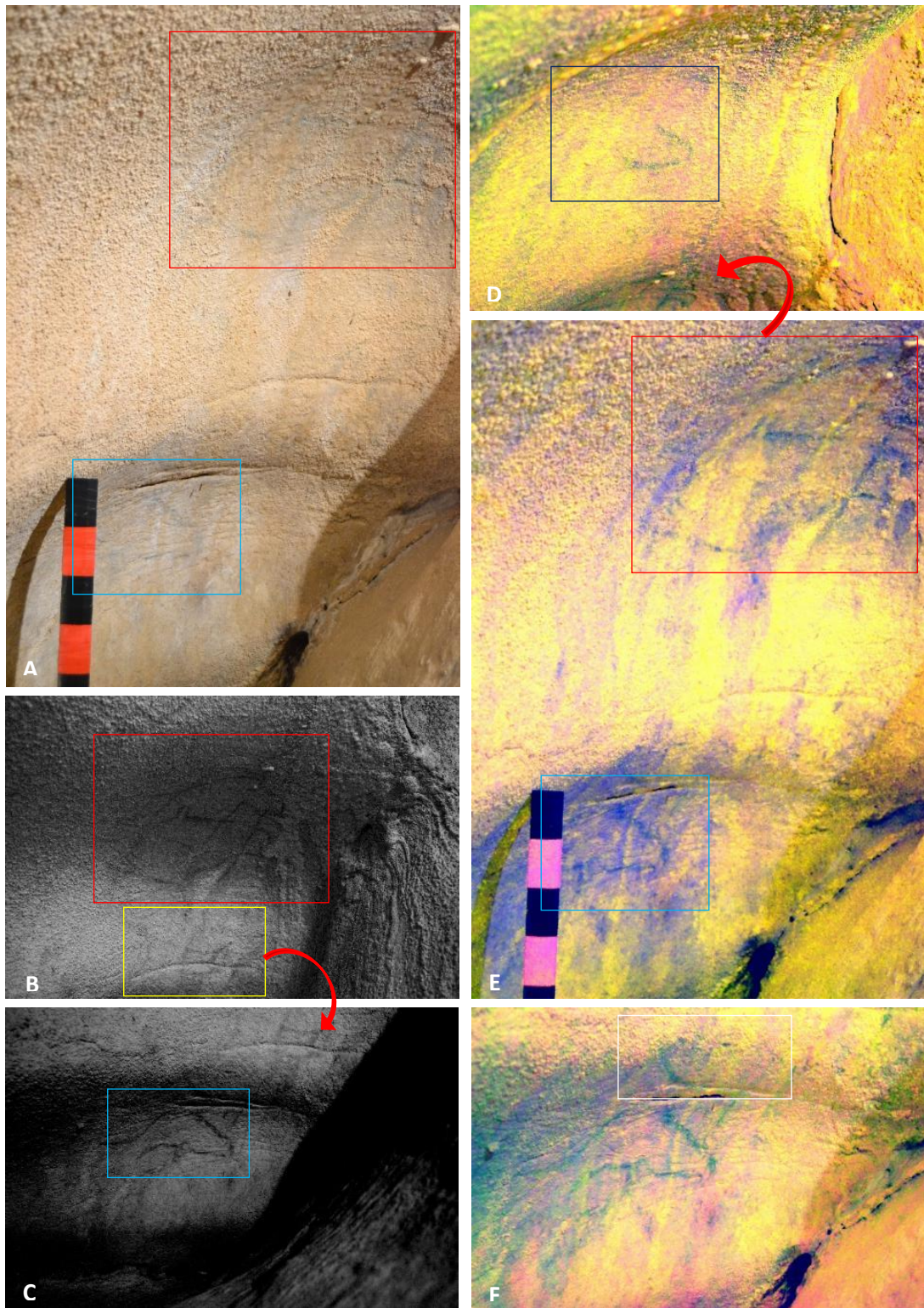
Figure 5: Letters A-H represent the complete panel of painting #7. (A) Visible light photography; (B-C) IR photography with 780nm filter; (D) DStretch software applied with colorspace YBK and auto contrast at 5% scale; (E) DStretch colorspace YBK at 12.5% scale; (F) DStretch colorspace YBK and auto contrast at 10% scale.
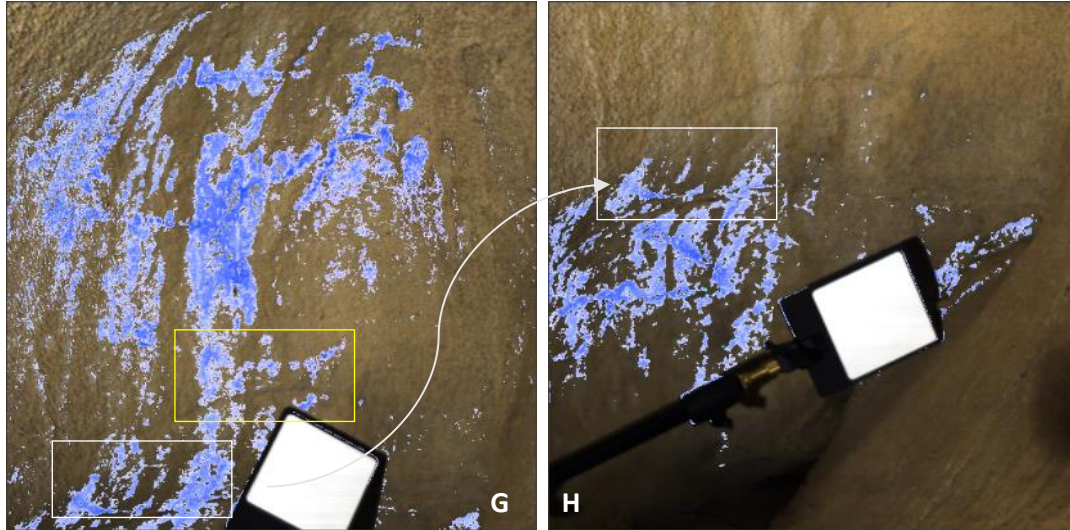
Figure 5(continued): (G-H) Hyperspectral image from Specim IQ studio (Painting #7).

Above in figure 5, are the various imaging technique results from painting #7. Photograph (A) is from visible light photography. As this painting is very difficult to see, the main figures have been highlighted with corresponding matching colored boxes. Photos (B) and (C) are both from IR photography and begin to reveal the hidden paintings. Overlapping Equidae heads can be seen in the upper half of (B), while the lower half resembles a small mammal, perhaps of the Bovidae family. The IR results for photo (C) can be shown to reveal another possible Equidae head. Photos (D-F) are altered with the DStretch plugin and depicts similar results to the IR photographs; however, an additional curved line, possibly a belly, of another Equidae can be seen above the lower Equidae head in photo (F); in photo (D) an additional head can be spotted with the alterations from DStretch. Lastly, photos (G-H) are from the hyperspectral Specim IQ studio; these photos reveal similar results to the IR and DStretch photographs.

PAINTING #8

Figure 6: Letters A-B represent the complete panel of painting #8. (A) Visible light photography; (B) Hyperspectral image from Specim IQ studio.

Figure 6 shows photos of the final painting, #8, analyzed at Escoural Cave. (A) is a visible light photo of an unknown figure. The majority of techniques used on this painting could not enhance it any further than the original visible light. (B) is a hyperspectral image from the Specim IQ studio which, as seen above, does not reveal any further details of painting #8.

ENGRAVNIGS #1E-4E

Raking light photography technique used on all engravings analyzed for this thesis at Escoural Cave did not reveal any new hidden elements of the rock art. The location and surrounding unevenness of the rock surface for most of the engravings analyzed were not ideal and proved extremely difficult to capture a proper raking light photograph (figure 7). Lighting positions of halogen lamps and tripod stabilization were difficult to set up in the confined positions determined by the location of the engravings. Engravings are best seen in the 3D models created.

Figure 7: Raking light photograph of engraving #1E.

Standards were created for calibration of the BWTEK i-Spec 25 Vis-NIR FORS detectors and for the creation of a spectral database to confirm field point analysis results. Research of traditional Palaeolithic rock art pigments and binders was conducted to determine which pigments, binders, and quantities would be best suited for the replication (Gay et al., 2016; Olivares et al., 2013; Ontañón, 2014; Rogerio-candelera, 2015; Smith, 2014). Previous research conducted at Escoural Cave in 2016 with pigment micro-sampling and EDXRF, weighed considerably into the decision of which pigments to use as well (Mauran, 2016).

Vis-NIR FORS investigations were conducted to determine whether or not the detectors could identify characteristic bands of Palaeolithic binders in the resulting spectra. These investigations were conducted through the use of reproductions created in a laboratory setting. The reproductions included various Palaeolithic pigments mixed with various Palaeolithic binders (see table 1). All colorants were painted in a ratio of 80% binder, 20% pigment for reproducibility; although, authentic Palaeolithic paint recipes are not believed to have followed a specific ratio. Reproductions were painted on substrates of various mediums including parchment paper, limestone, and glass slides (see figures 1-2).

Results from the various investigations determined that firstly, the Vis-NIR FORS was able to identify characteristic pigment bands in the visible range, but could not differentiate binders in the NIR range. Secondly, the resulting spectra were highly influenced by the substrate material which the reproductions were painted on.

Due to the results acquired from the laboratory investigations, efforts to reveal the possible binder spectra continued with the help of PCA. Binders alone were thickly painted on glass slides and allowed to dry for one day. Spectra were taken of the binders on glass and of the glass without a binder present, converted to TXT, and transferred to MATLAB. Using a set of mathematical equations, the standard deviation of all glass spectra was subtracted from the standard deviation of all binder on glass spectra and then plotted using a Savitzky–Golay smoothing with order=2 and framelen=7 [4]. Results showed that each binder contained a distinct spectrum but was found in extremely low levels of absorbance (see figure 3). All

---

[4] MATLAB calculations to subtract glass medium background from spectra with binder was devised by Silvia Bottura PhD. Candidate.

spectra of Palaeolithic binders subtracted from glass medium were converted to TXT for PCA and calibrated against the spectra from Escoural Cave.

CATEGORY	COLORANT/ BINDER	REFERENCE
RED PIGMENT	Red Ochre	Kremer 40090
	Cinnabar (Mercury (II) Sulfide)	Aldrich 243566-50G
YELLOW PIGMENT	Yellow Ochre	Kremer 40010
BLACK PIGMENTS	Charcoal (Beech)	Kremer 47800
	Bone Black	Kremer 47100
	Manganese Oxide	Local Pyrolusite (powdered)
BINDERS	Arabic gum	
	Parchment glue	
	Saliva	
	Lime water	
	Chicken Blood	
	Human Blood	
	Urine	
	Bone marrow	

Table 1: List of pigments and binders analysed for the spectral database.
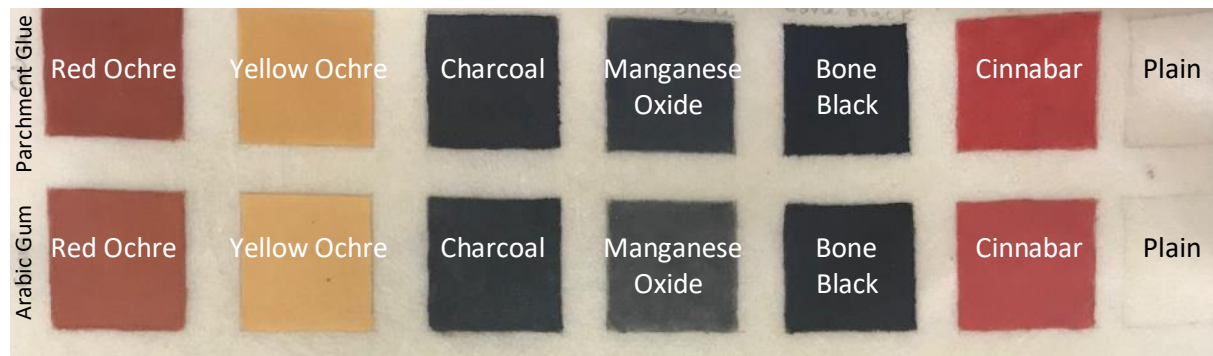
Figure 1: Reproduction of Palaeolithic pigment and binders on parchment paper.
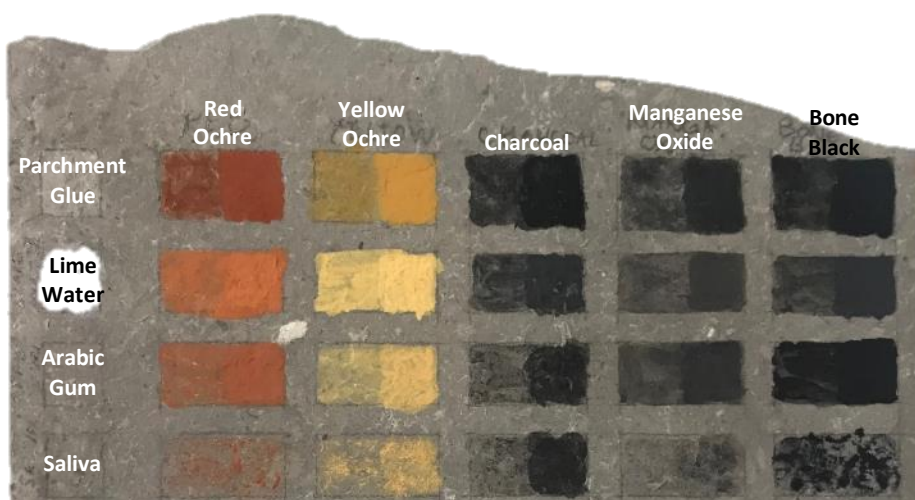
Figure 2: Reproduction of Palaeolithic pigment and binders on limestone.
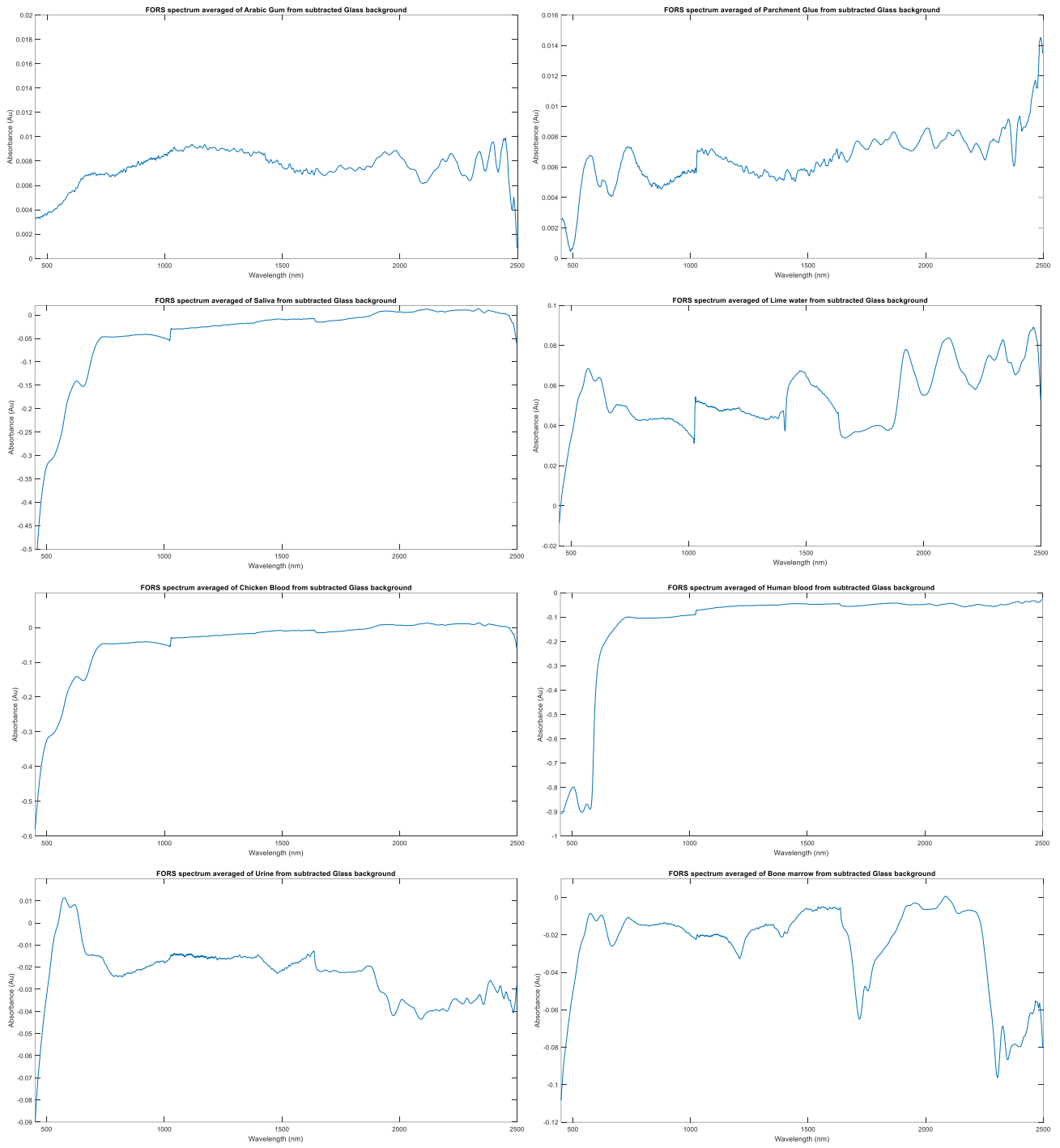
Figure 3: Spectra of Palaeolithic binder subtracted from glass medium. Smoothed with Savitzky–Golay.

Appendix 5

Below are the Vis-NIR FORS and EDXRF point analysis locations for each painting analyzed with these techniques. 3-5 points were taken at each location for reliability and representative sample results. White dots represent a limestone point, red dots represent a red pigment point, black dots represent a black pigment point.

Painting #1 (Main)

Painting #2 (Bird)

Painting #5 (Lines)
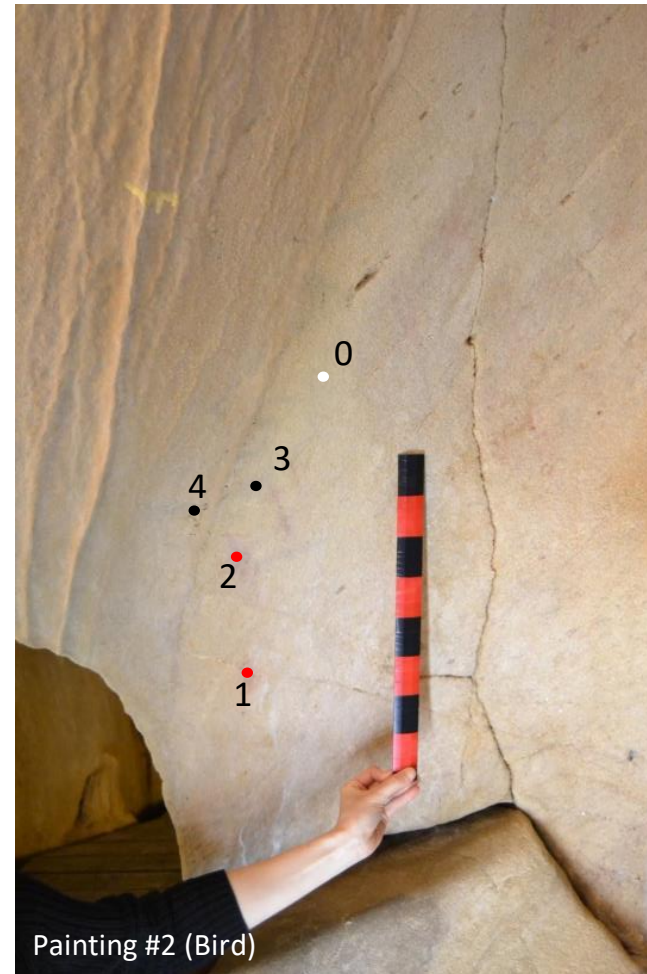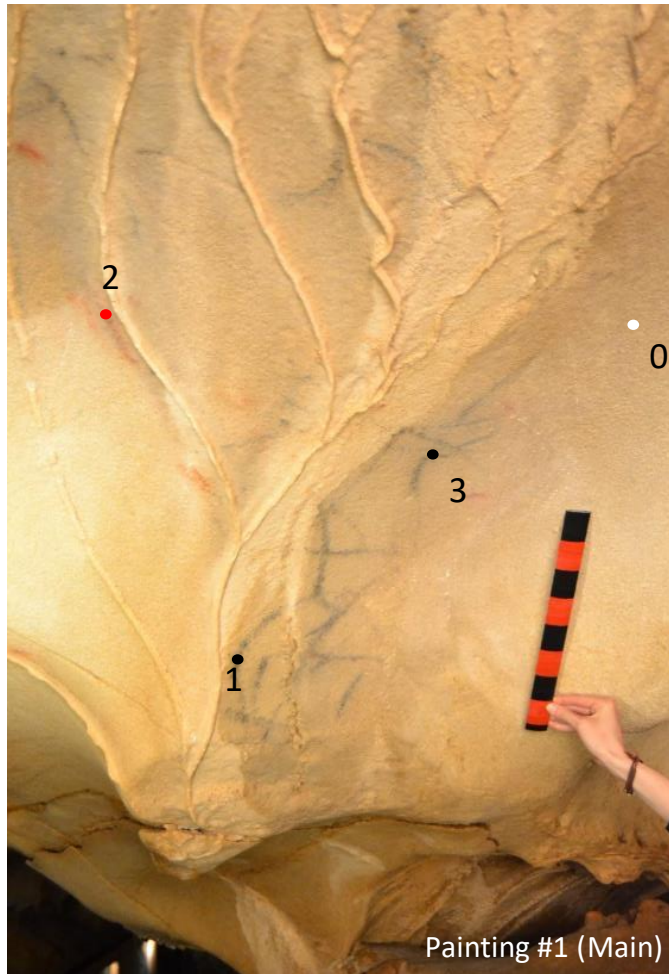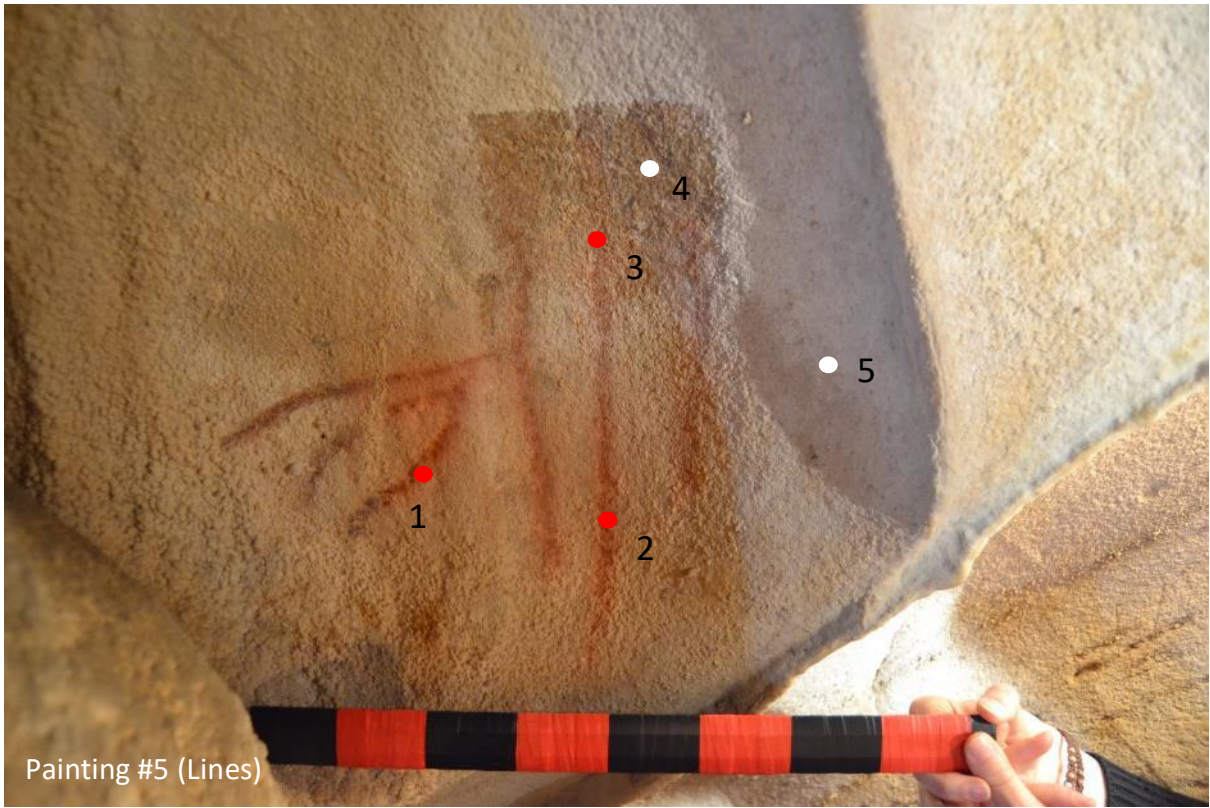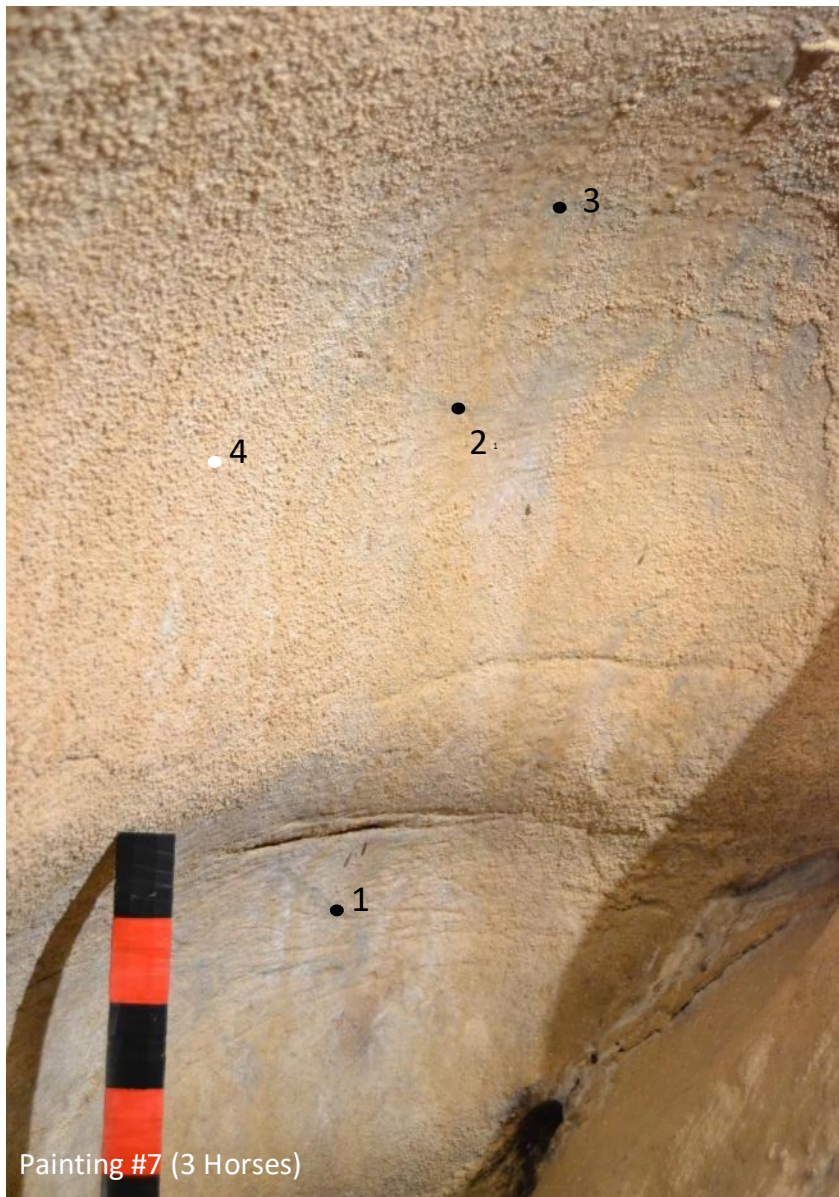
Painting #6 (MM)

Painting #7 (3 Horses)
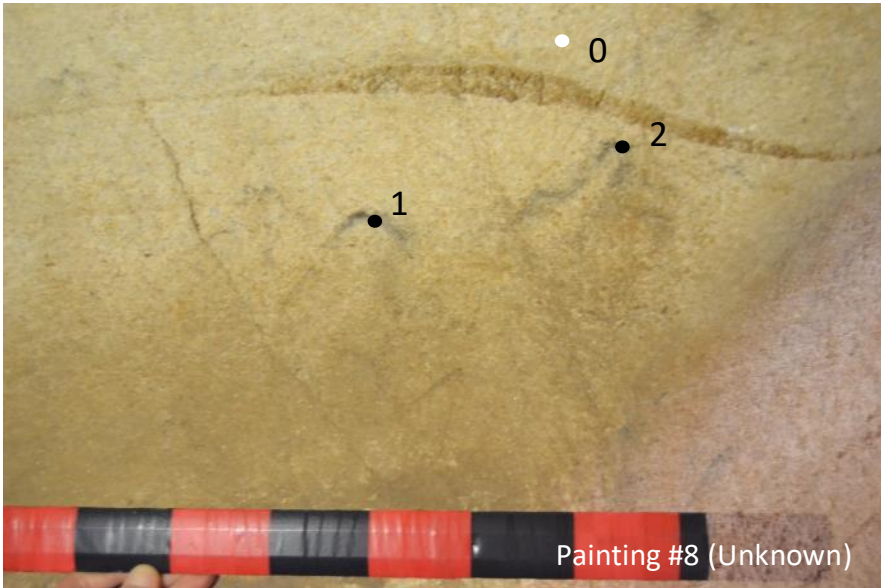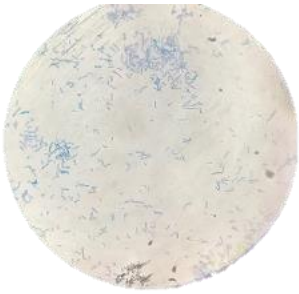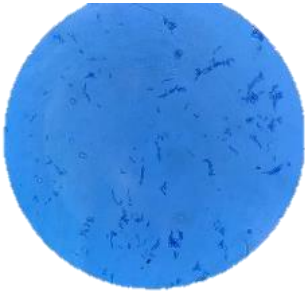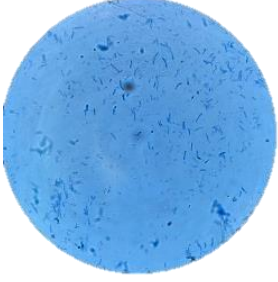
Painting #8 (Unknown)
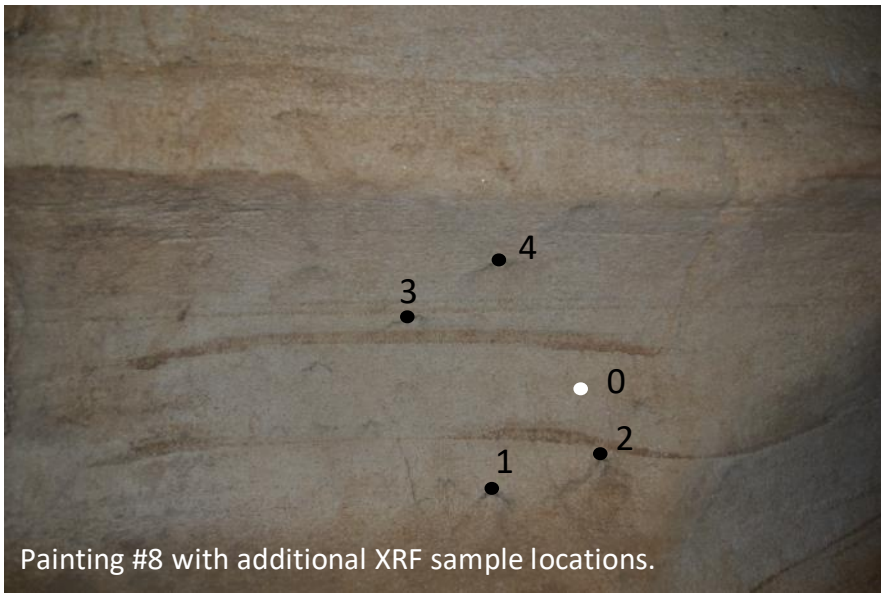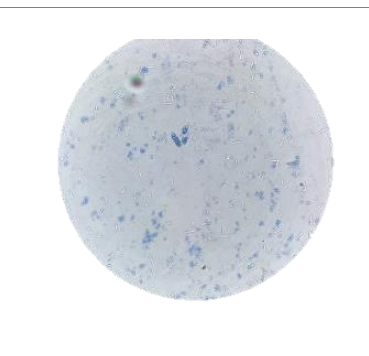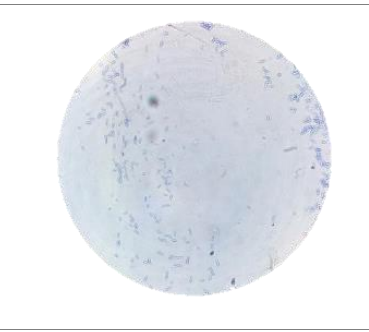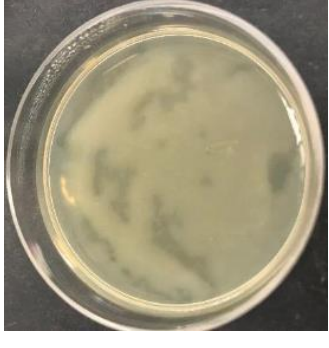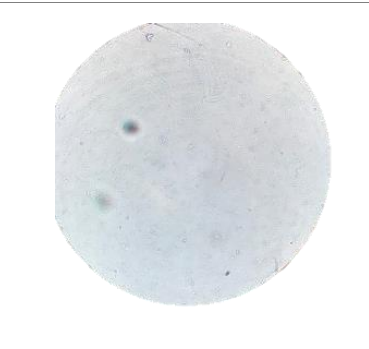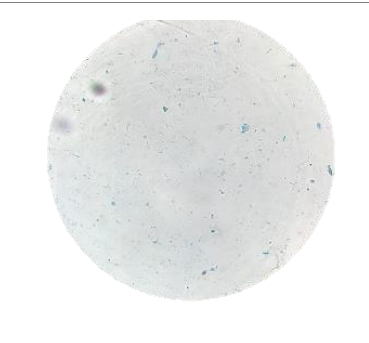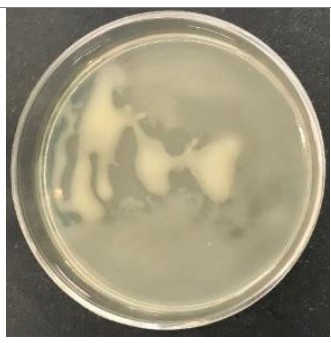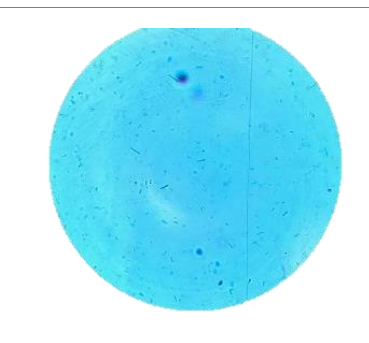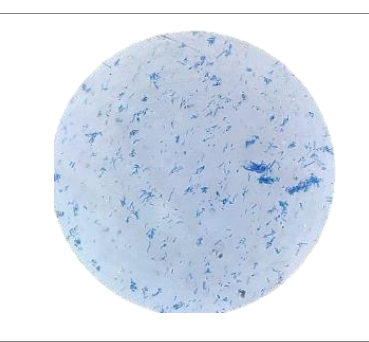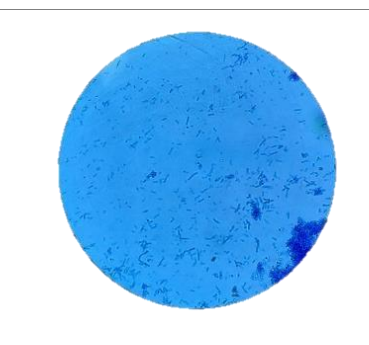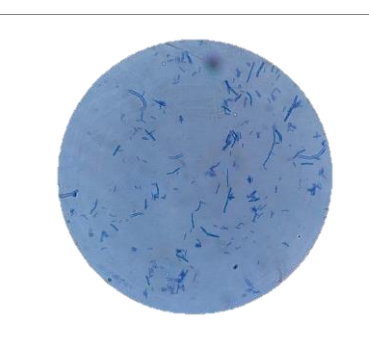
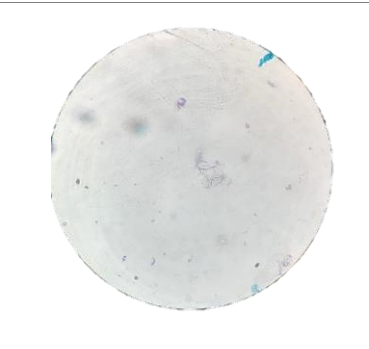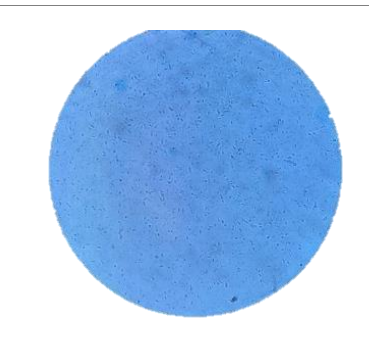Painting #8 with additional XRF sample locations.
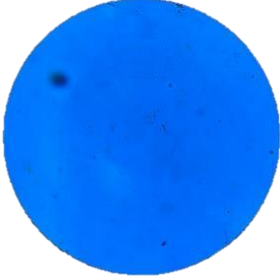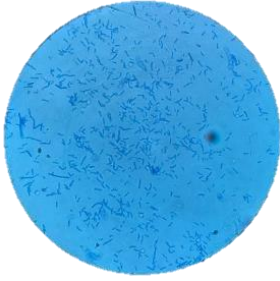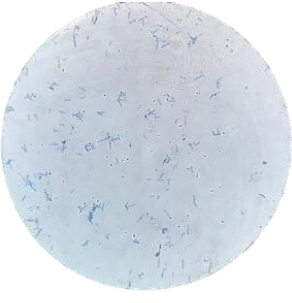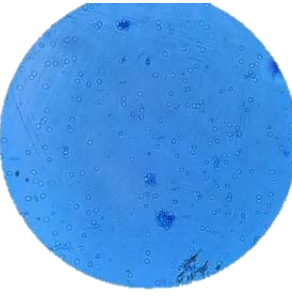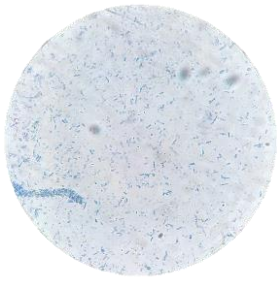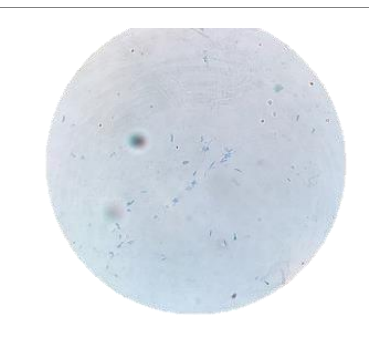
The remaining 27 of 28 bacteria isolates from Escoural Cave using culture-dependent methods.
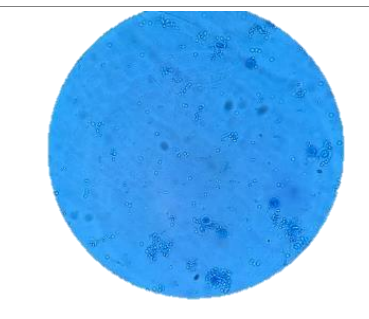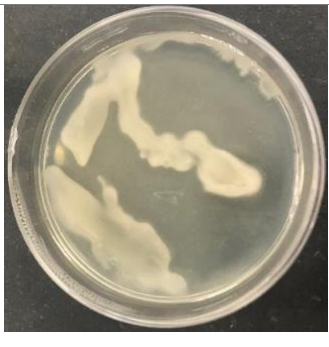
Strain	Genus	Macroscopic features	Microscopic features (100x)
A1-1	*Bacillus sp.3*		
A1-2	*Bacillus sp.13*		
A1-2--2	*Stenotrophomonas sp.1*		
A3-1	*Bacillus sp.2*		

$\underline{A}_{100}$-1	*Solibacillus sp.1*		
$\underline{A}_{100}$-2	*Bacillus sp.1*		
$\underline{A}_{1.100}$-1	*Streptomyces sp.1*		
$\underline{B}$1-1	*Enterobacter sp.2*		
$\underline{B}$3-1	*Enterobacter sp.4*		

$\underline{B}_{100}$-1--2	*Enterobacter sp.3*		
$\underline{C}_1$.1-1	*Bacillus sp.10*		
$\underline{C}_1$.2-1	*Bacillus sp.8*		
$\underline{C}_1$.3-1-1	*Bacillus sp.12*		
$\underline{C}_1$.3-1-2	*Bacillus sp.11*		

$\underline{C}_1$.4-1	*Bacillus sp.4*		
$\underline{C}_1$.4-2	*Bacillus sp.15*		
$\underline{C}_{1.100}$-1	*Bacillus sp.14*		
$\underline{C}_2$.1-1	*Bacillus sp.6*		
$\underline{C}_2$.2-1	*Bacillus sp.9*		

$\underline{C}_2.3\text{-}1$	*Bacillus sp.5*		
$\underline{C}_{2.100}\text{-}1$	*Bacillus sp.7*		
$\underline{D}1\text{-}1$	*Acinetobacter sp.1*		
$\underline{D}1\text{-}2$	*Stenotrophomonas sp.3*		
$\underline{D}2\text{-}2$	*Stenotrophomonas sp.2*		

D3-2	*Pseudomonas sp.3*		
D3-1-1	*Lysinibacillus sp.1*		
D100-1	*Pseudomonas sp.1*		
D100-2	*Pseudomonas sp.2*		

Pie charts depicting different taxonomic regions of each sample analyzed with NGS in Escoural Cave.

G

B

D(1)

112

D(12)

M

vancouverensis

Other
Pseudomonas

Unclassified
Pseudomonas

Bacteria
Proteobacteria
Gammaproteobacteria
Pseudomonadales
Pseudomonadaceae
Pseudomonas

Other
Bacteria

Alphaproteobacteria

Proteobacteria

Bacteria

Firmicutes

Bacilli

Bacillales

Actinobacteria

Actinobacteria

Actinomycetales

Y

Unclassified
Gluconacetobacter

Gluconacetobacter

Bacteria

Proteobacteria

Enterobacteriales

Enterobacteriaceae

Gammaproteobacteria

Yersinia

nurmii

Pseudomonadales

Pseudomonadaceae

Pseudomonas

brenneri

113

WORKS CITED

Agnew, N., Deacon, J., Hall, N., Little, T., Sullivan, S., & Tacon, P. (2015). *Rock Art; A cultural treasure at risk A cultural treasure at risk*.

Alberti, R., Fiorini, C., Guazzoni, C., Klatka, T., & Longoni, A. (2007). Elemental mapping by means of an ultra-fast XRF spectrometer based on a novel high-performance monolithic array of Silicon Drift Detectors. *Nuclear Instruments & Methods in Physics Research*, *580*, 1004–1007. https://doi.org/10.1016/j.nima.2007.06.056

Amann, R. I., Ludwig, W., & Schleifer, K. (1995). Phylogenetic Identification and In Situ Detection of Individual Microbial Cells without Cultivation. *American Society for Microbiology*, *59*(1), 143–169.

Araújo, A. C., & Gomes, M. rio V. (n.d.). *Gruta do Escoural - Arte Parietal*. Lisboa: Instituto Português do Património Arquitectónico.

Balas, C., Epitropou, G., Tsapras, A., & Hadjinicolaou, N. (2018). Hyperspectral imaging and spectral classification for pigment identification and mapping in paintings by El Greco and his workshop. *Multimedia Tools and Applications*. https://doi.org/10.1007/s11042-017-5564-2

Barquín, R. M. (2015). Estudio ambiental y medidas de conservación preventiva de las manifestaciones rupestres de la gruta de Escoural (Alentejo , Portugal). Actuaciones 2010-2012. *Almansor - Revista de Cultura*, *3*(1), 9–13.
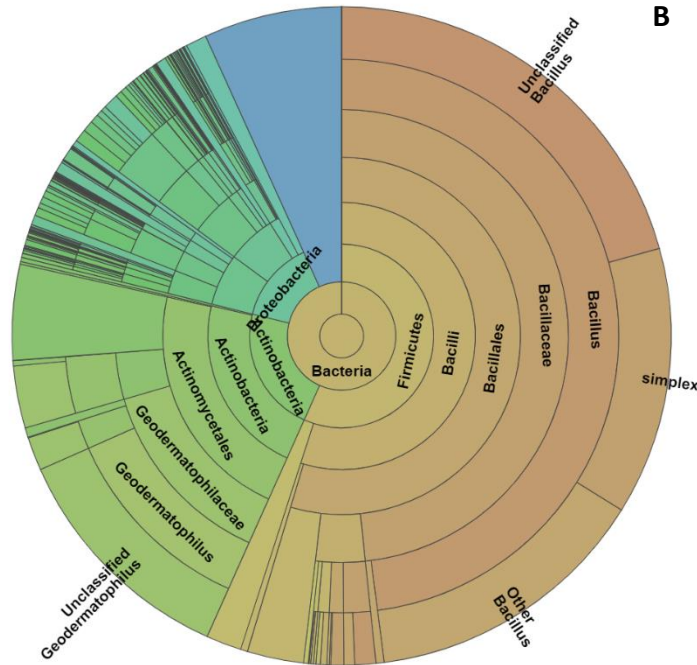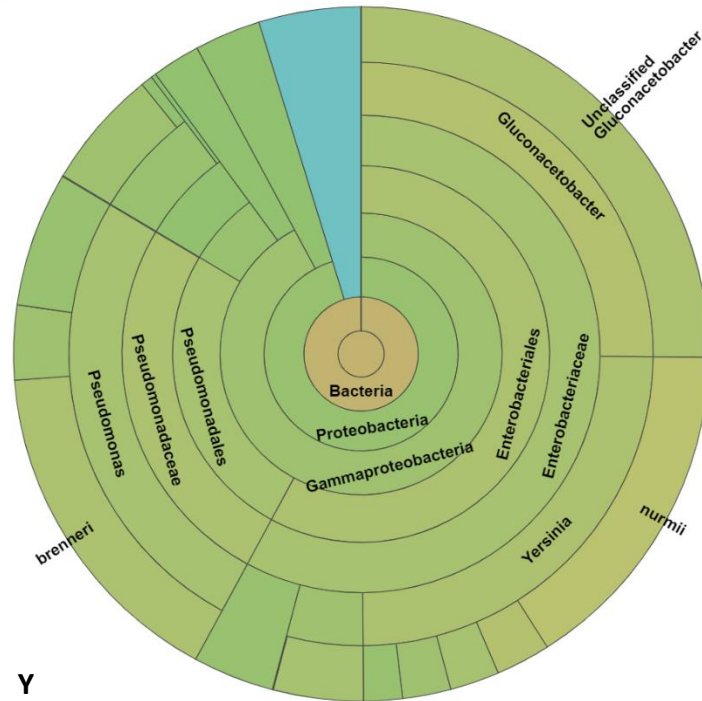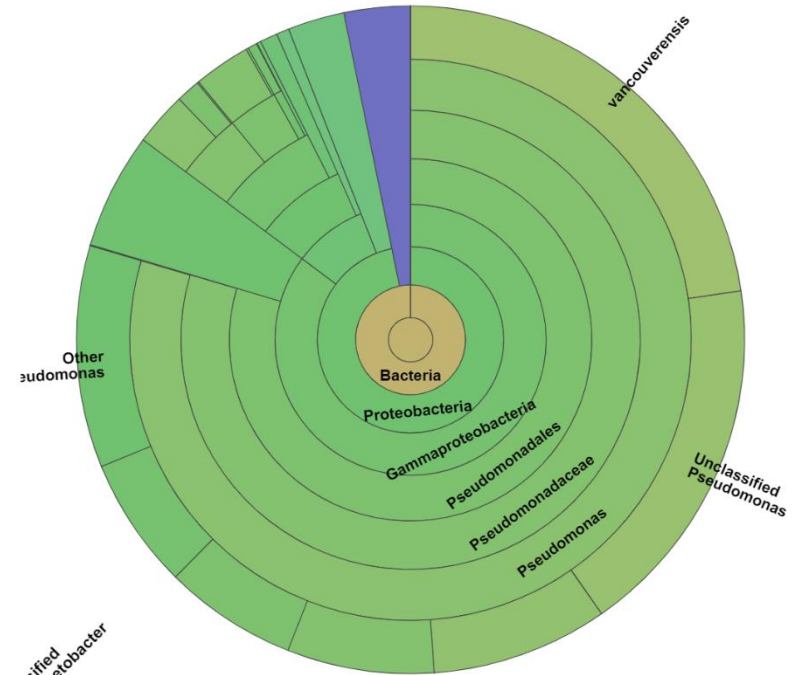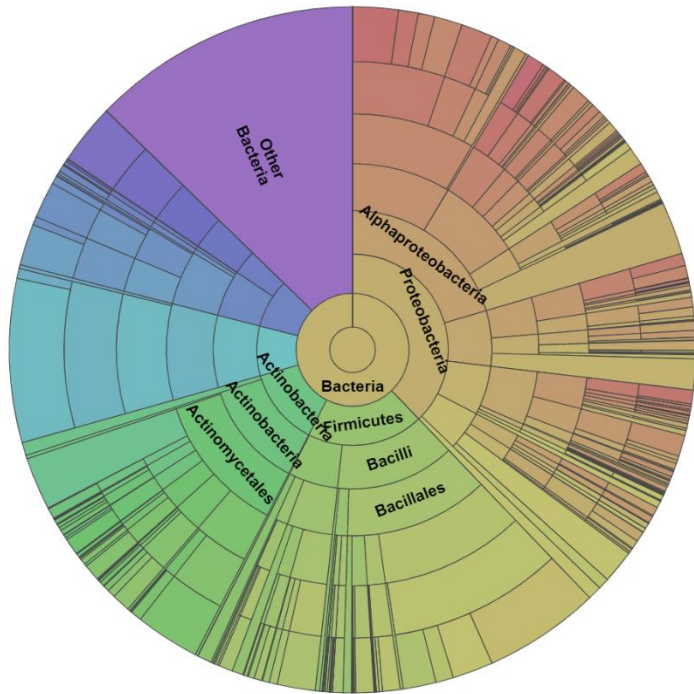
Bicho, N., Carvalho, A. F., Gonz, C., & Sanchidri, J. L. (2007). The Upper Paleolithic Rock Art of Iberia. *Journal of Archaeological Method and Theory*, *14*(1). https://doi.org/10.1007/s10816-007-9025-5

Bonifazi, G., Capobianco, G., Pelosi, C., & Serranti, S. (2019). Hyperspectral Imaging as Powerful Technique for Investigating the Stability of Painting Samples. *Journal of Imaging*. https://doi.org/10.3390/jimaging5010008

Bonizzoni, L., Caglio, S., Galli, A., & Poldi, G. (2008). A non invasive method to detect stratigraphy , thicknesses and pigment concentration of pictorial multilayers based on EDXRF and vis-RS : in situ applications. *Applied Physics A- Materials Science & Processing*, *210*, 203–210. https://doi.org/10.1007/s00339-008-4482-6

Brandshaw Foundation. (n.d.). The Cave Art Paintings of the Chauvet Cave. Retrieved April 27, 2019, from http://www.bradshawfoundation.com/chauvet/megaloceros.php

Cavaleri, T., Giovagnoli, A., & Nervo, M. (2013). Pigments and mixtures identification by Visible Reflectance Spectroscopy. *Procedia Chemistry*, *8*, 45–54. https://doi.org/10.1016/j.proche.2013.03.007

Chalmin, E., Menu, M., & Vignaud, C. (2003). Analysis of rock art painting and technology of Palaeolithic painters. *Measurement Science and Technology*, (July). https://doi.org/10.1088/0957-0233/14/9/310

Cheilakou, E., Troullinos, M., & Koui, M. (2014). Identification of pigments on Byzantine wall paintings from Crete (14th century AD) using non-invasive Fiber Optics Diffuse Re fl ectance Spectroscopy (FORS). *Journal of Archaeological Science*, *41*, 541–555. https://doi.org/10.1016/j.jas.2013.09.020

Clark, R. (1999). *Remote Sensing for the Earth Sciences: Manual of Remote Sensing*. (A. Rencz, Ed.) (3rd ed.). John Wiley & Sons Ltd.

Conservation Perspectives: Rock Art Conservation. (2019).

Contador, S. (2019). Escoural Cave Tour. Santiago do Escoural.

Cosentino, A. (2014). FORS Spectral Database of Historical Pigments in Different Binders. *E Conservation Journal*, (September). https://doi.org/10.18236/econs2.201410

Daniel, F., & Mounier, A. (2016). Mobile hyperspectral imaging for the non-invasive study of a mural painting Mobile hyperspectral imaging for the non-invasive study of a mural painting in the Belves Castle (France , 15th C). *STAR: Science & Technology of Archaeological Research*. https://doi.org/10.1080/20548923.2016.1183942

Delaney, J. K., Ricciardi, P., Glinsman, L. D., Facini, M., Thoury, M., Palmer, M., … Rie, E. R. De. (2015). Use of imaging spectroscopy , fiber optic reflectance spectroscopy , and X-ray fluorescence to map and identify pigments in illuminated manuscripts. *Studies in Conservatoin*, *3630*. https://doi.org/10.1179/2047058412Y.0000000078

Documentation and Conservation of Rock Art. (n.d.). *Technologies for Prehistoric and Historic Preservation*, 165–168.

Domingo, I., Carrión, B., Blanco, S., & Lerma, J. L. (2015). Evaluating conventional and advanced visible image enhancement solutions to produce digital tracings at el Carche rock art shelter. *Digital Applications in Archaeology and Cultural Heritage*, *2*(2–3), 79–88. https://doi.org/10.1016/j.daach.2015.01.001

Domingo, I., Villaverde, V., López-montalvo, E., Luis, J., & Cabrelles, M. (2013). Latest developments in rock art recording : towards an integral documentation of Levantine rock art sites combining 2D and 3D recording techniques. *Journal of Archaeological Science*, *40*(4), 1879–1889. https://doi.org/10.1016/j.jas.2012.11.024

Domingo Sanz, I. (2014). Rock Art Recording Methods : From Traditional to Digital, (January). https://doi.org/10.1007/978-1-4419-0465-2

Dooley, K. A., Lomax, S., Zeibel, J. G., Miliani, C., Ricciardi, P., Hoenigswald, A., & Delaney, J. K. (2013). Mapping of egg yolk and animal skin glue paint binders in Early Renaissance paintings using near infrared reflectance imaging spectroscopy. *Analyst*, 4838–4848. https://doi.org/10.1039/c3an00926b

Earle, S. (2019). *Physical Geology - 2nd Edition* (2nd ed.). Victoria, B.C.

Fernandez-Cortes, A., Cuezva, S., Sanchez-moral, S., Cañaveras, J. C., Porca, E., Jurado, V., … Saiz-jimenez, C. (2011). Detection of human-induced environmental disturbances in a show cave. *Environ*, 1037–1045. https://doi.org/10.1007/s11356-011-0513-5

Fischer, C., & Kakoulli, I. (2013). Multispectral and hyperspectral imaging technologies in conservation : current research and potential applications. *Studies in Conservatoin*. https://doi.org/10.1179/sic.2006.51.Supplement-1.3

Gaálová, B., Donauerová, A., Seman, M., & Bujdáková, H. (2014). Identification and ß-lactam resistance in aquatic isolates of Enterobacter cloacae and their status in microbiota of Domica Cave in Slovak Karst (Slovakia). *International Journal of Speleology*, *43*(January), 69–77.

Gallinaro, M. (2018). Rock art –theoretical and methodological issues. Rome, Italy.

Gay, M., Müller, K., Plassard, F., Cleyet-merle, J., Arias, P., Ontañón, R., & Reiche, I. (2016). Efficient quantification procedures for data evaluation of portable X-ray fluorescence – Potential improvements for Palaeolithic cave art knowledge. *Journal of Archaeological Science: Reports*, (June). https://doi.org/10.1016/j.jasrep.2016.06.008

General Method Policies for All Site Recordation. (2018).

Gonzalez, I., Laiz, L., Hermosin, B., Caballero, B., & Incerti, C. (1999). Bacteria isolated from rock art paintings : the case of Atlanterra shelter (south Spain). *Journal of Microbiological Methods*, *36*, 123–127.

Grady, E., MacDonald, J., Liu, L., Richman, A., & Yuan, Z. (2016). Current knowledge and perspectives of Paenibacillus: a review. *Microbial Cell Factories*.

Groth, I., & Saiz-Jimenez, C. (2010). Actinomycetes in Hypogean Environments. *Geomicrobiology Journal*, *0451*(1999). https://doi.org/10.1080/014904599270703

Gunn, J. (Ed.). (2004). *Encyclopedia of Caves and Karst Science*. New York: Taylor & Francis.

Harman, J. (2006). *Using Decorrelation Stretch to Enhance Rock Art Images*.

Hennings, J. K., Baumann, H., Sobottka, I., Schmiedel, S., & Klose, H. (2009). Enterobacter Cloacae as Cause of a Severe Community-Aquired Pneumonia. *American Thoracic Society Journal*.

Heyd, T., & Lenssen-erz, T. (2012). Rock art and human dimensions of climate change. In *Pleistocene art of the world*.

Jurado, V., Laiz, L., Rodriguez-nava, V., Boiron, P., Sanchez-moral, S., Saiz-jimenez, C., … Pathogenic, S. C. (2010). Pathogenic and opportunistic microorganisms in caves. *International Journal of Spel*, *39*(January), 15–24.

Jurado, V., Porca, E., Cuezva, S., Fernandez-cortes, A., Sanchez-moral, S., & Saiz-jimenez, C. (2010). Fungal outbreak in a show cave. *Science of the Total Environment*. https://doi.org/10.1016/j.scitotenv.2010.04.057

Lambert, D. (2007). Introduction to Rock Art Conservation: A guide to the preservation of Aboriginal rock art. *Culture and Heritage Division, Australia*.

Leona, M., & Winter, J. (2019). Fiber Optics Reflectance Spectroscopy : A Unique Tool for the Investigation of Japanese Paintings. *Studies in Conservatoin*, *46*(3), 153–162.

Leys, N., Ryngaert, A., Bastiaens, L., Verstraete, W., Top, E., & Springael, D. (2004). Occurrence and Phylogenetic Diversity of Sphingomonas Strains in Soils Contaminated with Polycyclic Aromatic Hydrocarbons. *Applied and Environmental Microbiology*.

Liang, H. (2011). Advances in Multispectral and Hyperspectral Imaging for Advances in multispectral and hyperspectral imaging for archaeology and art conservation. *Applied Physics A- Materials Science & Processing*. https://doi.org/10.1007/s00339-011-6689-1

Marques, J. A. (2001). Património Estudos: Conjunto Arqueológico do Escoural.

Mauran, G. (2016). *Rock paintings and microorganisms - a new insight on Escoural Cave*. University of Evora.

Mauran, G., Mirao, J., Candeias, A., & Caldeira, A. T. (2017). A arte rupestre da Gruta do Escoural – novos

dados analíticos sobre a pintura paleolítica. *Arqueologia Em Portugal*.

Mitova, M., Iliev, M., & Groudeva, V. (2015). Identification of Bacillus strains isolated from rock paintings in Magoura cave , Bulgaria. *Journal of BioScience and Biotechnology*, 303–306.

Mulec, J., & Kosi, G. (2009). LAMPENFLORA ALGAE AND METHODS OF GROWTH CONTROL. *Journal of Cave and Karst Studies*, (2), 109–115.

Novakova, A., Hubka, V., Saiz-Jiménez, C., & Kolarik, M. (2012). Aspergillus baeticus sp. nov. and Aspergillus thesauricus sp . nov ., two species in section Usti from Spanish caves. *International Journal of Systematic and Evolutionary Microbiology*, 2778–2785. https://doi.org/10.1099/ijs.0.041004-0

Oh, S., Hyun, C., & Park, H. (2017). Near-Infrared Spectroscopy of Limestone Ore for CaO Estimation under Dry and Wet Conditions. *Minerals*, (7), 1–11. https://doi.org/10.3390/min7100193

Olivares, M., Castro, K., Corchón, M. S., Gárate, D., Murelaga, X., Sarmiento, A., & Etxebarria, N. (2013). Non-invasive portable instrumentation to study Palaeolithic rock paintings : the case of La Peña Cave in San Roman de Candamo (Asturias , Spain). *Journal of Archaeological Science*, *40*(2), 1354–1360. https://doi.org/10.1016/j.jas.2012.10.008

Ontañón, R. (2014). The conservation of prehistoric caves in Cantabria , Spain.

Peyroteo-stjerna, R. (2018). The dead at Escoural Cave (Montemor-o-Novo, Portugal): early farmer's interactions in south-western Iberian Peninsula. *De Gibraltar Aos Pireneus*, 65–84.

Pronti, L., Ferrarai, P., Uccheddu, F., Pelagottii, A., & Piva, A. (2015). Identification of pictorial materials by means of optimized multispectral reflectance image processing. In *2015 IEEE International Workshop on Information Forensics and Security*. https://doi.org/10.1109/WIFS.2015.7368561

Quellec, J. Le, Duquesnoy, F., & Defrasne, C. (2015). Digital image enhancement with DStretch: Is complexity always necessary for efficiency? *Digital Applications in Archaeology and Cultural Heritage*, *2*(2–3), 55–67. https://doi.org/10.1016/j.daach.2015.01.003

Robinson, E., & Ware, G. (2002). *Multi-spectral Imaging of La Casa de las Golondrinas Rock Paintings*.

Rogerio-candelera, M. Á. (2015). Digital image analysis based study, recording, and protection of painted rock art . Some Iberian experiences. *Digital Applications in Archaeology and Cultural Heritage*, *2*(2–3), 68–78. https://doi.org/10.1016/j.daach.2014.11.001

Rogerio-Candelera, M. Á. (2016). Journal of Archaeological Science : Reports Digital image analysis-based strategies for quantitative monitoring of rock art sites. *Journal of Archaeological Science: Reports*, *10*, 864–870. https://doi.org/10.1016/j.jasrep.2016.06.041

Rogerio-Candelera, M. Á., Bueno, P., Balbín-Behrmann, R. De, Dias, M. I., García, L., Larsson, M., … Gaspar, D. (2018). Landmark of the past in the Antequera megalithic landscape : A multi- disciplinary approach to the Matacabras rock art shelter, *95*(May), 2–3.

Rosado, T., Silva, M., Dias, L., Candeias, A., Gil, M., Mirão, J., … Caldeira, A. T. (2017). Microorganisms and the integrated conservation-intervention process of the renaissance mural paintings from Casas Pintadas in Évora – Know to act , act to preserve. *Journal of King Saud Univeristy - Science*, 1–9. https://doi.org/10.1016/j.jksus.2017.09.001

Rosi, F., Daveri, A., Miliani, C., Verri, G., & Benedetti, P. (2009). Non-invasive identification of organic

materials in wall paintings by fiber optic reflectance infrared spectroscopy : a statistical multivariate approach. *Analytical and Bioanalytical Chemistry*. https://doi.org/10.1007/s00216-009-3108-y

Saiz-Jimenez, C. (Ed.). (2014). *The Conservation of Subterranean Cultural Heritage*. London: Taylor & Francis.

Silva, A. C. (2011). *Escoural* (2nd ed.). Direcção Regional de Cultura do Alentejo.

Silva, A. C., & Araújo, A. C. (1995). Roteiros Da Arqueologia Portuguesa 4: Gruta do Escoural.

Smith, C. (Ed.). (2014). *Encyclopedia of Global Archaeology*. New York: Springer. https://doi.org/10.1007/978-1-4419-0465-2

Ster, K., Little, B., Pinar, G., Pinzari, F., Rios, A. D. L., & Gu, J. (2018). Future directions and challenges in biodeterioration research on historic materials and cultural properties. *International Biodeterioration & Biodegradation*, *129*(February), 10–12. https://doi.org/10.1016/j.ibiod.2017.12.007

Stomeo, F., Gonzalez, J. M., & Saiz-Jimenez, C. (2007). ON THE PRESENCE OF ACIDOBACTERIA IN THE CAVE OF DOÑA TRINIDAD (MALAGA, SPAIN). In *7th International Symposium on the Conservation of Monuments in the Mediterranean Basin*.

Stomeo, F., Portillo, M. C., Gonzalez, J. M., & Laiz, L. (2008). Pseudonocardia in white colonizations in two caves with Paleolithic paintings. *International Biodeterioration & Biodegradation*, *62*(4), 483–486. https://doi.org/10.1016/j.ibiod.2007.12.011

Stuart, B. H. (2007). *Analytical Techniques in Materials Conservation*. Chichester, England: John Wiley & Sons Ltd.

TARA. (n.d.). Trust for African Rock Art. Retrieved April 12, 2019, from https://africanrockart.org/

Varmuza, K., & Filzmoser, P. (n.d.). *Introduction to Multivariate Statistical Analysis in Chemometrics*. CRC Press.

Whitley, D. S. (2001). *Handbook of Rock Art Research*. AltaMira Press.

Williams, K., & Shee, E. (2015). From sketchbook to structure from motion : Recording prehistoric carvings in Ireland. *Digital Applications in Archaeology and Cultural Heritage*, *2*(2–3), 120–131. https://doi.org/10.1016/j.daach.2015.04.002

Yasir, M. (2017). Analysis of bacterial communities and characterization of antimicrobial strains from cave microbiota. *Brazilian Journal of Microbiology*, *49*(2), 248–257. https://doi.org/10.1016/j.bjm.2017.08.005

Yivlialin, R., Galli, A., Raimondo, L., Martini, M., & Sassella, A. (2019). Detecting the NIR Fingerprint of Colors : The Characteristic Response of Modern Blue Pigments, 2255–2261. https://doi.org/10.3390/heritage2030137

Zucco, M., Pisani, M., & Cavaleri, T. (2017). Fourier Transform Hyperspectral Imaging for Cultural Heritage. *Fourier Transforms - High-Tech Application and Current Trends*.